# STUDIES OF THE EFFECTS OF CROSS-SECTIONAL AREA CHANGE AND BOUNDARY-LAYER GROWTH ON SHOCK-WAVE MOTION

Thesis by

David A. Russell

In Partial Fulfillment of the Requirements
For the Degree of
Doctor of Philosophy

California Institute of Technology

Pasadena, California

1961

# ACKNOWLEDGEMENTS

The author wishes to acknowledge the patient guidance of Dr. Anatol Roshko, and the many useful discussions with fellow students. I also wish to acknowledge the assistance of my wife, who typed the rough draft of this work, Mrs. Geraldine Krentler for the final draft, and Mrs. Dorothy Diamond for her painstaking preparation of the figures.

# ABSTRACT

Three problems concerned with the motion of a shock wave are discussed. The first is an analytical and experimental study of the performance of a shock tube with area change near the diaphragm. Interesting results of this section are the development of a simple shock-speed control through the use of area change, and the fact that a spread-out dissipation region was shown to exist for a configuration where a non-stationary secondary shock wave was originally expected. A general discussion of the use of this type of area change is also included.

The second problem is a study of the effects of boundary-layer growth on the motion of a shock wave. A simple theory for predicting the attenuation of a shock wave on entering an upstream-facing tube is developed from the analysis of Spence and Woods. When simple laminar boundary-layer approximations are applied, the theory shows good agreement with measurements.

The final problem is an experimental study of the motion of a shock wave downstream of a finite-length area contraction. Normalized results are presented which show that the shock wave emerges from the area change at a speed close to the "linearized" theory value, and is then attenuated by second-order disturbances until it reaches the speed predicted for the steady-state configuration. The results are presented in a form which is shown to be insensitive to both the incident shock Mach number and the amount of the area reduction.

# TABLE OF CONTENTS

TABLE OF CONTENTS (Cont'd.)

TABLE OF CONTENTS (Cont'd.)

# LIST OF FIGURES

## LIST OF FIGURES (Cont'd.)

# LIST OF SYMBOLS

| | | |
|---|---|---|
| $a$ | = | speed of sound |
| $A$ | = | cross-sectional area |
| $A^*$ | = | throat cross-sectional area (M = 1) |
| $d$ | = | channel diameter |
| $f$ | = | arbitrary function or Blasius Function |
| $F$ | = | arbitrary function |
| $g$ | = | arbitrary function or amplification factor (Appendix I, equation 9) |
| $G$ | = | arbitrary function |
| $k$ | = | coefficient of thermal conductivity |
| $K_1$ | = | $\delta_1^* \sqrt{u_2/(\nu x)}$ |
| $K_2$ | = | $\delta_2^* \sqrt{u_2/(\nu s)}$ |
| $K_3$ | = | $\delta_3^* \sqrt{u_2/(\nu s)}$ |
| $\ell_o$ | = | nozzle length |
| $M$ | = | Mach number |
| $M_o$ | = | unperturbed shock Mach number ($u_o/a_1$) |
| $M_s$ | = | actual perturbed or transmitted shock Mach number ($u_s/a_1$) |
| $M_L$ | = | shock Mach number predicted by the linear theory |
| $M_{ss}$ | = | shock Mach number predicted by the steady-state calculation |
| $p$, $P$ | = | pressure |
| $Pr$ | = | Prandtl number |
| $P_{Tg}$ | = | total pressure after probe normal-shock wave |
| $r$ | = | radial distance |
| $R$ | = | channel radius |
| $R_{ed}$ | = | Reynolds number based on diameter and flow conditions 'e' |

## LIST OF SYMBOLS (Cont'd.)

$R_{2d}$ = Reynolds number based on diameter and flow conditions '2'

s = slope of fine-wire response

= shock fixed variable ($U_o t - x$)

t = time

= ideal-theory calculated time of arrival of event (measured from passage of primary shock wave)

- $t_{cs}$ contact-surface arrival
- $t_{s2}$ secondary shock arrival
- $t_e$ secondary expansion-wave arrival
- $t_{ee}$ end of secondary expansion wave

T = temperature

u = velocity

$U_o$ = unperturbed shock speed

$U_s$ = perturbed or transmitted shock speed

$U_{s2}$ = speed of secondary shock wave down the shock tube

v = vertical velocity

x = distance along shock-tube axis or gauge spacing

y = distance perpendicular to shock-tube axis

$\alpha$ = parameter for matching steady and unsteady boundary layers

$\gamma$ = ratio of specific heats

$\delta$ = boundary-layer thickness

$\delta_1^*$ = displacement thickness, steady boundary layer

$\delta_2^*$ = displacement thickness, shock-boundary layer

$\delta_3^*$ = displacement thickness of shock-boundary layer in laboratory reference frame

## LIST OF SYMBOLS (Cont'd.)

| | | |
|---|---|---|
| $\eta$ | = | characteristic variable, $x - (u_2 + a_2)t$ |
| $\mu$ | = | coefficient of viscosity |
| $\nu$ | = | kinematic viscosity |
| $\xi$ | = | characteristic variable, $x - (u_2 - a_2)t$ |
| $\rho$ | = | density |

Subscripts:

| | |
|---|---|
| $( )_1$ | parameter in region 1, the undisturbed driven gas |
| $( )_2$ | parameter in region 2, downstream of contact surface (also denotes unperturbed flow) |
| $( )_3$ | parameter in region 3, upstream of contact surface |
| $( )_4$ | parameter in region 4, the undisturbed driver gas |
| $( )_3'$ | |
| $( )_3''$ | parameters in or adjacent to the area change (see fig. 1) |
| $( )_4'$ | |
| $( )_a$ | parameter in general region a |
| $( )_b$ | parameter in general region b |
| $( )_e$ | parameter in core flow |
| $( )_w$ | parameter evaluated at shock-tube wall |
| $( )_*$ | parameter at throat |
| $\overline{( )}$ | quantity averaged over a distance |

N.B. other symbols are defined as they are used in the text.

# GENERAL INTRODUCTION

This work is divided into three main parts. The first, a study of area change near the diaphragm of a shock tube, was reported earlier (ref. 1). The primary concern in part I is with the effect of area change at the diaphragm location on the shock speed at large distances from the diaphragm. The wave systems in this case have reached a steady-state velocity, and hence analytical solutions are obtained simply by matching conditions across the various waves of the assumed model. Measurements were made to check the validity of the theory and some interesting conclusions were reached. Principal among these is the postulation of a spread-out dissipation region for the configuration where a traveling secondary shock wave was originally postulated. This work has practical importance for the design of shock tubes, and the results of this section were used extensively for the control of the incident shock speed for the models used in parts II and III.

In part II, the motion of a shock wave which has entered an upstream facing tube is studied. This work was initiated in order to learn something of the viscous attenuation effects on the shock wave in the third problem studied. It is treated as a separate section because of the concise attenuation theory that was developed, and the possibilities of using this model to gain more insight into the phenomenon of viscous attenuation of shock-waves.

In part III, the motion of a shock wave downstream of a finite length area convergence is studied. Both part II and part III are essentially studies of the effect of the flow behind the shock wave on the

shock-wave motion. In part II the governing one-dimensional equations can be linearized and a simple solution obtained. For the problem of part III this is not so, for the effect studied is intimately tied to the higher-order terms in the one-dimensional equations of motion.

When a shock wave travels through a region of continually decreasing cross-sectional area, very large increases in shock speed are predicted by the theory based on the linearized equations of motion. This theory relates the strength of the accelerating shock wave directly to the local cross-sectional area at the shock-wave location. Now if the shock wave emerges from the converging section into a section of constant area, according to this theory its speed should remain constant (since the area is constant). On the other hand, far downstream the region of varying area will appear identical to an instantaneous area change, for which a lower transmitted shock speed may be calculated by matching parameters across the steady-state wave model. Thus the shock wave must actually decelerate downstream of the area change until it reaches the final steady-state velocity, and the linear theory fails to predict this deceleration.

This problem is studied in detail in part III. Normalized experimental results are presented which (in combination with the results of part II) allow finite-length area changes to be designed to provide a specified shock-wave attenuation per foot at a fixed position downstream. This is of considerable importance for the practical use of the large shock-strength enhancement possible with converging cross sections, and the results themselves help to shed more light on the re-reflected disturbances (represented by the higher-order terms in the

equations of motion).

When viscous effects can be neglected, it is convenient to divide problems involving the effects of cross-sectional area change into three inter-related groups. The first group, typified by part I and by the asymptotic steady-state solution of part III, involves non-accelerating wave systems and can generally be solved by a process of matching parameters across an assumed wave model. Next in mathematical complexity is the group involving montonically accelerating or decelerating wave systems, an example being the motion of a shock wave down a continuously-converging duct. For this type of problem useful solutions may often be found by solving the linearized one-dimensional equations of motion. Finally, there is the class of problems typified by part III. Here the wave system is not monotonically accelerating, the shock wave actually accelerating through the area convergence and then decelerating to finally attain a steady-state configuration of the form of the first classification. For problems of this type, which involve non-monotonically accelerating wave systems, the flow history behind the shock wave affects the shock-wave motion and any mathematical treatment must involve the higher-order terms in the one-dimensional equations of motion.

# I. A STUDY OF AREA CHANGE NEAR THE DIAPHRAGM OF A SHOCK TUBE

## 1. INTRODUCTION

It was mentioned in the General Introduction that the types of cross-sectional area change that affect wave motion in a duct may be conveniently classified on the basis of the type of acceleration exhibited by the resulting wave systems. The configurations involving no wave acceleration have similarity solutions in the x-t plane about some origin. They may be further divided into those configurations for which there are waves entering as well as leaving this origin (i.e., problems involving wave reflection (ref. 2)), and those for which there are only waves leaving the similarity origin. For a shock tube, the latter group is referred to as having area change "near the diaphragm". This implies that, for flow times of interest, the various waves have attained a state of constant velocity, wave reflection has ceased to be important, and the contact surface has passed through the region of varying area. The purpose of part I is to study this type of area change in a shock tube.

Shock tubes with area change near the diaphragm may be treated in ideal theory (see section 2) as though the area change were an isentropic nozzle located at the diaphragm. The calculation of shock-tube performance is then basically a problem of matching pressure and velocity across the contact surface. In general, an upstream-facing secondary wave, between the nozzle exit and the contact surface, will be found necessary in order to achieve the contact-surface matching (see fig. 1). For very high shock Mach numbers, this wave will be a non-steady expansion wave; for lower Mach numbers, a non-steady normal shock wave is required; for still lower Mach numbers, the normal shock wave

moves into the nozzle and becomes stationary; while at the very low Mach numbers, the nozzle flow becomes subsonic, and thus incapable of supporting any secondary wave.

The above wave configurations are the only possible ones for a shock tube with area change near the diaphragm; however, a given shock tube may not produce them all. Previous work, notably by Resler, Lin, and Kantrowitz (ref. 3) and by Alpher and White (ref. 4)*, has been concerned with the use of area change at the diaphragm for the attainment of high speed shocks, and thus has only partially considered the first configuration (the case where the secondary wave is isentropic). In this report, the existing work is extended to all four configurations, and thus covers the whole range of shock Mach numbers and possible area changes at the diaphragm.

The ideal theory for the different configurations is discussed in the first section of part I. (Detailed calculation procedures are presented in Appendix I.) Curves of range of application and of initial pressure ratio versus shock Mach number are presented for Nitrogen-Air and Helium-Air shock tubes. The second section discusses the usefulness of various area configurations with the aid of the ideal theory. Particular attention is given to the use of a simple drilled plate inserted at the diaphragm,as a means of gaining additional flexibility in shock tube operation.

The agreement between experimental and theoretical curves of initial pressure ratio versus shock Mach number is discussed in the next

---

* Reference 4 includes a critical review of earlier work, and in particular points out an error in a previous study of the expansion wave configuration made at this laboratory. (Yoler, Y.A.: Hypersonic Shock Tube. GALCIT Hypersonic Research Project, Memorandum No. 18, July 19, 1954.)

section, where the fine wire and piezo-electric pressure gauge observations of the secondary waves are shown to indicate the necessity for a new model for the non-steady, non-isentropic configuration.

A simple model, based on the concept of the Fanno process, or spread-out compression region, is presented in the fourth section. With this new theory the remarkable agreement with experimental basic performance is shown, and the insensitivity of the basic performance curves to the type of model is demonstrated. The inadequacies of this new theory are discussed, and more realistic models are indicated.

## I - 2. IDEAL THEORY

The ideal theory is based on the assumptions of no heat transfer and no boundary layers or associated viscous-interaction regions. These restrictive assumptions, which allow the use of isentropic nozzles and simple plane waves, will turn out to be remarkably good for predicting most of the performance characteristics of shock tubes with area change near the diaphragm. The procedure is based on matching conditions across the contact surface, and is set up so as to avoid the iterative calculations that are common to this type of problem.

The shock tube configurations studied are illustrated in figure 1. Each model shown is similar to a plain shock tube, except for the changing area at the diaphragm station and the resultant secondary waves. The notation used is adapted from the accepted shock-tube notation, where region 1 refers to the undisturbed driven gas, regions 2 and 3 to the gas downstream and upstream of the contact surface, and region 4 to the undisturbed driver gas. The primed numbers refer to the gas immediately upstream and downstream of the area change as shown. It should be noted that the secondary waves are always upstream of the contact surface, and are always upstream-facing waves (although non-steady waves are swept downstream by the flow). It can be shown that any other secondary wave configuration is unstable, for the wave will either tend to change its position to correspond to one of the configurations in figure 1, or it will catch up with one of the primary waves.

The assumption that the area change may be treated as an isentropic nozzle allows the shock-tube geometry to be completely specified by $A_4/A_1$ (the ratio of driver to driven tube area) and $A^*/A_1$ (the ratio of the

throat area to the driven tube area). For a given shock tube with specified gases (i.e., $a_4$, $\gamma_4$, $a_1$, $\gamma_1$), the velocity downstream of the contact surface is uniquely determined by $M_s$ (the shock Mach number), while the velocity upstream of the contact surface is fixed by the nozzle geometry (if the nozzle exit flow is assumed supersonic). Thus, there is only one value of $M_s$ for which the velocity will match across the contact surface. For shock speeds above this value a secondary expansion wave is necessary to further expand the nozzle exit flow. This is the "expansion wave configuration" depicted in figure 1a. For shock speeds below the critical value, a normal shock wave will, in general, be expected (figure 1b). As mentioned in the Introduction, this wave increases in strength as $M_s$ is lowered, until it becomes stationary in the nozzle... the "shock-in-nozzle" configuration (figure 1c). Finally, for very low shock speeds, the nozzle flow becomes completely subsonic and no secondary waves can exist. Curves illustrating the regions of application of these various configurations are presented in figure 2, for $A_4/A_1 = 1$.

The actual analyses are worked out in Appendix I. The ideal theory for the expansion wave configuration has been previously demonstrated for $A_4/A_1 > 1$ and $A^*/A_1 = 1$ (ref. 3 and 4)*, but is reviewed both as a background for the other configurations, and to show its extension to all values of these area ratios. It is seen that the solution of the basic shock-tube relation is available in closed form for this case. Indeed, an "equivalent standard shock tube" may be defined as shown in Appendix I. A. In this analysis it is not necessary to consider the speed of the secondary

---

* Reference 4 also considers the energy aspects of the problem ... considerations of energy transfer efficiency across the various wave systems affords a useful qualitative understanding of the whole process.

expansion wave itself, for the ratio of the parameters across the wave depends only on the flow Mach numbers on either side. For the normal shock-wave configuration, however, the expression for the pressure ratio across the secondary shock involves the speed of the shock wave, and elimination of this speed in terms of the flow Mach numbers involves the solution of a high-degree algebraic equation. The resulting calculation becomes so unwieldy that the usefulness of a closed form solution for the normal shock case is questionable. The procedure presented provides a relatively fast means of calculating performance, avoiding the necessity for iteration by not attempting to solve the direct problem in which $M_s$ is specified. The shock-in-nozzle configuration is an extension of the shock-wave case, simplified because the shock is stationary, but complicated because of the additional steady expansion.

Illustrative performance curves are shown in figures 3 and 4 for the high $M_s$ regions. These curves are for varying $A^*/A_1$ only. Figures 5a and 5b allow determination of the performance of a Helium-Air shock tube of any geometry, but for the expansion-wave case only. Figure 12 shows the low $M_s$ solution for a Nitrogen-Air shock tube again with varying $A^*/A_1$ only. Since the effect of the nozzle depends solely on $A_4/A_1$ for the "subsonic nozzle" configuration, that part of the curves of figure 12 corresponds to the conventional shock-tube curve.

The dividing line between the regions of application of the expansion-wave and shock-wave model does not readily come out of the expansion-wave theory. It is arrived at by taking the limit of the normal shock-wave theory, that is, where the secondary shock has zero strength

$$\left(M_{3'} - \frac{U_{s2}}{a_{3'}} = 1\right).$$

The lower limit for the normal-shock model is where the shock first becomes stationary ($U_{s2} = 0$); the lower limit for the shock-in-nozzle theory is where the shock is at the throat and has zero strength. These boundaries are depicted in figure 2 for shock tubes with varying $A^*/A_1$.

## I - 3. APPLICATION OF AREA CHANGE AT THE DIAPHRAGM

One of the first studies of area change at the diaphragm was that of Lukasiewicz (ref. 5). Both he and subsequent authors (ref. 3 and 4) have been primarily concerned with the interesting fact that area change may be used to increase available shock speed for a given shock tube. This effect is a maximum for $A^*/A_1 = 1$ and $A_4/A_1 \rightarrow \infty$; however, from figures 5a and 5b it is seen that a small increase in $A_4$ produces very nearly the same effect as the limit of infinitely large $A_4/A_1$. The actual per cent increase in $M_s$ over that of a conventional shock tube is a complicated function of $M_s$ itself, but figures 5a and 5b illustrate it to be of the order of ten per cent for a practical shock tube operating at near maximum pressure ratio. Information contained in reference 4 shows that this figure is reasonable for shock tubes operating with other gas combinations. While the figure of ten per cent is appreciable in some instances, other techniques will generally produce more spectacular increases (i.e., different gas combinations, a heated driver, or a double-diaphragm shock tube (ref. 6)).

A study was made of the use of area change at the diaphragm for the economical operation of large shock tubes. The diaphragm cost (proportional to $A^{*3/2}$) turns out to be negligible when compared with that of the driver gas at the high pressure ratios where cost becomes significant. The gas volume is proportional to $P_4A_4$, and it is readily shown that $A^*/A_1$ must be unity for optimum economy at a given $M_s$. The optimum value of $A_4/A_1$, however, is not obvious, and curves of $A_4/A_1$ versus $P_4A_4$ must be plotted for each value of $M_s$. Such curves

are presented in figure 6. It is seen that the value of $A_4/A_1$ at which $P_4A_4$ is a minimum is a function of $M_s$ as expected. The trend to higher optimum values of $A_4/A_1$ with increasing $M_s$ is a result of the asymptotic behavior of the basic performance curves, such that the high values of $M_s$ cannot reasonably be achieved in a plain shock tube where the $M_s$ asymptote is low. For operation at moderate $M_s$ it is seen from figure 6 that a conventional shock tube ($A_4/A_1 = 1$) is not far off optimum for economical operation. For operation at high $M_s$, however, the above logic shows that the use of $A_4/A_1 > 1$ is most efficient, and figure 6 illustrates that factors of ten or greater decrease in operating costs can be realized for a Helium-Air shock tube. Studies of this nature aid in the choice of driver size, and they may result in a significant decrease in operating cost for a large shock tube.

The use of area change can provide additional flexibility in shock tube operation. Since the nozzle used in the ideal theory has no characteristic axial length, it may be assumed to have negligible length and to consist merely of a drilled plate placed perpendicular to the flow at the diaphragm station. Separation losses and consequent violation of the assumptions inherent in the ideal theory might now be expected, however the experimental evidence presented in the next section shows these losses to be negligible. Thus the use of a simple insert in a conventional shock tube enables any reduced-diaphragm-area shock tube to be easily obtained. The insert plates provide an additional control on Reynolds number, and they are a logical way to produce low shock speeds. *

*In addition, the ideal theory for the normal-shock-wave configuration predicts a jump in pressure after the primary shock wave, and a jump back to essentially the initial pressure after the passage of the secondary wave. This pressure pulse might have useful application, but the experimental evidence indicates that it is not to be expected for small shock tubes operating at reasonable pressure levels.

Figures 3, 4, and 12 show the performance of such a modified shock tube; figure 7 shows the diaphragm insert section used for obtaining the experimental results presented in this report. Placement of the drilled plate just far enough downstream to clear the opening diaphragm provides model and instrument protection from possible diaphragm fragments, and circumvents the rippage and uncertain breaking-pressure problems associated with the alternative use of very thin diaphragms. For large shock tubes it may be desirable to reduce the diaphragm size and thickness, and this may be facilitated by clamping the diaphragm directly over the plate orifice.

## I - 4. EXPERIMENTAL RESULTS

An experimental study of area change near the diaphragm of a shock tube was undertaken in the GALCIT 3-inch-square tube. The purpose of this study was to check the validity of the ideal theory, both by observing the basic performance of a modified shock tube, and by an investigation of the secondary waves. This shock tube has an area ratio of $A_4/A_1 = 0.855$, and was modified by the diaphragm insert of figure 7. Nitrogen-Air runs were made with various insert plates giving a range of $A^*/A_1$ from 0.855 to 0.03. Varying the initial pressure from 5 - 500 mm. gave enough range in $M_s$ to enable measurements to be made in all of the flow regimes involving secondary waves. A description of the shock tube and instrumentation used is presented in Appendix II.

The ideal theory predicts initial pressure ratio as a function of $M_s$ with no attenuation. In order to experimentally verify these curves with $M_s$ measured some distance down the tube, the attenuation must be taken into account. Thus, for the initial measurements, $M_s$ was obtained at two stations along the shock tube.

The resulting values of per cent attenuation per foot showed considerable scatter, and only crude correlation with theory (ref. 7). This was presumably due to the uncertain effect of diaphragm opening time, the appearance of turbulence in the boundary layer, and the relatively short distance over which it was possible to make the measurements. The measurements did show, however, that for a given $M_s$ there is no consistent or appreciable dependence of attenuation on $A^*/A_1$. This means that a value of $M_s$, measured in a modified shock tube, may be corrected

for attenuation by adding to it the difference between the ideal and the best-fit experimental curves for the unmodified shock tube with the same $M_s$. Figure 8 presents the original $P_4/P_1$ versus $M_s$ data. (Note that the ideal theory curves are plotted for $A_4/A_1 = 0.855$ and thus differ from those of figure 12.) Figure 9 shows the data replotted with the small attenuation correction applied. The experimental points were obtained on different days and are accurate to the order of the symbol size. A few points, for which the diaphragms were only partially opened, fell understandably low and have been omitted.

The agreement between the theory and the corrected experimental results is seen to be excellent for the shock-in-nozzle configuration. The experimental points also appear to fair into the ideal theory curve for the expansion-wave case. The validity of the ideal theory for the expansion wave configuration was also noted by Alpher and White (ref. 8), who made measurements at high $M_s$ in a shock tube with various values of $A_4/A_1$ and observed that the change in basic performance agrees with the theory. These results emphasize the general validity of the ideal theory and they imply that any nozzle plate losses are insignificant (from the standpoint of the ideal theory). Indeed, nozzle losses could be easily added into the theory (if the experimental data were available), but it is felt that the remaining uncertainties in attenuation are of more significance.

The discrepancy between theory and experiment for the normal shock configuration remains unexplained. In order to shed more light on this situation, the actual details of the secondary waves were investigated for the normal-shock-wave and expansion-wave configurations. The primary tool for this investigation was the fine unheated wire (ref. 9), for which the analysis techniques are discussed in Appendix IIB.

Tungsten wires with diameters ranging from 1.5 - 0.2 mils. were used, affording a wide range of sensitivity. The wire response was expected to exhibit a sharp change in slope when a secondary shock wave passed over it, or a gradual change of slope through an expansion wave. The slope on each side of the secondary wave, together with the expected time of arrival of the wave at the gauge, was calculated and compared with the experimental results. The use of slope ratios eliminates some of the wire calibration properties, and it is felt that the resulting slope predictions are accurate to within ten per cent. Principal errors in this calculation are due to end losses, the cumbersome calculation procedure, and the extension of existing hot-wire data to the current situation.

Typical results are presented in figure 10, where the relevant theoretical and experimental slope ratios are also listed. Figure 10a, for the expansion-wave case, shows reasonable agreement, both in times and slope ratios. The normal-shock-wave case, however, did not show the expected change in slope. Indeed, there was no definite slope change observed for this configuration with any of the wires tested, and the predicted slope ratio was always considerably different from the observed value, indicating that the secondary-normal-shock model is incorrect.

An examination of the slope ratios for the normal shock configuration revealed that the experimental slope is always nearer to the predicted values of $s_2/s_3$, than it is to $s_2/s_3$. Since no change in slope occurs after the contact surface, this might indicate that the secondary shock occurred at the contact surface. To check this unlikely possibility, and to provide additional information concerning this configuration, static

pressure measurements were made using a commercially available crystal transducer. (Kistler Piezo-Calibrator Model 2 with S. L. M. pickup) A sample trace is shown in figure 11a. These traces did not show the expected sharp pressure drop through the secondary shock wave. Instead, they showed the gradual pressure rise that has been observed in conventional shock tubes (ref. 15).

It is unlikely that the shock wave is masked out at the wall by boundary layer inter-action, but total pressure measurements were made to check this possibility. A small total-pressure probe was constructed, using a Barium Titanite crystal modeled after that of reference 10. A trace from this instrument is shown in figure 11b. There is a suggestion of a drop in total pressure, but it is not conclusive in that it is unfortunately obscured by hash from the diaphragm and a natural frequency of the crystal mounting. Since the total pitot pressure is relatively insensitive to the existence of a secondary normal shock, this study was not pursued further than a few unsuccessful attempts to clean up the response. It is felt that the measurements tended to support the previous findings of no secondary normal shock wave.

A final experimental study was made with a four-inch wooden nozzle attached to the downstream side of the 0.03 inch orifice plate. The purpose of this nozzle was to check the effect of the plate itself on the existence of the normal shock wave. Fine wire results were essentially identical with and without the nozzle on the plate. The points on the $P_4/P_1$ versus $M_s$ curves of figures 8 and 9 fall a little high, but the results are too few to be conclusive, and are probably due to a change in the attenuation history. A smoothly contoured nozzle appears to

produce the same shock-tube flow as the orifice plates.

## I - 5. FRICTIONAL THEORY FOR THE NON-ISENTROPIC SECONDARY WAVE CONFIGURATIONS

The experimental results of the last section indicate that the normal-shock model is marginal for predicting $M_s$ and thus conditions in region 2, and quite inadequate for describing the flow details upstream of the contact surface. To agree with the measurements, a new theory for this non-isentropic configuration is needed which will predict no static pressure jump and no sharp slope changes in the fine wire response. The new theory must, in addition, predict nearly the same basic performance as the ideal theory, and must fair into the valid solutions for the other configurations.

The starting point for the new theory might logically be to consider the secondary shock to be replaced by many weak shocks, resulting in a spread-out compression region. The existence of a spread-out compression region in a supersonic duct has been studied in connection with wind-tunnel nozzles (ref. 11 and 12). Indeed, in reference 12 it is pointed out that the shock wave reflecting off the end of a shock tube has been observed to take this form. It would seem quite possible that the interaction between the secondary shock wave and the thick boundary layer from the diaphragm could also result in a spread-out region for the configuration under study.

Appendix III. A shows the relevant calculations for a new model based on the replacement of the secondary shock wave with such a stationary interaction region. The functional relationship of the flow variables across this region is that of a Fanno curve, and the model will be referred to as the Fanno-process model. The relationship is obtained by writing the energy and continuity equations for the average cross

sectional flow values, replacing the momentum equation by a statement of the overall pressure ratio. This allows for arbitrary frictional processes and still enables the shock-tube performance to be calculated, although the details in the Fanno region itself remain arbitrary. It should be mentioned that in the calculations that lead to the Fanno model, the exit Mach number may come out to be subsonic. Since a frictional process in a constant area duct cannot result in a transition from supersonic to subsonic flow (ref. 13), a stationary shock wave must exist within the Fanno regions for these cases.

Figure 12 shows the results of the Fanno process model for $A_4/A_1 = 1$.* Figure 9 shows the remarkable agreement between this model and the experimental data. It is seen that the new curves fair in with both the expansion wave and subsonic nozzle solutions, even though they may cross the ideal theory curve before doing so. It is interesting to note that there is no slope discontinuity corresponding to that which occurs at the junction of the normal shock and shock-in-nozzle solutions, and that the shock-in-nozzle solution itself is unchanged by the new theory.

An attempt was made to choose a combination of shock-tube gases so as to further separate the two solutions and thus experimentally check the validity of the Fanno model under more severe conditions, but the relative $M_s$ difference was quite insensitive to the gases used. The insensitivity of the basic performance to the model used is further exemplified by the fact that solutions which consist of part stationary Fanno

---

* The plain shock tube curve was obtained with the use of a Fanno process from sonic velocity, replacing that part of the driver expansion wave which was downstream of the diaphragm.

process and part drifting secondary normal shock lie in the small enclosed region between the two pure solutions.

The agreement with the detailed flow measurements is also improved with the Fanno model. The calculated fine-wire slope ratio for figure 10b is -5.4 as compared with an experimental value of -7.7, and an ideal theory value of -2.0. The static pressure is now expected to remain constant, and while it actually tends to rise, this feature has been observed in plain shock tubes (ref. 15) and is thus not directly connected with the area change.

There is another interesting reason for accepting the Fanno model. From reference 14 it can be inferred that the nozzle starting process is important for times as short as those involved in shock-tube operation, and, in fact, the nozzle may not attain fully developed supersonic flow before the end of the run. A quasi-steady model of this situation might be to consider isentropic flow to a given station in the nozzle exit, and a Fanno process through the remainder of the nozzle. As time proceeds, more and more of the nozzle will be occupied with the isentropic flow and the Fanno region will move out of the nozzle. It is shown in Appendix III. B that for this model the flow parameters downstream of the Fanno process are independent of the location of the beginning of the Fanno process in the nozzle, and depend only on the overall pressure ratio across the whole region. Thus this quasi-stationary model must give results identical with the previous Fanno curve model, a fact which lends further credence to that model.

The simple stationary Fanno model has shown appreciably better agreement with experiment than the ideal-theory model; indeed, the remaining unexplained differences are of the same nature as those which

have been observed in a plain shock tube (ref. 15). The use of the basic Fanno-process idea, inter-related with a time-dependent mechanism for attenuation, may be a key to more complete understanding of these flows. The Fanno region may be combined with non-steady waves, may be allowed to drift down the tube, or may be assumed to grow with time (i.e., the downstream boundary moving with the speed of the contact surface). In the latter case, the time-dependent equations may be simplified by the introduction of a conical flow parameter, but the detailed history of one variable is needed to replace the momentum equation, and solution difficulties arise for all but the most simple assumed profiles.

A model, consisting of a stationary Fanno curve with a weak expansion wave downstream, was tried in an attempt to explain the wall pressure rise with time that existed for all shock-tube configurations. Some agreement with experiment was obtained, but more detailed measurements are necessary in order to justify the existence of this type of model, and to provide a thorough understanding of the Fanno-type of frictional process in a shock tube. In particular, it would be useful to learn more of the way in which this process may be advantageously used in place of the more complicated boundary-layer approaches.

## I - 6. CONCLUSIONS

The ideal theory presented in this report accurately predicts $M_s$ for shock tubes with area change near the diaphragm, with the exception of those configurations where a moving secondary shock wave is expected. For these cases, it is shown that the secondary shock wave can be replaced by a spread-out dissipation region. The resultant Fanno-process model accurately predicts $M_s$ and provides agreement with flow details to the same degree that flow measurements agree with theory for a plain shock tube. Further refinement of the theory, to coincide more closely with observation, awaits a more detailed experimental investigation. It is suggested that the Fanno-type of frictional process might have useful application to other shock-tube problems.

It appears that the most practical applications of area change at the diaphragm are the use of $A_4/A_1 > 1$ for increased $M_s$, and the use of simple insert plates to provide an additional control on shock-tube performance. In addition to these, and certain advantages that may occur in large shock tubes, area change near the diaphragm offers an interesting research tool for a further understanding of shock-tube flows.

# II. A STUDY OF THE VISCOUS ATTENUATION OF A SHOCK WAVE ENTERING A TUBE

## 1. INTRODUCTION

It is a well established fact that a shock wave attenuates due to the boundary-layer growth behind it. Since this effect can be important to an understanding of shock-tube flows, most actual shock-wave attenuation studies have been directly concerned with predicting the attenuation in a shock tube. Perhaps the most widely accepted of these studies is the theory of Mirels (ref. 7), in which the shock-tube boundary layer is replaced by a mass addition term in the continuity equation. Another treatment of shock-wave attenuation in a shock tube is that of Trimpi and Cohen (ref. 22). They replace the boundary layer by averaging its wall shear and heat transfer over the whole cross-section, using this information to modify the momentum equation. These theories are quite different in nature and cannot be expected to yield the same results. Of particular interest is the fact that Mirel's approach predicts a decrease in shock attenuation due to the driver expansion-wave boundary layer, while the theory of Trimpi and Cohen predicts the opposite effect!

The complete shock-tube boundary layer is complicated by the existence of the driver expansion-wave boundary layer and the problem of boundary-layer matching at the contact surface. In the above analyses, these complications are reduced by simplifying assumptions which are justified by the fact that the major contribution to attenuation comes from the boundary layer between the contact surface and the shock itself. The actual flow in a shock tube however, is also affected by the non-ideal diaphragm opening, and this is extremely hard to predict in a general

fashion. The result is that definitive measurements as to the actual mechanisms of attenuation are difficult to make, both theories providing roughly the same agreement with experiment. To provide more insight into the attenuation mechanism a much simpler configuration than the complete shock-tube flow is needed.

The problem studied in this section provides such a configuration. This is the problem of the motion of a shock wave after it has entered a sharp-edged tube which faces upstream into the flow (see figure 13). Here it is assumed that the impinging shock wave is produced in a shock tube of sufficient size so that the only significant attenuation occurs in the open-ended tube itself. Thus the attenuation of the shock wave is determined entirely by the boundary layer developed in the small tube, and there are no uncertain diaphragm effects to contend with. There is however, a problem provided by the fact that the complete boundary layer in the tube is as yet unsolved* (ref. 23), and must therefore be approximated by arbitrarily picking a condition for matching the known leading-edge-boundary layer with the known shock-boundary layer. Various criteria may be used for the matching of the two boundary layers, each providing a different relative position for the matching point and consequently affecting the predicted attenuation. This source of error does not occur in the shock-wave analyses referred to above (where the position of the matching point is known to be very near the contact surface.) However, it will be shown in what follows that displacement-thickness matching will yield results that agree with experiment to at least the same degree that

*In reference 23 Lam and Crocco cannot demonstrate the existence of a solution in the matching region between the two boundary layers, but they present arguments that the boundary layer equations are capable of producing a continuous solution which satisfies the boundary conditions.

has been observed in complete shock-tube attenuation studies. Moreover, in this case the disagreement can arise only from the approximations used in the theory, the measurements being in principle quite clean and repeatable. Thus, as more information on the tube boundary layer becomes available, the theory can be improved and better agreement expected.

An appropriate theory for the motion of a shock wave in a tube might be developed from the previously mentioned studies (ref. 7 and 22); however, a recent paper by Spence and Woods (ref. 24) contains a more concise approach to the problem of shock-wave attenuation. They integrate the complete continuity equation across the duct, and obtain a linearized one-dimensional continuity equation for the motion of the core-flow. The boundary-layer terms enter this equation in a simple way. The new system of linearized one-dimensional equations is written in characteristic form and integrated to obtain general expressions for the velocity and pressure in the core flow. The undetermined functions in these expressions are evaluated by the appropriate boundary conditions at the shock and the interface, and the expression for the shock motion is obtained in a relatively simple form.

Spence and Woods used this technique to calculate the attenuation in a shock tube with a turbulent boundary layer extending from the shock to the contact surface. They also went on to treat interesting combustion effects in the same manner. Their work is an extension of the earlier work of Demyanov (ref. 25), who treated the motion of a shock wave with a laminar Polhausen-type boundary layer.

In what follows, the theoretical treatment of Demyanov and Spence and Woods is further extended to deal with the problem of the shock-wave

motion on entering an upstream-facing tube. Analytical expressions are presented for the case of laminar boundary layers, and good agreement with experiment is shown.

## II - 2. ANALYSIS

### A. The Continuity Equation:

The axially-symmetric continuity equation is

$$\frac{\partial \rho}{\partial t} + \frac{\partial}{\partial x}(\rho u) + \frac{1}{r}\frac{\partial}{\partial r}(r\rho v) = 0. \tag{1}$$

Multiplying by $r$ and integrating across the duct from 0 to $d/2$ yields

$$\frac{\partial}{\partial t}\int_0^{d/2} \rho r\, dr + \frac{\partial}{\partial x}\int_0^{d/2} \rho u r\, dr = 0 \tag{2}$$

Following Spence and Woods (ref. 24), put $\rho = \rho_e$, $u = u_e$, for $0 < r < (d/2 - \delta)$ (where $\delta$ is the boundary-layer thickness). Performing the integration results in

$$\frac{\partial \rho_e}{\partial t} + \frac{\partial}{\partial x}(\rho_e u_e) = \frac{4}{d}\left[\frac{\partial}{\partial t}\int_0^{\delta}(\rho_e - \rho)\,dy + \frac{\partial}{\partial x}\int_0^{\delta}(\rho_e u_e - \rho u)\,dy\right], \tag{3}$$

where the right-hand side, representing the boundary-layer contribution, is of order $\delta/d$ (higher-order terms have been neglected). Since the right-hand side is of lower order, it will be consistent for the following linearized theory to evaluate it from the two-dimensional boundary layer solutions for the unperturbed shock speed $U_o$. Thus, for the stationary laminar boundary layer, the definition of the displacement thickness $\delta_1^*$ and its known dependence on Reynolds number and $x$ (ref. 26), results in

$$\frac{4}{d}\left[\frac{\partial}{\partial t}\int_0^{\delta}(\rho_e-\rho)dy + \frac{\partial}{\partial x}\int_0^{\delta}(\rho_e u_e-\rho u)dy\right] \cong 4\rho_e u_e \frac{d\delta_1^*}{dx} = 2K_1\frac{\rho_e u_e}{d}R_{ed}^{-1/2}\left(\frac{x}{d}\right)^{1/2}, \qquad (4)$$

where $K_1$ is a constant which will be evaluated later.

For the shock-boundary layer, it is most convenient to transform the right-hand side of equation 3 to shock-fixed coordinates, such that $s = U_o t - x$. Evaluating this quantity in the shock-fixed coordinates results in

$$\frac{4}{d}\left[\frac{\partial}{\partial t}\int_0^{\delta}(\rho_e-\rho)dy + \frac{\partial}{\partial x}\int_0^{\delta}(\rho_e u_e-\rho u)dy\right]$$

$$= \frac{4}{d}\rho_e(U_o-u_e)\frac{d\delta_2^*}{ds} = -2K_2\rho_e\frac{(U_o-u_e)}{d}R_{ed}^{-1/2}\left(\frac{U_o t-x}{d}\right)^{1/2}, \qquad (5)$$

where $\delta_2^*$, the displacement thickness in the shock-fixed coordinate system, is defined by

$$\rho_e(U_o-u_e)\delta_2^* = \int_0^{\infty}\left[\rho(U_o-u)-\rho_e(U_o-u_e)\right]dy,$$

and is a positive quantity.

B. Solution of the Linearized Equations:

The momentum and isentropic equations for the core flow are:

$$\rho_e\left(\frac{\partial u_e}{\partial t} + u_e\frac{\partial u_e}{\partial x}\right) + \frac{\partial p_e}{\partial x} = 0 \tag{6}$$

$$a_e^2 = \left(\frac{\partial p_e}{\partial \rho_e}\right)_s. \tag{7}$$

For small perturbations such that

$$\rho_e = \rho_2 + p;\ u_e = u_2 + u;\ \text{etc.}, \tag{8}$$

there is obtained from equations 3, 4, 5, 6, and 7 (after some re-arrangement)

$$\frac{1}{a_2^2\rho_2 u_2}\left(\frac{\partial p}{\partial t} + u_2\frac{\partial p}{\partial x}\right) + \frac{1}{u_2}\frac{\partial u}{\partial x} = \begin{cases} \frac{2K_1}{d}R_{2d}^{-1/2}\left(\frac{x}{d}\right)^{-1/2} \\ -\frac{2K_2}{d}\left(\frac{U_o - u_2}{u_2}\right)R_{2d}^{-1/2}\left(\frac{U_o t - x}{d}\right)^{-1/2} \end{cases}$$

$$\rho_2\left(\frac{\partial u}{\partial t} + u_2\frac{\partial u}{\partial x}\right) + \frac{\partial p}{\partial x} = 0. \tag{9}$$

Writing the equations in terms of the characteristic variables $\eta = x - (u_2 + a_2)t$ and $\xi = x - (u_2 - a_2)t$ results in:

on $\eta$ = constant:

$$\frac{d}{d\xi}\left[\rho_2 a_2 u + p\right] = \begin{cases} \frac{a_2\rho_2 u_2}{d}K_1 R_{2d}^{-1/2}\left(\frac{x}{d}\right)^{-1/2} \\ -\frac{a_2\rho_2}{d}(U_o - u_2)K_2 R_{2d}^{-1/2}\left(\frac{U_o t - x}{d}\right)^{-1/2} \end{cases} \tag{10}$$

on $\xi$ = constant:

$$\frac{d}{d\eta}\left[\rho_2 a_2 u - p\right] = \begin{cases} \frac{a_2\rho_2 u_2}{d}K_1 R_{2d}^{-1/2}\left(\frac{x}{d}\right)^{-1/2} \\ -\frac{a_2\rho_2}{d}(U_o - u_2)K_2 R_{2d}^{-1/2}\left(\frac{U_o t - x}{d}\right)^{-1/2}. \end{cases}$$

Putting $x$ and $(U_o t - x)$ in terms of $\eta$ and $\xi$, and performing the integration finally yields

$$\rho_2 a_2 (u - u_2) = f\left(\frac{\eta}{m}\right) + g\left(\frac{\xi}{n}\right) - \frac{4\rho_2 a_2^3 u_2}{(u_2^2 - a_2^2)} K_1 R_{2d}^{-1/2} \left(\frac{x}{d}\right)^{1/2}$$

$$p - p_2 = f\left(\frac{\eta}{m}\right) - g\left(\frac{\xi}{n}\right) + \frac{4\rho_2 a_2^2 u_2^2}{(u_2^2 - a_2^2)} K_1 R_{2d}^{-1/2} \left(\frac{x}{d}\right)^{1/2} \qquad (11a)$$

for the set of equations for the stationary-boundary layer, and

$$\rho_2 a_2 (u - u_2) = F\left(\frac{\eta}{m}\right) + G\left(\frac{\xi}{n}\right) - \frac{4\rho_2 a_2^3 (u_o - u_2)}{(u_o - u_2)^2 - a_2^2} K_2 R_{2d}^{-1/2} \left(\frac{U_o t - x}{d}\right)^{1/2}$$

$$p - p_2 = F\left(\frac{\eta}{m}\right) - G\left(\frac{\xi}{n}\right) - \frac{4\rho_2 a_2^2 (u_o - u_2)^2}{(u_o - u_2)^2 - a_2^2} K_2 R_{2d}^{-1/2} \left(\frac{U_o t - x}{d}\right)^{1/2} \qquad (11b)$$

for the shock-boundary layer. Here f, g, F, and G are the arbitrary functions arising from the integration. They are to be determined from the boundary conditions for each set of equations. m and n are constants chosen to simplify the notation in the following section;

$$m = u_o - (u_2 + a_2) \; ; \quad n = u_o - (u_2 - a_2).$$

C. Application of the Boundary Conditions:

The boundary conditions must be applied at the positions in the x-t plane given by the unperturbed flow. Thus, at the shock ($x = U_o t$) the linearized Rankine-Hugoniot relations together with equations 11b yield:

$$(\rho_2 a_2)\frac{2a_1}{\gamma+1}\left(1+\frac{1}{M_o^2}\right)\phi(t) = F(t) + G(t)$$

$$\frac{4\gamma}{\gamma+1}\, p_1 M_o\, \phi(t) = F(t) - G(t), \tag{12a}$$

where

$$\phi(t) = \frac{u_s - u_o}{a_1} = M_s - M_o. \tag{12b}$$

From equations 12a, eliminating G(t)

$$\left[\frac{\rho_2 a_2 a_1}{\gamma+1}\left(1+\frac{1}{M_o^2}\right) + \frac{2\gamma}{\gamma+1} p_1 M_o\right]\phi(t) = F(t). \tag{12c}$$

In a similar fashion, application of the conditions that $u = u_2$ and $p = p_2$ at the entrance of the tube ($x = 0$) results from equations 11a in:

$$F = g = 0. \tag{12d}$$

The connection between the stationary-boundary-layer region and the shock-boundary-layer region may be assumed to be some line $x = \alpha U_o t$ in the $x$- t plane. On this line perturbed velocities and pressures must match. Thus equations 11a and 11b, together with 12d yield

$$-\frac{4\rho_2 a_2^3 u_2}{u_2^2 - a_2^2} K_1 R_{2d}^{-1/2}\left(\frac{\alpha u_o t}{d}\right)^{1/2} = F\left[\left(\frac{\alpha u_o - (u_2+a_2)}{u_o - (u_2+a_2)}\right)t\right] +$$

$$+ G\left[\left(\frac{\alpha U_0 - (u_2 - a_2)}{U_0 - (u_2 - a_2)}\right)t\right] - 4\frac{\rho_2 a_2^3 (U_0 - u_2)}{(U_0 - u_2)^2 - a_2^2} K_2 R_{2d}^{-1/2} \left(\frac{(1-\alpha) U_0 t}{d}\right)^{1/2},$$

and (12e)

$$\frac{4\rho_2 a_2^2 u_2^2}{u_2^2 - a_2^2} K_1 R_{2d}^{-1/2} \left(\frac{\alpha U_0 t}{d}\right)^{1/2} = F\left[\left(\frac{\alpha U_0 - (u_2 + a_2)}{U_0 - (u_2 + a_2)}\right)t\right] -$$

$$- G\left[\left(\frac{\alpha U_0 - (u_2 - a_2)}{U_0 - (u_2 - a_2)}\right)t\right] - \frac{4\rho_2 a_2^2 (U_0 - u_2)^2}{(U_0 - u_2)^2 - a_2^2} K_2 R_{2d}^{-1/2} \left(\frac{(1-\alpha) U_0 t}{d}\right)^{1/2}.$$

Adding the above two equations eliminates the function G and gives an expression for $F\left[\left(\frac{\alpha U_0 - (u_2 + a_2)}{U_0 - (u_2 + a_2)}\right)t\right]$. Changing time scales, this value may be inserted into equation 12c to obtain the solution for $\phi$ (t). After some re-arranging there is obtained

$$R_{2d}^{1/2} \left(\frac{x}{d}\right)^{-1/2} \left(\frac{M_s}{M_0} - 1\right) = J(M_0) \left[\frac{u_2}{u_2 + a_2} K_1 - \left(\frac{U_0 - u_2}{u_2 + a_2 - U_0}\sqrt{\frac{1-\alpha}{\alpha}}\right) K_2^{1/2}\right] \left[\alpha\left(\frac{(u_2 + a_2) - U_0}{(u_2 + a_2) - \alpha U_0}\right)\right]^{-1/2} \quad (13)$$

where $J(M_0) = \frac{\gamma + 1}{M_0} \left[\frac{a_1}{a_2}\left(\frac{M_0^2 + 1}{2 M_0^2}\right) + \frac{p_1}{p_2} M_0\right]^{-1}$,

and the $K_1$ and $K_2$ are the boundary-layer constants defined by equations 4 and 5 respectively. In the next section both these values and the value of $\alpha$ will be derived for certain simple assumptions.

D. Evaluation of Boundary Layer Constants:

Simplifying assumptions are made in the following calculations. For most practical cases, these assumptions will introduce little error in the attenuation analysis; however, they can be relaxed if the appropriate boundary-layer solution is available.

For the steady compressible-boundary layer, assuming $Pr = 1$, $T_w = T_1$, and $\frac{d^2T}{du^2} = -\mu/k$ there is obtained (ref. 26)

$$\frac{T-T_2}{T_1} = \left(1 - \frac{T_2}{T_1}\right)\frac{u}{u_2} + \frac{\gamma-1}{2} M_2^2 \frac{u}{u_2}\left(1 - \frac{u}{u_2}\right). \tag{14a}$$

Transforming the definition for the displacement thickness by the use of the Howarth-Dorodnitzyn variable, and utilizing the fact that $\rho T = \text{const.}$ in the boundary layer, results in

$$\delta_1^* \sqrt{\frac{u_2}{\nu_2 x}} = \frac{T_1}{T_2}\int_0^\infty F(\eta)\,d\eta + \frac{\gamma-1}{2} M_2^2 \int_0^\infty \frac{df(\eta)}{d\eta}\left(1 - \frac{df(\eta)}{d\eta}\right)d\eta, \tag{14b}$$

where the $f(\eta)$ are the Blasius functions, and the numerical values of the integrals are given in reference 26. Finally, from the definition of $K_1$ (see equation 4)

$$K_1 \equiv \delta_1^* \sqrt{\frac{u_2}{\nu_2 x}} = 1.73\frac{T_1}{T_2} + 0.664\left(\frac{\gamma-1}{2}\right)M_2^2. \tag{14c}$$

With the assumption that $\rho\mu$ = constant, the shock-boundary layer displacement-thickness in the shock-fixed coordinates is given in convenient form by Rott and Hartunian (ref. 27). Transforming to the notation of the present report, (and assuming Pr = 1, $T_w = T_1$),

$$\frac{\delta_2^*}{\Delta} = \frac{u_2}{u_0 - u_2}\left[1 + \frac{2u_0 - \sqrt{2}\,u_2}{\left(\frac{2}{\gamma+1}\right)u_0 + u_2}\right]$$

$$\Delta = \sqrt{\frac{\nu_2 s}{u_2}}\sqrt{\frac{4}{\pi}\frac{u_2}{\left[u_0 - u_2(\sqrt{2}-1)\right]}}. \qquad (15a)$$

Thus

$$K_2 \equiv \delta_2^*\sqrt{\frac{u_2}{\nu_2 s}} = \frac{u_2}{u_0 - u_2}\left[1 + \frac{2u_0 - \sqrt{2}\,u_2}{\frac{2}{\gamma+1}u_0 - u_2}\right]\sqrt{\frac{4}{\pi}\frac{u_2}{\left[u_0 - u_2(\sqrt{2}-1)\right]}}. \qquad (15b)$$

The value of $\alpha$ (that is, the location in the x-t plane of the matching line for the cross over from the stationary-boundary layer to the shock-boundary layer) will be determined by equating the laboratory-reference-frame displacement thicknesses on the line $x = \alpha U_o t$. This would seem to be the most reasonable physical criterion for the boundary-layer matching; however, since the boundary layer enters the attenuation calculation through the vertical velocity at its edge*, an argument can be presented for matching this velocity. It is found that this latter type of matching results in a lower value of $\alpha$ and hence slightly more attenuation than the $\delta^*$ matching.

*The terms involving the slope of the boundary-layer thickness in equations 4 and 5 may be rewritten as functions of the actual vertical velocity at the boundary-layer edge.

Since it will be shown that this will provide poorer agreement with the experimental measurements, vertical-velocity matching will not be considered further.

To match the displacement thicknesses, the displacement thickness of the shock-boundary layer in the laboratory-coordinate system is needed. This was found by writing the definition for the displacement thickness in the laboratory system, and then transforming to the shock-fixed system in order to evaluate the integrals. Again using the work of Rott and Hartunian (ref. 27) and the assumptions used above in determining $\delta_2^*$, there is obtained

$$\frac{\delta_3^*}{\Delta} = 1 - \frac{u_2}{u_0 - u_2}\left[\frac{2u_0 - \sqrt{2}\,u_2}{\left(\frac{2}{\gamma-1}\right)u_0 + u_2}\right] = \frac{u_0}{u_0 - u_2} - \frac{\delta_2^*}{\Delta} \tag{16a}$$

$$\Delta = \sqrt{\frac{\nu_2 s}{u_2}}\sqrt{\frac{4}{\pi}\frac{u_2}{\left[u_0 - u_2(\sqrt{2}-1)\right]}}$$

Thus

$$K_3 \equiv \delta_3^*\sqrt{\frac{u_2}{\nu_2 s}} = \frac{u_0}{u_0 - u_2}\sqrt{\frac{4}{\pi}\frac{u_2}{\left[u_0 - u_2(\sqrt{2}-1)\right]}} - K_2 \tag{16b}$$

Now the line where the displacement thicknesses are equal may be found by putting

$$K_3\sqrt{\frac{\nu_2 s}{u_2}} = K_3\sqrt{\frac{\nu_2(u_0 t - x)}{u_2}} = K_1\sqrt{\frac{\nu_2 x}{u_2}}.$$

Solving for x:

$$x = \frac{K_3^2}{K_1^2 + K_3^2}u_0 t, \quad \text{thus } \alpha = \frac{K_3^2}{K_1^2 + K_3^2}. \tag{16c}$$

The boundary-layer constants $\alpha$, $K_1$, $K_2$, and $K_3$ are shown plotted against $M_o$ in figure 14. It is interesting to note that $\alpha$ is always less than 0.5, that is, the matching point always occurs nearer to the leading edge of the tube than to the shock itself. The attenuation parameter defined by equation 13 is presented in figure 15 for the constants of figure 14. Also shown is the value of this parameter obtained by putting $K_1 = \alpha = 0$, that is with the shock-boundary layer extending all the way from the shock to the leading edge of the tube. It is seen that the leading edge-boundary layer accounts for more than a 15 per cent correction, and that this correction takes the form of a reduction in the amount of attenuation predicted.

## II - 3. EXPERIMENTAL RESULTS

An experimental study of attenuation in open-ended tubes was undertaken in order to check the validity of the theory. The pertinent factors that must be considered in the design of this type of attenuation experiment are the length of shock-tube test gas available, the length of the laminar boundary layer behind the shock wave, and the ratio $\delta^*/d$. These parameters are illustrated in figure 16. A discussion of figure 16, as well as a brief description of the models and instrumentation used, may be found in Appendix II C. It is noted here that the tubes used were approximately 2 feet long, and had inside diameters of 1", 5/8", or 3/8". An initial pressure of 5 mm. was ordinarily used, although some runs were made at 50 mm.

Figure 17 presents the collected experimental results, and it is seen that attenuations varying from 1 to 6 per cent per foot were recorded. The shock-tube attenuation per foot at the model location, calculated by the theory of Mirels (ref. 7) for the case of laminar boundary layers, was always less than 10 per cent of the above attenuation. It was therefore assumed that the basic shock-tube attenuation would have little effect on the present measurements, *except for the 50 mm. points where a relatively larger amount of basic attenuation would be expected due to the increased importance of turbulence in the shock-tube boundary layer.

The accuracy of the experimental points was essentially dependent on counter error and gauge response. The latter error was due to the

---

*For a detailed study of this effect, the pressure and velocity perturbations at the tube entrance could be obtained from Mirels' theory and applied as a boundary condition on the present problem (i.e., modifying equation 12d).

finite axial width of the upstream wall gauge compared to the infinitesimal width of the gauge on the face of the movable plug (see fig. 13). The plug gauge had essentially instantaneous response, while the side wall gauge was observed to have a rise time of as long as 1 $\mu$ sec. This error, combined with the fact that 1 $\mu$ sec. counters were used, resulted in an overall accuracy of $\pm$ 2 $\mu$ sec. on each counter reading. Since the attenuation depends on the ratio of the two counter readings (corrected for any length discrepancy), the maximum error thus roughly corresponded to the case where one count was 2 $\mu$ sec. high and the other 2 $\mu$ sec. low. Referring to figure 17, this error amounted to approximately $\pm$ 5 per cent uncertainty in the value of $\overline{(M_s/M_o)}$. It is felt that this effect, in combination with the basic shock tube attenuation scatter, could account for the scatter observed for the individual set of points.

The measurements give the average value of $M_s$ over a distance x. In order to compare this with the theory, it is necessary to integrate the local theoretical value of $M_s$ over the same distance. For laminar boundary layers, $\overline{(M_s/M_o - 1)}$ over a distance x is found to be equal to two thirds of the local value of $(M_s/M_o - 1)$ at x. Using this fact, the theoretical curves in figures 17 and 18 were readily obtained from figure 15.

The experimental data are presented in concise form in figure 18. Here it is seen that the agreement between theory and experiment is generally to within 10 per cent. Since individual points have been plotted and not the averages of sets of points, this agreement is <u>at least</u> as good as that which has been reported for shock-tube attenuation studies (ref. 22). On figure 18, the accuracy of the 3/8"

tube points is again ± 5 per cent. For the other points the actual measured value of $\overline{(M_s/M_o - 1)}$ was much smaller, and hence the previously mentioned ± 5 per cent error in $\overline{(M_s/M_o)}$ becomes much more significant. Indeed, the error for the 50 mm. points would be almost ± 100 per cent when plotted on figure 18. As mentioned above, these 50 mm. points were expected to involve turbulent boundary layers and therefore more attenuation. This trend is observed in figure 17, where the 50 mm. points all fall lower with respect to the theory than do the 5 mm. points. For these reasons the 50 mm. points were not carried over to figure 18.

Also shown in figure 18 is the theory with the matching point fixed half way between the shock and the leading edge. This seems to exhibit better agreement with the experimental results and raises questions about the validity of the assumptions used in the original theory. The possibility of using matching conditions other than continuity of displacement thickness has been briefly discussed (see section 2-D), and until the complete boundary-layer solution is available, there appears to be little justification for any other matching scheme. However, the assumptions used for the evaluation of the boundary-layer thicknesses themselves may warrant further consideration. Lowering the Prandtl number to 0.72 will affect $\delta^*$, as does increasing the wall temperature above $T_1$. These effects are small, but if they affect one boundary layer more than the other they will change the position of the matching point. In spite of these possibilities, it is felt that more accurate measurements are needed before the theory is further refined.

These measurements might be accomplished with faster counters and matched gauges in a larger shock tube where less inherent attenuation is present.

## II - 4. CONCLUSIONS

The study of the motion of a shock wave on entering an open-ended tube offers possibilities for obtaining more insight into the problem of shock-wave attenuation. A simple theory has been developed for this configuration and experimental agreement to within 10 per cent has been observed.

It would be of considerable interest to carry out more precise measurements for this configuration, and also to investigate the effects of larger ratios of boundary-layer thickness to tube diameter on the agreement with the linearized theory. Once this is done, further refinement of the theory would be justified; including extension to more complicated situations involving turbulence in the boundary layers.

# III. AN EXPERIMENTAL STUDY OF THE INTERACTION OF A SHOCK WAVE WITH AN AREA CHANGE OF FINITE LENGTH

## 1. INTRODUCTION AND REVIEW OF THE LITERATURE

The passage of a shock wave through a converging or diverging tube offers possibilities of very great shock-speed modification. Many authors (ref. 30-35) have studied this problem analytically by assuming one-dimensionality of the flow. In each case, however, the complexity of the motion has necessitated linearizing assumptions in order to obtain a useful result.

An interesting example is the work of Chisnell (ref. 30), in which it is assumed that the desired relationship for an arbitrary area change may be obtained by a simple summation of the incremental effects of a shock wave passing through a series of infinitesimal area changes. Each infinitesimal area change is assumed to produce a slightly modified transmitted-shock wave, a reflected sound wave, and a weak contact surface (see fig. 19). For strong shocks, Chisnell's integrated result is essentially the same as the strong-shock similarity solution of Guderley (ref. 31), while for weak shocks Rayleigh's sonic-wave solution is obtained.

Chisnell's theory indicates that the shock strength is a function only of the local duct area at the shock location, and not of the flow behind it. This is because the second-order effects of re-reflected disturbances are neglected, since there is no mechanism supplied for the interaction of the elemental reflected-sound waves and contact surfaces with the changing area and with each other. Chisnell estimates

the effects of these second-order disturbances and shows them to be small for a continuously slowly-varying area change. This conclusion is further documented by the fact that Payne (ref. 36) has numerically solved the equations of motion for a converging cylindrical shock and finds good agreement with Chisnell's linearized theory.

Different approaches to the study of the motion of a shock wave through a continuously-varying area change are provided by Chester (ref. 32) and Whitham (ref. 33). Chester's approach is based on a linearized study of the diffraction pattern behind the shock, while Whitham linearizes the one-dimensional equations of motion and follows a characteristic integration procedure similar to that used in part II of this report. (For convenience, and because of the similarity to part II, Whitham's approach is reviewed in Appendix IV.) Both of these studies result in the same final expression for the relation between area change and shock strength. This expression is also identical to that obtained by Chisnell, since re-reflections are neglected in all three analyses.

The linear solution of Chisnell, Chester, and Whitham is shown in figure 20 for overall area ratios of 10 and 4*. Also shown on this figure is the steady-state solution for an instantaneous area change. This solution was obtained by assuming a wave pattern as shown in figure 19. For sonic flow at the exit of the area change, the reflected shock is readily calculated from the Rankine-Hugoniot relations. With this information the transmitted shock speed may be found by an iterative

*It is useful to note that a specific area-ratio curve can be used repeatedly to find the transmitted shock speed for a larger area ratio which is equal to a simple power of the first area ratio. I.e., for $M_o = 2$ into an area ratio of 100, the transmitted shock speed for an area ratio 10 is first found, and then used as the input into another area ratio 10. This provides the final transmitted shock speed for an area ratio of 100.

procedure based on assuming different pressure ratios across the expansion wave. The choice of the correct wave pattern and the calculating procedure itself have been dealt with before (i.e., ref. 34, 37, and 38), and will not be further discussed.* The main interest here is in the fact that for a given area change and initial shock Mach number, two solutions for the transmitted shock Mach number are available -- that provided by the steady-state solution for an instantaneous area change, and the higher (see fig. 20) value given by the linear theory for a continuously varying area change. The difference between these two solutions can become very large, since, when the overall area-ratio approaches infinity, the linear theory value for the transmitted shock Mach number goes to infinity while the steady-state value remains finite (and not much greater than that predicted for an area ratio of 10).

The shock speed history through and downstream of a finite-length area change must involve elements of both of the above limiting solutions. While the shock wave is in the region of gradually changing area its behavior is expected to follow the prediction of the linear theory. On the other hand, when the shock wave has progressed far downstream of the convergent section its motion must be given by the steady-state calculation, since the region of gradually changing area will now appear as an instantaneous area change. As the transmitted shock speed given by the linear theory is much higher than that of the steady-state-calculation, the shock wave must actually decelerate from the end of the convergence

*It should be mentioned that the area ratios used for this study are large enough so that no ambiguity exists in the assumed wave pattern (see ref. 37).

until it finally reaches the steady-state velocity at some point downstream.*

The linear theory relates the shock Mach number directly to the local cross-sectional area at the shock location, and hence cannot predict the deceleration in the constant-area duct downstream of the convergence. The deceleration stems from the higher-order terms neglected in the linearized theory, these terms representing the complex wave interactions taking place in the flow behind the shock wave and their ultimate effect on the shock itself. For a continuous monotonic area convergence these re-reflected disturbances fortuitously have little effect on the shock wave motion (ref. 30). For a finite-length area convergence however, the upstream moving disturbances will usually re-enforce each other to form a reflected shock wave, and the downstream moving disturbances will modify the transmitted shock wave as discussed above.

The motion of a shock wave downstream of a finite-length area convergence is studied in this report. The above arguments show that the solution to the problem will be time dependent, and any analytical approach must consider the second-order effects neglected in the linear theory. The author's attempts to modify the boundary conditions applied to the linearized equations, or to use simple integral approaches based on the linear solutions, have been unsuccessful. It appears that a useful solution is dependent on the inclusion of higher-order terms in

---

*The argument that the shock speed varies downstream of the nozzle may be illustrated by sketching an x-t diagram of one instantaneous area change followed by another. It is immediately seen that the secondary waves will interact with the various area changes and with each other, and that some disturbances must eventually catch up with the transmitted shock wave.

the one-dimensional flow equations.

Friedman (ref. 39) has made a study in which some of the higher-order terms have been included, and has found that the extra terms result in the negative characteristics joining together to form a reflected shock for cases where a reflected shock is expected from the steady-state model. This reflected shock formation (non-existent in the linear theory) is closely coupled with the transmitted shock speed reduction; however, it appears to be impossible to obtain a useful closed-form solution for the present problem from the improved equations of motion used by Friedman. Indeed, Friedman himself was not able to find a convenient general expression for the motion of the negative characteristics, finding it necessary to make further assumptions in order to exhibit this motion.

The remaining possibilities for a solution to the problem of shock wave motion through a finite-length area change are the tedious numerical characteristics calculation procedure, and possibly a more physical approach of the type used by Chisnell to estimate the effect of the second-order disturbances (see above). The first step in the latter approach might logically be to obtain careful experimental information, and attempt to get some ideas about the parametric dependencies. Both this and the characteristics calculation procedure are used in this paper.

Little experimental information is available for the motion of a shock wave through an area change, and what little evidence is available is concerned primarily with the flow behind the shock wave (ref. 40, 41). An exception is the work of Hertzberg and Kantrowitz (ref. 42) which illustrates the validity of the one-dimensional x-t characteristics calculations for the shock-wave motion. Of specific interest is the

more recent study of Bird (ref. 43) which provides some insight into the relationship between the linear and steady-state theories. Bird reasoned that the transmitted shock strength should vary from the steady-state value for a $90^{\circ}$ nozzle to the linear theory value for a $0^{\circ}$ nozzle, and he was qualitatively able to show this.

In the following work the effect of nozzle angle on transmitted shock motion is investigated more fully. Measurements are made at different distances downstream of the nozzles in order to study the approach of the shock speed to the steady-state value. In any practical application of a finite-length area change (as for example shock strength augmentation in a large shock tube), boundary-layer effects must be considered, and use of the theory of part II is made here in order to develop a scheme for estimating these effects. Section 2 presents the experimental data and the application of the viscous corrections. This is followed by a discussion of the experimental results and some interesting conclusions concerning the shock-speed parametric dependencies.

## III - 2. EXPERIMENTAL RESULTS

### A. Basic Measurements:

An area-change model, typical of those studied in this report, is illustrated in figure 21. Conical nozzles of 5, 10, and 30° angle were used with downstream tubes of 1" and 5/8" inside diameter, providing overall area ratios of 4 and 10.24. (A description of the models and instrumentation, as well as the choice of operating conditions, is presented in Appendix IID.) As shown in the figure the average downstream shock speed, $\overline{M}_s$, was measured by two thin-film gauges, one fixed near the nozzle exit and the other on the movable end-wall plug. x, the distance between these gauges, was fixed at either 6", 12", 18", or 24". The initial pressure was set at 50 mm. for most of the measurements, although some runs were made at 5 mm.

The raw data thus obtained are presented in figure 22, where $M_o$ refers to the shock Mach number measured just upstream of the convergent section. It is immediately seen that all of the data fall below the linear theory and that there is a strong dependency on nozzle angle and x. It is also noted that these effects are reduced for the smaller area ratio, and that there is more scatter in the points for this case than for the area ratio 10 (see fig. 22c). This trend is to be expected since the shock-speed modification is weakest for the smaller area ratio.

The main source of inaccuracy in the measurements comes from the finite width of the gauge at the nozzle exit,* and the possible counter

*The gauge used had a rise time in the neighborhood of 1 $\mu$ sec. Before constructing narrower gauges, the effects of possible shock-wave curvature and tilt should be considered.

error of 1 $\mu$ sec. Considering these effects, the inaccuracy in the data corresponds roughly to the scatter observed. It is further noted that whereas the 6" points would be expected to show the most scatter from these effects, the 24" points will involve some turbulence in the boundary layer behind the shock wave, and this may provide an additional source of scatter for the longer lengths (see fig. 16).

Figure 23 shows a typical cross-plot of the raw data, in this case for an area ratio of 10 and $M_o = 3$. In the absence of two-dimensional and viscous effects, the significant non-dimensional length for this study must be the distance downstream divided by the nozzle length. This fact emerges quite naturally in the one-dimensional characteristics calculation (Appendix V), and it is used in this figure where the number of nozzle lengths refers to the non-dimensional distance measured downstream of the nozzle exit. In plotting the points, it was assumed that the measured value of $\overline{(M_s/M_o)}$ over a fixed x was equivalent to the actual value at x/2. The justification for this is provided by the fact that each set of points in figure 23 very closely approximates a straight line.

It is observed in figure 23 that the uncorrected data-points approach the linear-theory value at the zero nozzle length position, and fall off towards the steady-state value downstream. It would be of interest to obtain points nearer to the nozzle exit; however, it was impractical to construct nozzles of angle smaller than $5^o$, and measurement inaccuracies would make the use of shorter gauge spacing questionable.

B. Viscous Corrections:

Because of the model size and the operating conditions used, some viscous effects were expected. It was originally planned to keep these effects small, and to correct for them by making identical measurements at various initial pressures and extrapolating to the point where the effects were negligible. This turned out to be difficult to do, principally because of the changing laminar-turbulent nature of the boundary layer as the initial pressure was varied. It was therefore decided to keep the pressure low enough to avoid transition, and to make a theoretical correction based on the results of part II of this report.

The primary assumption necessary in developing the theoretical correction procedure was that the viscous effects on the downstream measurements may be considered to result solely from a non-steady laminar-boundary layer extending from the shock wave to the nozzle exit. On the basis of this assumption, the attenuation parameter for the viscous effects may be found from the upper curve of figure 15. For a specific configuration and distance x, the average value of the shock Mach number downstream of the nozzle was estimated from the measurements of figure 22 and used to provide the input value of $M_o$ on figure 15. The actual viscous attenuation at a distance x, $M_s/M_o - 1$, was then obtained. However, since the measurements to be corrected actually represented the average value of the shock Mach number over a distance x, it is the average viscous attenuation over a distance x that is needed, and this is found by taking 2/3 of the actual attenuation at x (see part II-3). The viscous $\overline{(M_s/M_o)}$ thus obtained was divided into the measured transmitted shock Mach number to obtain the corrected value.

The results of the application of this correction are illustrated

in figure 23, where it is seen that the 5 mm. corrected points fall very nearly onto the 50 mm. corrected points. There is some slight discrepancy; however, it shows no systematic trend and is well within the accuracy of the individual points. Excellent agreement was also observed with the $M_o = 2$ cross-plot, and it is concluded that the attenuation correction accurately eliminates the viscous effects occurring downstream of the nozzle.

No correction was made for the effect of the boundary layer within the nozzle itself, however it should be noted that the nozzle boundary layer would be expected to reduce the transmitted shock strength. This effect could, in principle, be estimated by including a boundary-layer term in Whitham's analysis (see Appendix IV).

## III - 3. DISCUSSION

The corrected experimental points are shown plotted in figure 24 for incoming shock Mach numbers of 2 and 3 and area ratios of 10 and 4. Here the ordinate is the difference between the actual transmitted shock speed and the calculated steady-state value, divided by the difference between the linear and steady-state values. The experimental points would thus be expected to approach the value of one at zero nozzle lengths, and to taper off to zero at some position downstream. It is seen from the figure that this behavior is observed, the collected points falling off to zero at 14 to 17 nozzle lengths downstream.*

A careful study of figure 24 will reveal that the observed scatter in the experimental points roughly corresponds to the magnitude of the discrepancies between different nozzle angles. These discrepancies are clearly illustrated in figure 23. From figure 24 it may be seen that the discrepancies show the same trend for all the configurations studied; for a specified value of $M_o$ and area ratio, the last point for a specific nozzle invariably falls on a line which is lower than the first point of the next larger angle nozzle. This effect is not completely understood. It may be due to two dimensionality, to the fact that the boundary layer in the nozzle has not been accounted for, or to the fact that for the longer distances between gauges, a portion of the boundary layer is probably turbulent (see fig. 16). The latter two mechanisms would result in an additional small decrease in $M_s$,

*The fact that the larger area ratio was actually 10.24 instead of 10.00 was taken into account in the calculation of the theoretical quantities that appear in the ordinate.

and this would essentially be a function of position downstream. It is felt, however, that more experimental work is necessary in order to justify making any further corrections to the data. In particular, it would be of interest to investigate and isolate the effects of two-dimensionality.

The main purpose of the normalized method of presenting the data was to allow direct comparison of the measurements from different configurations. From figure 24 it can be seen that, neglecting the discrepancies mentioned above, the collected experimental points plot out as a single curve for all of the configurations tested. This single curve is estimated by the best-fit curve shown on figure 24. Since the actual attenuation of the shock wave downstream of the area change is due to weak disturbances catching up with it from behind, and these disturbances must travel with speed u + a, a measure of the scale of this effect may be assumed to be provided by the parameter

$$\frac{(u+a) - u_s}{u_s}.$$

Here the numerator represents the closing speed of the disturbance on the shock wave. For values of $M_s$ above 2, this parameter is an extremely weak function of $M_s$. This may explain why there is little dependence on $M_o$, and suggests that the normalized curve of figure 24 can be extended to arbitrarily large values of $M_o$ and overall area ratio!

The success of the above simple argument immediately raises the possibility of applying simple approaches to a determination of the number of nozzle lengths necessary for the transmitted shock Mach number to fall off to the steady-state value. Unfortunately, this length is dependent upon complicated re-reflection processes, and approximate

schemes for calculating it will be found to be too simple to involve the correct physics or too complicated to justify the use of simple assumptions. On the question of this decay length, it should be mentioned that it would be of some interest to make measurements at nozzle lengths greater than 16 in order to make sure that the corrected value of the transmitted shock speed ceases to fall off.*

Also shown on figure 24 is the characteristics calculation for an area ratio 10 conical nozzle with $M_o = 2$. The only assumption made for this calculation was flow one-dimensionality, and consequently, because of the tediousness of the calculation (see Appendix V), it was only carried to 4 nozzle lengths downstream. The x-t plot of the calculation is presented to a 1/5 scale in figure 25, while the calculation procedure itself is discussed in Appendix V. Of interest here is the fact that the experimental data fall below the characteristics solution, even though the slope of the points roughly corresponds to the calculated value. This effect could be attributed to two-dimensionality, but if this were the case more difference might be expected between the 30 and $5^{o}$ nozzles. Another possible cause of this effect might be the boundary layer within the nozzle (see section II-B). It should be mentioned, however, that the extrapolated value of $\frac{M_s - M_{ss}}{M_L - M_{ss}} = 0.85$ at zero nozzle lengths corresponds to an actual value of $M_s$ that is only 3-4 per cent below the linear-theory value. Thus, if the results were plotted in terms of $M_s$ versus nozzle lengths, the per cent agreement would be considerably better.

From the above discussions it is concluded that the normalized curve of figure 24 exhibits the expected transition from the linear to the

---

*The downstream tubes used in the experiments were not long enough to provide nozzle lengths $> 16$ with the existing nozzles. Larger angle nozzles were not used because of expected two-dimensional effects.

steady-state theoretical value for the transmitted shock speed. Furthermore this curve, together with the procedure developed for estimating viscous effects (section III-2B), may be used to predict the shock wave history downstream of any small-angle conical nozzle for any value of the overall area ratio and any value of $M_o$ above 2. Since the deceleration history has been shown to depend on nozzle length, a nozzle can thus be chosen so as to combine the large increase in shock strength predicted by the linear theory with a specified allowable shock-wave deceleration rate downstream.

## III - 4. CONCLUSIONS

A normalized curve of the shock-wave history downstream of finite-length converging area ratios has been experimentally obtained. When shock-speed measurements are plotted in this form, they are shown to be insensitive to both the value of the incident shock Mach number and the overall area ratio. It has also been shown that the shock Mach number at the exit of the area change agrees reasonably well with the prediction of the linearized theory, and that the second-order re-reflections neglected in that theory eventually attenuate the shock wave to the steady-state value.

The effect of viscosity on the shock-wave history downstream of an area change has been studied, and a method for estimating this effect has been developed from the theory of part II. When the measurements are corrected for these viscous effects, they exhibit reasonable agreement with the shock history calculated by the full one-dimensional characteristics method. It would be of interest to investigate this agreement more closely by studying the viscous and two-dimensional effects associated with more abrupt area convergences.

# APPENDIX I

## IDEAL THEORY CALCULATION PROCEDURES

It may readily be shown from one-dimensional shock theory that

$$P_a/P_b = 1 + \left(2\gamma/(\gamma+1)\right)\left(M_b^2 - 1\right); \tag{1}$$

transforming velocity so as to apply to a shock tube results in

$$P_2/P_1 = 1 + \left(2\gamma_1/(\gamma_1+1)\right)\left(M_s^2 - 1\right). \tag{2}$$

A similar procedure results in

$$u_2/a_1 = \left(2/(\gamma_1+1)\right)\left(M_s - \frac{1}{M_s}\right). \tag{3}$$

Hence,

$$u_2/a_1 = \left(\frac{P_2}{P_1} - 1\right)\left[\gamma_1\,\frac{(\gamma_1+1)}{2}\left(\frac{P_2}{P_1} - 1\right) + \gamma_1^2\right]^{-\frac{1}{2}}. \tag{4}$$

The Riemann invariant applied across a non-steady isentropic wave results in:

$$P_a/P_b = \left[\rho_a/\rho_b\right]^{\gamma} = \left[a_a/a_b\right]^{\frac{2\gamma}{\gamma-1}} = \left[\frac{1 + \frac{\gamma-1}{2} M_b}{1 + \frac{\gamma-1}{2} M_a}\right]^{\frac{2\gamma}{\gamma-1}}, \tag{5}$$

while the energy relation applied across a steady isentropic process results in

$$P_a/P_b = \left[\rho_a/\rho_b\right]^{\gamma} = \left[a_a/a_b\right]^{\frac{2\gamma}{\gamma-1}} = \left[\frac{1 + \frac{\gamma-1}{2} M_b^2}{1 + \frac{\gamma-1}{2} M_a^2}\right]^{\frac{\gamma}{\gamma-1}}. \qquad (6)$$

In the following analyses, extensive use is made of the tables for the parametric relationships across a stationary normal shock wave, and tables for steady isentropic flow with area change (ref. 16 and 17). The calculations are arranged so that only these tables and curves of equation 4 need be obtained in order to calculate the complete performance of a given shock tube. In the following calculations, perfect gases have been assumed throughout.

A. Expansion-Wave Configuration (fig. 1a)

Referring to figure 1a, the overall pressure ratio may be written as

$$P_4/P_1 = \left(P_4/P_4'\right)\left(P_4'/P_3'\right)\left(P_3'/P_3\right)\left(P_3/P_2\right)\left(P_2/P_1\right). \tag{7}$$

Applying equation 5 across the non-steady expansion waves (regions 4-4' and 3'-3), equation 6 through the supersonic nozzle (4'-3'), and applying the pressure boundary condition, $P_3 = P_2$, yields:

$$P_4/P_1 = \left[1 + \frac{\gamma_4-1}{2} M_4'\right]^{\frac{2\gamma_4}{\gamma_4-1}} \left[\frac{1 + \frac{\gamma_4-1}{2} M_3'^2}{1 + \frac{\gamma_4-1}{2} M_4'^2}\right]^{\frac{\gamma_4}{\gamma_4-1}} \times \left[\frac{1 + \frac{\gamma_4-1}{2} M_3}{1 + \frac{\gamma_4-1}{2} M_3'}\right]^{\frac{2\gamma_4}{\gamma_4-1}} P_2/P_1 . \tag{8}$$

Now, extending the results of reference 3, define an "amplification factor"

$$g = \left[\frac{1 + \frac{\gamma_4-1}{2} M_4'^2}{1 + \frac{\gamma_4-1}{2} M_3'^2}\right]^{\frac{\gamma_4}{\gamma_4-1}} \left[\frac{1 + \frac{\gamma_4-1}{2} M_3'}{1 + \frac{\gamma_4-1}{2} M_4'}\right]^{\frac{2\gamma_4}{\gamma_4-1}}. \tag{9}$$

g is a constant, depending only on the driver gas and the parameters $A_4/A_1$ and $A^*/A_1$. It may readily be determined with the use of tables (ref. 16 and 17). Curves of g for all values of the area parameters are shown in figure 5a for a Helium-Air shock tube. Since $A_4/A_1$ cannot be less than $A^*/A_1$ by definition, the line where these ratios are

equal forms the left-hand boundary and each curve for a given value of $A_4/A_1$ must terminate on this boundary. Previous work (ref. 3 and 4) has been concerned only with the case where $A^*/A_1 = 1$; inclusion of the effect of $A^*/A_1$ results in a complete surface as shown.

Equations 8 and 9 result in

$$P_4/P_1 = \frac{1}{g\left(\frac{A_4}{A_1}, \frac{A^*}{A_1}, \gamma_4\right)}\left[1 + \frac{\gamma_4 - 1}{2} M_3\right]^{\frac{2\gamma_4}{\gamma_4 - 1}} P_2/P_1. \qquad (10)$$

The velocity boundary condition, $u_2 = u_3$, enters through $M_3$:

$$M_3 = (u_3/a_3) = (u_2/a_3) = (u_2/a_1)(a_1/a_4)(a_4/a_4')(a_4'/a_3')(a_3'/a_3). \qquad (11)$$

Using equations 5, 6, and 9,

$$M_3 = (u_2/a_1)(a_1/a_4)\, g^{\frac{\gamma_4 - 1}{2\gamma_4}}\left[1 + \frac{\gamma_4 - 1}{2} M_3\right]. \qquad (12)$$

Solving equation 12 for $M_3$, and inserting into equation 10 there is obtained

$$P_4/P_1 = 1/g\,(P_2/P_1)\left[1 - \frac{\gamma_4 - 1}{2}(u_2/a_1)\left((a_1/a_4)\, g^{-\frac{(\gamma_4 - 1)}{2\gamma_4}}\right)\right]^{-\frac{2\gamma_4}{\gamma_4 - 1}}. \qquad (13)$$

Thus, assuming a given $M_s$, one may calculate $u_2/a_1$ and $P_2/P_1$ from relations 2 and 3. Knowing g, $P_4/P_1$ may be calculated, and in a similar manner any of the flow parameters arrived at.

Reference should be made to the well-known connection between the above theory and that of a standard shock tube. The standard shock

tube equation may be obtained by putting g = 1 in equation 13

$$P_4/P_1 = P_2/P_1\left[1 - \frac{\gamma_4 - 1}{2}(u_2/a_1)(a_1/a_4)\right]^{\frac{-2\gamma_4}{\gamma_4 - 1}} \tag{14}$$

Comparing equations 13 and 14, it is seen that the area-ratio tube produces the same shock speed for a given $P_4/P_1$ as a standard tube with the following modifications:

$$(a_1/a_4)_{\text{standard}} = g^{-(\gamma_4 - 1)/(2\gamma_4)} (a_1/a_4)_{\text{area ratio}} \tag{15}$$

$$(P_4/P_1)_{\text{standard}} = g\,(P_4/P_1)_{\text{area ratio}} .$$

B. Normal Shock-Wave Configuration (Fig. 1b)

Starting as in the previous case, applying the pressure boundary condition and relations 5, 6, and 9, the overall pressure ratio becomes

$$P_4/P_1 = \left(P_{3'}/P_3\right)\left(P_2/P_1\right)\frac{\left[1+\frac{\gamma_4-1}{2}M_{3'}\right]^{\frac{2\gamma_4}{\gamma_4-1}}}{g}$$

$$= C_1\left(\frac{A_4}{A_1},\frac{A^*}{A_1},\gamma_4\right)\left(P_{3'}/P_3\right)\left(P_2/P_1\right), \tag{16}$$

where the notation is that of figure 1b.

The velocity boundary condition results in

$$u_2/a_1 = u_3/a_1 = \left(u_3/u_{3'}\right)\left(u_{3'}/a_{3'}\right)\left(a_{3'}/a_{4'}\right)\left(a_4/a_1\right). \tag{17}$$

Again using equations 5, 6, and 9

$$u_2/a_1 = u_3/u_{3'}\left(a_4/a_1\right)\frac{M_{3'}}{1+\frac{\gamma_4-1}{2}M_{3'}}\,g^{\frac{\gamma_4-1}{2\gamma_4}}$$

$$= C_2\left(\frac{A_4}{A_1},\frac{A^*}{A_1},\gamma_4,\frac{a_4}{a_1}\right)\left(u_3/u_{3'}\right). \tag{18}$$

Now consider region 3 - 3' and define the secondary shock velocity as $U_{s2}$. Transforming to a stationary shock system, the flow Mach number into the shock becomes

$$\left(M_{3'} - \frac{u_{s2}}{a_{3'}}\right).$$

Equation 1 then yields

$$P_3/P_{3'} = 1 + \frac{2\gamma_4}{\gamma_4+1}\left[\left(M_{3'}-\frac{U_{s2}}{a_{3'}}\right)^2 - 1\right]. \tag{19}$$

The calculation procedure is as follows:

(1) Assuming supersonic flow out of the nozzle, obtain $M_{3'}\left(\frac{A_4}{A_1}, \frac{A^*}{A_1}, \gamma_4\right)$ from the tables and evaluate $C_1$ and $C_2$ in equations 16 and 18.

(2) Now assume a value for $U_{s2}/a_3$, and calculate $P_3/P_{3'}$ from equation 19. Knowing the flow Mach number into the shock, $\left[M_{3'} - (U_{s2}/a_{3'})\right]$, calculate or obtain from the tables the exit-flow Mach number $\left[M_3 - (U_{s2}/a_3)\right]$, and the speed of sound ratio $a_{3'}/a_3$.

(3) $M_3$ may be found from the relation

$$M_3 = \text{exit-flow Mach number} + \frac{U_{s2}}{a_{3'}}\,(a_{3'}/a_3). \tag{20}$$

The velocity ratio across the moving shock becomes

$$u_3/u_{3'} = M_3/M_{3'}\left(a_3/a_{3'}\right). \tag{21}$$

(4) Knowing $u_3/u_{3'}$, equation 18 determines $u_2/a_1$; equations 4 and 2 determine $P_2/P_1$ and $M_s$. It is suggested that the $P_2/P_1$ versus $u_2/a_1$ curves referred to at the beginning of the section be used to determine $P_2/P_1$, and $M_s$ be either calculated from this value (equation 2) or picked out of the tables.

(5) With $P_2/P_1$ and $P_{3'}/P_3$ known, $P_4/P_1$ is readily calculated from equation 16.

C. Shock-In-Nozzle Configuration (Fig. 1c)

In this case, the shock is stationary, and it is necessary to assume the shock position in the nozzle. Denoting the nozzle area at this position as $A_s$, the equation analogous to equation 16 is

$$P_4/P_1 = (P_{3''}/P_{3'})(P_{3'}/P_3)(P_2/P_1)\frac{\left[1 + \frac{\gamma_4 - 1}{2} M_{3''}\right]^{\frac{2\gamma_4}{\gamma_4 - 1}}}{g_s}, \quad (22)$$

where $g_s = g\left(\frac{A_4}{A_s}, \frac{A^*}{A_s}\right)$ and the notation is as in figure 1c.
The velocity boundary condition yields

$$u_2/a_1 = u_3/a_1 = M_3(a_3/a_{3'})(a_{3'}/a_{3''})(a_{3''}/a_{4'})(a_{4'}/a_4)(a_4/a_1). \quad (23)$$

Applying equations 5, 6, and 9

$$u_2/a_1 = M_3(a_3/a_{3'})(a_{3'}/a_{3''})(a_4/a_1)\frac{g_s^{\frac{\gamma_4 - 1}{2\gamma_4}}}{1 + \frac{\gamma_4 - 1}{2} M_{3''}}. \quad (24)$$

The knowledge of $A_4/A_s$, $A^*/A_s$, and $\gamma_4$, enables $g_s$ and $M_{3''}$ to be calculated (ref. 16 and 17). The shock tables and the value of $M_{3''}$ then give $P_{3''}/P_{3'}$, $a_{3'}/a_{3''}$, and $M_{3'}$. Allowing the subsonic flow at station 3' to expand, $M_3$, $P_{3'}/P_3$, and $a_3/a_{3'}$, can be obtained by using the tables and the value of $M_{3'}$ and $A_s/A_1$. Thus $u_2/a_1$ can be found from equation 24 and $P_2/P_1$ then obtained from the curves of equation 4. The value of $P_2/P_1$ and the shock tables yield $M_s$, and $P_4/P_1$ is determined from equation 22.

D. Subsonic Nozzle Configuration (Fig. 1d)

In this case the nozzle flow is completely subsonic and conditions between regions 4' and 3 depend only on $A_4/A_1$. The performance may be calculated by the procedure of Appendix I. A, putting conditions in region 3' equal to those in region 3 (since no secondary expansion wave exists), and choosing the subsonic value for $M_3$. As expected, the resulting relations are identical with those for a plain shock tube when $A_4/A_1 = 1$, and there is an effect on performance only if $A_4/A_1 \neq 1$.

# APPENDIX II

## EXPERIMENTAL EQUIPMENT AND INSTRUMENTATION

### A. General Description of Facilities and Techniques Used

The GALCIT three-inch-square shock tube was used for all of the experiments. This is essentially the shock tube reported in reference 18, but the pressure seals have been improved and the two-dimensional nozzle at the end of the tube has been removed. This nozzle was replaced by a dump chamber for the first series of experiments, while for parts II and III the dump chamber itself was removed and was replaced by a flange assembly. The flange assembly was designed to hold the various models, and was located 18 feet downstream of the diaphragm section.

The shock tube has a circular driver such that $A_4/A_1 = 0.885$, and it was modified by the diaphragm insert section of figure 7. Soft aluminum diaphragms 0.006 inches thick were used in combination with 20-100 psi. nitrogen or helium drivers. Air was used as the driven gas. The shock speed was controlled by careful diaphragm scoring and by the use of area ratio 0.4 - 0.01 diaphragm insert plates.

The basic shock speed was detected with two matched platinum thin-film gauges spaced two feet apart. The gauges had high resistance (500$\Omega$) in order to maximize sensitivity, a gauge current of $10^{-2}$ amperes providing enough sensitivity to enable shock speeds as low as 1.04 to be readily measured. The gauge outputs were fed through low noise-level amplifiers to a Beckman 1 $\mu$sec. counter. For situations

where two separate shock-speed measurements were required (i.e., parts II, III, and the attenuation measurements of part I), each pair of gauges was connected in series and fed into a single amplifier. The differentiated output was then applied to the period function of a 1 $\mu$sec. counter.

For the downstream shock-speed measurements of parts II and III it was found most convenient to machine the insulated backing for the thin-film gauges from lucite. Electrical lead-outs were provided by copper wires cemented into holes drilled through this backing material. Epoxy cement was used, and the wire ends were ground off flush on the inner surface of the lucite plug. Since it is difficult to evaporate a thin film directly onto lucite, the gauges themselves were made from thin strips of Mylar adhesive tape onto which an aluminum film had been evaporated. Mystic Type 7300 was found to be the most satisfactory tape for this application, since it is stable at relatively low pressure and high temperature, and it has an overall thickness of under .002". Painted silver connections were made from the tape to the flush ends of the copper lead-out wires. The conflicting requirements of durability and sensitivity resulted in the use of relatively low resistance (50 $\Omega$) films. Gauges made from these films lasted typically for fifty shots, and were easily repaired by lifting off the old film and pressing a new one into place.

The initial pressure was measured with a Wallace and Tiernan 0-50 mm. gauge and an aircraft type manometer. When it was required, the driver pressure was measured with an 0-100 psi. Bourdon gauge. All gauges were carefully calibrated with either a McLeod gauge or known reference volumes. It was estimated that the corrected 50 mm.

gauge reading was accurate to $\pm$ .1 mm. The shock-tube leak rate was always considerably less than 1 mm. per hour.

The distances between the film centers of the various sets of gauges was measured to within .01".

B. Specific Details Pertinent to Part I

The average distance of the two shock-speed gauges from the diaphragm was 16.7 feet for these experiments. For the attenuation measurements of this section, two pairs of platinum gauges were used, the center of the extra pair being located at 12.7 feet from the diaphragm.

The fine wires were constructed as in reference 9. A constant excitation current was applied and the voltage across the wire was directly sensed by an oscilloscope. The wire acts like a calorimeter, and thus its response to a given flow change is roughly exponential with time. Thus, for small times relative to the characteristic time, the slope of the wire response will be constant; for very long times, the wire response will be a step function. It was found that a wire chosen so as to have the former response characteristic was the most practical for these tests.

Given a specific $M_s$ and $P_1$, all the flow variables could be calculated from the ideal theory. Approximate Nusselt numbers for the various flow regions could then be found from the calculated Reynolds and Mach numbers through the use of references 19 and 20. The Nusselt number is defined as

$$Nu = \frac{qd}{K(T_r - T_w)}, \tag{1}$$

where d is the wire diameter, K the thermal conductivity of the fluid (evaluated at total temperature, ref. 21), $T_r$ the recovery temperature, and $T_w$ the initial wire temperature. The heat transfer per unit area of wire, q, may be shown to be directly proportional to s, the response slope (ref. 9). Thus,

$$S_2/S_3 = q_2/q_3 = \frac{K_2(T_{r2} - T_1)}{K_3[T_{r3} - (T_{r1} + \Delta T_2)]} \, Nu_2/Nu_3. \qquad (2)$$

It may also be shown that

$$\Delta T_2 = \frac{\Delta E_2}{\alpha I_w R_w}, \qquad (3)$$

where $I_w$ is the wire current ($\sim 2(10)^{-3}$ amp.), $R_w$ the wire resistance at $T_1$ ($\sim 2\Omega$), $\alpha$ the coefficient of resistivity (taken as 0.004 $/^{\circ}C$ for tungsten), and $\Delta E$ the voltage jump on the experimental response trace. $\Delta T_2$ was of the order of $50^{\circ}C$ for the $1\frac{1}{2}$ mil. wire.

Equation 2 predicts the slope ratio between regions 2 and 3 when the recovery factors and Nusselt numbers have been found. The equation may easily be extended to other regions if care is taken in obtaining the wire temperature at the beginning of each change in slope.

C. Specific Details Pertinent to Part II

For this series of experiments, the tube and flange assemblies of part III were reversed. This provided open-ended tubes of 1" and 5/8" inside diameter which protruded roughly 2 feet upstream from the end of the shock tube. (See fig. 21 and 13). The upstream ends of these tubes had a .004" wall thickness, tapering back 2" to the full 1/8" thick wall. A 3/8" inside diameter open-ended tube was also used, this tube being obtained by sliding a long insert into the 5/8" tube. Each tube was aligned with the shock-tube center line to within $1^{o}$, and was provided with a movable plug at its downstream end. The plugs were positioned at either 26" or 14" from the leading edge of the tubes. These distances were chosen in order to provide a length of shock-wave travel sufficiently long to make the shock-wave attentuation easily discernible.

The shock speed upstream of the tube entrance was measured by two platinum thin-film gauges located two feet apart, the downstream gauge being on the shock-tube wall in a position directly in line with the small tube entrance. The average shock speed in the small tube was measured between this latter gauge and an aluminum-tape gauge on the movable plug face. The gauge outputs were amplified, differentiated, and fed into two 1 $\mu$ sec. counters. The ratio of the two counts, corrected for the length discrepancies, directly provided the value of $\overline{(M_s/M_o)}$.

In order to check the theory of this section accurately, three factors had to be considered in the design of the experiment. The first of these was the length of the shock-tube testing region, which must be such that the experiment is over before the shock-tube contact

surface reaches the leading edge of the model. This length was evaluated by the theory of Roshko (ref. 28), and is shown in figure 16 for an 18 foot length of the 3-inch-square shock tube, and for initial pressures of 50, 5, and 0.5 mm. It is seen that there is a significant reduction in this parameter as the pressure is lowered, in contrast to the ideal theory which predicts no pressure effect.

The second important consideration is that the boundary layer must be laminar in order to justify comparison with the theory. As the shock-boundary layer is most important in the attenuation mechanism, a reasonable criterion is that this boundary layer must have a distance to transition of at least half the length of the open-ended tube being studied. The length of laminar boundary layer behind the shock was obtained from figure 4 of the experimental study of Hartunian et al (ref. 29), and is shown in figure 16 of this report. As expected, a reduction of initial pressure increases the probability of a complete laminar-boundary layer in the tube.

The final important factor is the ratio $\delta^*/d$, since the theory is only valid for boundary-layer thicknesses that are small compared with the tube diameter. The maximum displacement thickness occurs at the matching point of the leading-edge and shock boundary layers. This maximum thickness is shown in figure 16 for a pressure of 5 mm. and a tube length of 26". Since $\delta^*$ is inversely proportional to the square root of the pressure, the values of $\delta^*_{max}$ at 50 and 0.5 mm. can be easily obtained from the 5 mm. curve. It was felt that keeping $\delta^*_{max}/d < 0.1$ should provide agreement with the assumptions of the theory. (It would, however, be interesting to investigate the effects of larger $\delta^*_{max}/d$.)

From a study of the above effects it was decided to use an initial pressure of 5 mm. for the bulk of the attenuation measurements. This choice ensured both adequate testing time and the existence of laminar boundary layers in the 26" and 14" tubes. Figure 16 indicates that 26" tubes with diameters as small as 3/8" still satisfy $\delta^*_{max}/d < 0.1$ as long as the initial shock Mach number is not much less than 2.

In addition to the 5 mm. shots, runs were made with the 1" and 5/8" tubes at an initial pressure of 50 mm. in order to check the prediction that some boundary-layer turbulence would exist at this pressure.

## D. Specific Details Pertinent to Part III

The nozzle assembly used for these experiments is depicted in figure 21, the "O" ring seals and other construction details having been left off for clarity. The steel insert was necessary in order to convert the square shock tube to an axially-symmetric geometry. This was desirable because it allows larger area ratios for a given downstream channel height, and hence helps alleviate viscous boundary-layer effects. The insert itself was 13" long and had a 2" inside diameter. Its sharp leading edge (.003" thick wall with a $2^{o}$ bevel) was assumed to have no effect on the propagating shock wave.

The nozzles and downstream tube assemblies were made of brass with their inner surfaces polished. 5, 10, and $30^{o}$ conical nozzles were used with downstream tubes of 1" and 5/8" I. D. This provided area ratios of 4 and 10.24. The incoming shock speed was measured by two platinum thin-film gauges located two feet apart, the downstream gauge being on the shock-tube wall directly in line with the leading edge of the steel insert. The average downstream shock speed was measured over a distance x (see figure 12) between an aluminum-tape wall gauge located 1" downstream of the nozzle exit, and another aluminum tape gauge located on the movable end-wall plug. As in part II of this report, the gauge outputs were fed into two counters, and the ratio of the two counts (again corrected for length discrepancies) directly yielded $\left(\overline{M_s/M_o}\right)$. The temperature in the laboratory was recorded for each run and used to determine $M_o$. The maximum value of $M_o$ was limited by the necessity of keeping the initial pressure high enough to ensure both

small viscous effects and a long shock-tube test gas region (see fig. 16). An initial pressure of 50 mm. was found to be the most satisfactory for these experiments, although runs were also made at 5 mm. in order to check the validity of the viscous corrections used.

# APPENDIX III

## THE FANNO-PROCESS MODEL

### A. Constant-Area Fanno Model

In this study, the secondary normal shock of figure 1b is replaced with a stationary compression region supported by shock-boundary layer interaction. This interaction region is assumed to take place in the constant-area duct, and, as in the ideal theory, the entering flow (region 3') is assumed known.

Assuming a perfect gas, the steady energy equation is

$$\left(a_a/a_b\right)^2 = \frac{1 + \frac{\gamma-1}{2} M_b^2}{1 + \frac{\gamma-1}{2} M_a^2} = \left(P_a/P_b\right)\left(\rho_b/\rho_a\right). \qquad (1)$$

The continuity equation, applied between regions 3 and 3' may be written as

$$\left(P_3 M_3\right)/a_3 = \left(P_{3'} M_{3'}\right)/a_{3'}, \qquad (2)$$

where it is understood that flow parameters describing the Fanno region are the average values across the cross-section.

Applying equation 1 across the Fanno region, and substituting $a_3/a_{3'}$ from equation 2 yields

$$\left(1 + \frac{\gamma-1}{2} M_{3'}^2\right)\left[\frac{P_{3'} M_{3'}}{P_3}\right]^2 = M_3^2\left(1 + \frac{\gamma-1}{2} M_3^2\right). \qquad (3)$$

Solving for $M_3$

$$(\gamma-1)M_3^2 = -1 + \left[1 + 2(\gamma-1)\left(1 + \frac{\gamma-1}{2}M_3^2\right)\left\{(P_3'/P_3)M_3'\right\}^2\right]^{\frac{1}{2}}. \quad (4)$$

The shock-tube performance is readily calculated by first assuming $P_{3'}/P_3$. Then, since $M_{3'}$ is known, $M_3$ may be found. From this information $a_3/a_{3'}$ is obtained from equation 2. $u_3/a_1$ may now be determined and the performance calculated in a manner analogous to that of Appendix I.

B. Varying-Area Fanno Model

For this model, the Fanno process is assumed to take place in the nozzle itself. The flow is assumed to expand isentropically from the sonic throat to some station 3' and then proceed along a Fanno curve to a station downstream of the nozzle. (See sketch.) The entering flow is known, as well as $A^*/A_3$, $A_{3'}/A_3$, and $P_*/P_3$.

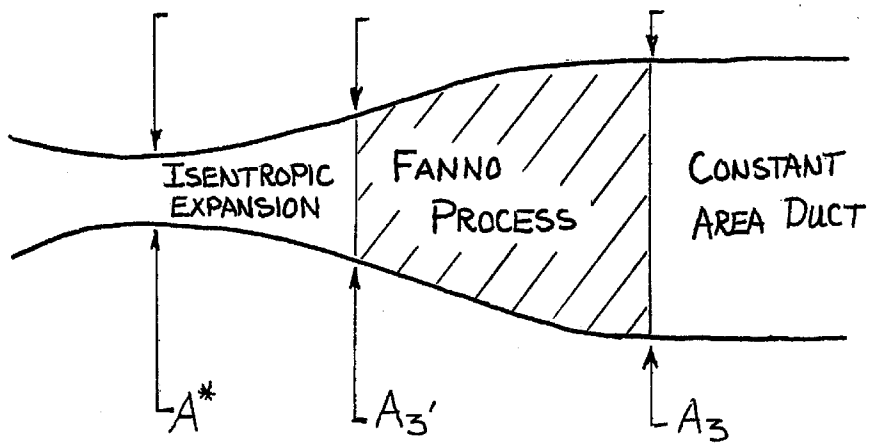


The isentropic relation between the throat and station 3' gives

$$P_*/P_{3'} = \left[\rho_*/\rho_{3'}\right]^{\gamma} = \left[a_*/a_{3'}\right]^{\frac{2\gamma}{\gamma-1}} \qquad (5)$$

Appropriately applying equations 1 and 5, the overall density ratio may be written

$$\rho^*/\rho_3 = (\rho_*/\rho_{3'})(\rho_{3'}/\rho_3) = \left[\frac{1+\frac{\gamma-1}{2}M_{3'}^2}{\frac{\gamma+1}{2}}\right]^{\frac{1}{\gamma-1}} \left[\frac{1+\frac{\gamma-1}{2}M_{3'}^2}{1+\frac{\gamma-1}{2}M_3^2}\right]\frac{P_{3'}}{P_3}; \qquad (6)$$

but

$$P_{3'}/P_3 = (P_{3'}/P_*)(P_*/P_3) = \left[\frac{\frac{\gamma+1}{2}}{1+\frac{\gamma-1}{2}M_{3'}^2}\right]^{\frac{\gamma}{\gamma-1}} \frac{P_*}{P_3} \qquad (7)$$

Thus, collecting terms

$$\rho_*/\rho_3 = \frac{\frac{\gamma+1}{2}}{1+\frac{\gamma-1}{2}M_3^2}\frac{P_*}{P_3}, \tag{8}$$

and the continuity equation and perfect gas relation yield

$$M_3 = (\rho_*/\rho_3)(a_*/a_3)(A_*/A_3) = \left[\rho_*/\rho_3\right]^{\frac{1}{2}}\left[P_*/P_3\right]^{\frac{1}{2}}(A_*/A_3). \tag{9}$$

Applying equation 8 to equation 9 and solving the algebraic relation

$$(\gamma-1)M_3^2 = -1+\left[1+(\gamma^2-1)\left\{(P_*/P_3)(A_*/A_3)\right\}^2\right]^{\frac{1}{2}}; \tag{10}$$

but, again, applying continuity and equation 8

$$u_3/a_* = (\rho_*/\rho_3)(A^*/A_3) = \frac{\frac{\gamma+1}{2}}{1+\frac{\gamma-1}{2}M_3^2}\left(\frac{P_*}{P_3}\right)\left(\frac{A_*}{A_3}\right), \tag{11}$$

and equation 11 together with equation 10

$$u_3/a_* = \frac{(\gamma+1)\left[(P_*/P_3)(A_*/A_3)\right]}{1+\left[1+(\gamma^2-1)\left\{(P_*/P_3)(A_*/A_3)\right\}^2\right]^{\frac{1}{2}}} \tag{12}$$

Equations 8, 10, and 12 demonstrate that the exit flow is independent of the position of station 3'. Thus the Fanno process could be completely outside of the nozzle, so that this solution is identical to that of part A above.

# APPENDIX IV

## WHITHAM'S ANALYSIS FOR THE MOTION OF A SHOCK WAVE THROUGH A REGION OF CHANGING AREA

The following analysis for the motion of a shock wave through a continuous area change will be seen to bear a strong resemblance to the theory for shock-wave attenuation presented in part II of this report. For a discussion of additional shock-wave interaction problems for which this type of analysis yields useful results, the reader is referred to Whitham's paper (ref. 33).

The axially-symmetric continuity equation for the flow in a varying area duct is

$$\frac{\partial \rho}{\partial t} + \frac{\partial}{\partial x}(\rho u) + \frac{1}{r}\frac{\partial}{\partial r}(r\rho v) = 0. \tag{1}$$

Multiplying by $r$ and integrating across the duct from 0 to R yields

$$\frac{\partial \rho}{\partial t}\int_0^R r\,dr + \frac{\partial}{\partial x}(\rho u)\int_0^R r\,dr = -r\rho v\Big|_0^R = -\rho u R\frac{dR}{dx}, \tag{2}$$

where $\rho$ and $u$ are assumed to be only functions of x, and

$$(v/u)_{r=R} = dR/dx.$$

For small perturbations such that

$$\rho = \rho_2 + \rho' \;;\; u = u_2 + u' \;;\; A(x) = A_2 + A' \;;\; \text{etc.}, \tag{3}$$

equation 2 may be re-written in terms of the cross-sectional area as

$$\frac{\partial \rho'}{\partial t} + \rho_2 \frac{\partial u'}{\partial x} + u_2 \frac{\partial \rho'}{\partial x} = -\frac{\rho_2 u_2}{A_2} \frac{dA'}{dx}. \tag{4}$$

Replacing the primed quantities in equation 4 by the complete flow quantities (equation 3), and introducing the isentropic relation and the linearized momentum equation (see part II, equations 6, 7, and 8) there is obtained

$$\frac{1}{a_2^2 \rho_2 u_2}\left(\frac{\partial P}{\partial t} + u_2 \frac{\partial P}{\partial x}\right) + \frac{1}{u_2}\frac{\partial u}{\partial x} = -\frac{1}{A_2}\frac{dA}{dx},$$

$$\rho_2\left(\frac{\partial u}{\partial t} + u_2 \frac{\partial u}{\partial x}\right) + \frac{\partial P}{\partial x} = 0. \tag{5}$$

These equations may be compared directly with equations 9 of part II, the difference between the two problems coming in through the right hand side of the first equation in each set.

Following the procedure of part II, equations 5 are written in terms of the characteristic variables $\eta = x - (u_2 + a_2)t$ and $\xi = x - (u_2 - a_2)t$:

$$\underline{\text{on}}\ \eta = \underline{\text{constant}}: \quad \frac{d}{d\xi}\left[\rho_2 a_2 u + p\right] = -\frac{\rho_2 a_2^2 u_2}{u_2 + a_2}\frac{dA}{A_2} \tag{6a}$$

$$\underline{\text{on}}\ \xi = \underline{\text{constant}}: \quad \frac{d}{d\eta}\left[\rho_2 a_2 u - p\right] = \frac{\rho_2 a_2^2 u_2}{u_2 - a_2}\frac{dA}{A_2}. \tag{6b}$$

Integrating equations 6 results in

$$\rho_2 a_2 (u - u_2) = F(\eta) + G(\xi) + \frac{\rho_2 a_2^3 u_2}{u_2^2 - a_2^2}\frac{A(x) - A_2}{A_2}$$

$$p - p_2 = F(\eta) - G(\xi) - \frac{\rho_2 a_2^2 u_2^2}{u_2^2 - a_2^2}\frac{A(x) - A_2}{A_2}. \tag{7}$$

The next step in the solution of equations 7 is to evaluate the constants F and G by applying the appropriate boundary conditions. It is immediately realized that one of these boundary conditions is that the shock relations must be satisfied at $x = U_o t$. The other boundary condition is supplied by the statement that $F(\eta)$ must be identically zero, since F represents disturbances catching up with the shock wave from behind, and such re-reflected disturbances are of second order. Thus this boundary condition is necessary for a consistent linear analysis, and the use of it precludes any possibility of the final solution being useful for the problem considered in part III.

Now, the function F arises from the integration of equation 6a, thus when F is put equal to zero equation 6a must hold for the complete flow, and not just on lines of $\eta$ = constant. Applying equation 6a at the shock wave and using the linearized Rankine-Hugoniot relations, there is obtained

$$\frac{dA}{A} = -\frac{2M_o}{(M_o^2-1)K(M_o)}\, dM_s ,$$

where

$$K(M_o) = 2\left[\left(1+\frac{2}{\gamma+1}\,\frac{1-\mu^2}{\mu}\right)\left(2\mu+1+M_o^{-2}\right)\right]^{-1}, \tag{8}$$

and

$$\mu^2 = \frac{(\gamma-1)M_o^2+2}{2\gamma M_o^2-(\gamma-1)} .$$

This is the result of Chester (ref. 32) and Chisnell (ref. 30) for an infinitesimal area change. It is seen from this relation that the

shock Mach number is a function only of $M_o$, $\gamma$, and the area at the shock location. When equation 8 is integrated, the linear solution for an arbitrarily-large continuous area change is obtained

$$A\, f(M_s) = \text{constant}. \tag{9}$$

where $f(M_s)$ is a complicated function of $M_s$ and $\gamma$, (see ref. 30).

# APPENDIX V

## ONE-DIMENSIONAL CHARACTERISTICS CALCULATION FOR THE MOTION OF A SHOCK WAVE DOWNSTREAM OF AN AREA CHANGE

In this section some details concerning the characteristics calculation of figure 25 are discussed.* The procedure used was developed from Rudinger's book (ref. 44), to which frequent reference is made. It should be mentioned that much simpler characteristic schemes are available for problems where only the flow in the nozzle just behind the shock wave is desired. Typical of these is the isentropic calculation procedure discussed in detail in reference 45. Approximations such as this however, are of little use for the present problem for which a more thorough analysis is necessary.

The "quasi-one-dimensional" equations of motion for the flow in a duct with changing cross-sectional area may be written (ref. 44)

$$\begin{aligned} \frac{\delta_+ P}{\partial \tau} &= -\bar{a}\bar{u}\frac{\partial \ln A}{\partial \chi} + \bar{a}\frac{\delta_+ \bar{S}}{\partial \tau} \\ \frac{\delta_- Q}{\partial \tau} &= -\bar{a}\bar{u}\frac{\partial \ln A}{\partial \chi} + \bar{a}\frac{\delta_- \bar{S}}{\partial \tau} \\ \frac{D\bar{S}}{D\tau} &= 0, \end{aligned} \qquad (1)$$

* It should be noted that figure 25 is a 1/5 scale reproduction of the actual calculation, and hence it has not been possible to show the complete details for the smaller cells near the nozzle exit.

where $\tau = \frac{a_o t}{\ell_o}$ ; $\chi = \frac{x}{\ell_o}$ ; $\bar{u} = \frac{u}{a_o}$ ; $\bar{a} = \frac{a}{a_o}$ ; $\bar{S} = \frac{S}{C_p(\gamma-1)}$

$$\frac{\delta^{\pm}}{\delta\tau} = \frac{\partial}{\partial\tau} + (\bar{u} \pm \bar{a}) \frac{\partial}{\partial\chi}$$

$$\frac{D}{D\tau} = \frac{\partial}{\partial\tau} + \bar{u} \frac{\partial}{\partial\chi}$$

and $$P = \frac{2}{\gamma-1}\bar{a} + \bar{u} \quad ; \quad Q = \frac{2}{\gamma-1}\bar{a} - \bar{u}.$$

$\ell_o$ is a reference length (taken as the nozzle length and $a_o$ a reference velocity (taken as the speed of sound in the undisturbed gas).

Equations 1 indicate how the parameters P, Q, and $\bar{S}$ vary in the $\chi, \tau$ plane along curves that are given by

$$\begin{aligned} \frac{d\chi}{d\tau} &= \bar{u} + \bar{a} \quad \text{for } P \\ &= \bar{u} - \bar{a} \quad \text{for } Q \\ &= \bar{u} \quad \text{for } \bar{S}. \end{aligned} \tag{2}$$

Now consider the following segment of figure 25, and assume that P, Q, and $\bar{S}$ are known at points 1, 2, and 3.

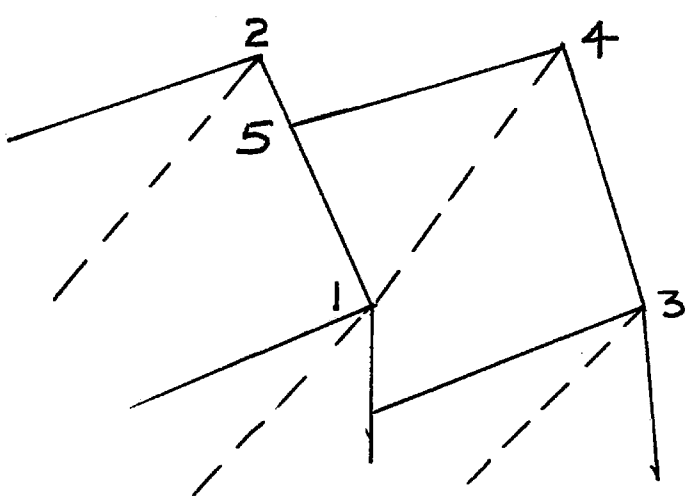

The following procedure was used to determine the location of point 4 and the values of $P_4$, $Q_4$ and $\bar{S}_4$:

(1) Point 4 is chosen to lie on the particle path from point 1, thus $\bar{S}_4 = \bar{S}_1$. Assume values for $P_4$, $Q_4$ and calculate $\bar{u}_4$, $\bar{a}_4$, $(\bar{u} + \bar{a})_4$, $(\bar{u} - \bar{a})_4$.

(2) Project a line from point 1 with slope $(\bar{u})_{1,4} = \frac{\bar{u}_1 + \bar{u}_4}{2}$ and one from point 3 with slope $(\bar{u} - \bar{a})_{3,4}$. The intersection of these lines determines the first trial position for point 4. From this position project a line with slope $(\bar{u} + \bar{a})_4$ to locate the trial position for point 5.

(3) With the trial position of point 5 known, interpolate between points 1 and 2 to obtain $P_5$, $Q_5$, $\bar{S}_5$, and thus calculate $\bar{u}_5$ and $\bar{a}_5$.

(4) The initial values and positions having been determined, calculate new values $P_4'$ and $Q_4'$ from equations 1 and 2:

$$P_4' = P_5 + \left(\frac{\delta_+ P}{\partial \tau}\right)_{4,5} (\tau_4 - \tau_5)$$

where

$$\left(\frac{\delta_+ P}{\partial \tau}\right)_{4,5} = -\frac{1}{2}\left[\bar{a}_4 \bar{u}_4 \left(\frac{\partial \ln A}{\partial \chi}\right)_4 + \bar{a}_5 \bar{u}_5 \left(\frac{\partial \ln A}{\partial \chi}\right)_5\right] + \left(\frac{\bar{a}_4 + \bar{a}_5}{2}\right)\left[\bar{S}_4 - \bar{S}_5\right]. \qquad (3)$$

$$Q_4' = Q_3 + \left(\frac{\delta_- Q}{\partial \tau}\right)_{4,3} (\tau_4 - \tau_3)$$

where

$$\left(\frac{\delta_+ Q}{\partial \tau}\right)_{4,3} = -\frac{1}{2}\left[\bar{a}_4 \bar{u}_4 \left(\frac{\partial \ln A}{\partial \chi}\right)_4 + \bar{a}_3 \bar{u}_3 \left(\frac{\partial \ln A}{\partial \chi}\right)_3\right] + \left(\frac{\bar{a}_4 + \bar{a}_3}{2}\right)\left[\bar{S}_4 - \bar{S}_3\right].$$

(The value of $\partial \ln A/\partial \chi$ may be determined from a curve of $\partial \ln A/\partial \chi$ versus $\chi$ for the configuration studied.)

(5) From $P_4'$ and $Q_4'$ determine $\bar{u}_4'$, $\bar{a}_4'$, $(\bar{u} + \bar{a})_4'$, and $(\bar{u} - \bar{a})_4'$. Locate a new position 4' by projecting new lines from points 1 and 3 with slopes $(\bar{u})_{1,4}'$ and $(\bar{u} - \bar{a})_{3,4}'$ respectively. From this new position project a line with slope $(\bar{u} + \bar{a})_{4',5}$ to locate a new position 5'. Now calculate the various parameters at 5' (by interpolation), and use this information with equations 3 to calculate $P_4''$ and $Q_4''$. The whole procedure is repeated until convergence is achieved, usually requiring 2-3 iterations.

Some care must be exercised when a cell involves the shock wave as one of its boundaries. For this case the flow is no longer particle-isentropic, there being an entropy jump at the shock wave. In addition, the Rankine-Hugoniot relations must be satisfied across the shock wave. The calculation procedure is discussed in Rudinger's book where useful tables are also presented.

The characteristics calculation for a specific configuration can become quite lengthy, especially for large area changes where many cells are necessary to achieve an accurate solution. Rudinger (ref. 44) suggests that the cell sizes should correspond to steps in $\partial \ln A/\partial \chi$ not much greater than 0.2. Slightly larger cells were used for the calculation of figure 25; however, excellent agreement with the linear theory for local shock speed was maintained. By taking all numbers to four significant figures and plotting slopes to 1 per cent, it is estimated that the calculated values $M_s$ are good to within $\pm \frac{1}{2}$ per cent. This was checked by plotting the specific values of $M_s$ versus their axial position, and observing less than $\frac{1}{2}$ per cent scatter.

The characteristics calculation presented in figure 25 is for the shock-wave motion through, and downstream of, an area ratio 10 conical convergent nozzle. The shock Mach number entering the nozzle was chosen equal to 2, and it can be seen to increase through the nozzle and then start to fall off downstream. The cell size decreases near the exit of the nozzle since the rate of area change for the conical nozzle is increasing. Downstream of the nozzle exit the cell size becomes very large, the area terms have dropped out of equations 1 and 3, and the shock speed is dependent only on the flow behind it. It is also interesting to note on the figure that the "Q" waves (lines of $(\bar{u} - \bar{a})$) are tending to coalesce to form the reflected shock wave inside the nozzle.

# REFERENCES


1. Russell, D. A.: "A Study of Area Change Near the Diaphragm of a Shock Tube". GALCIT Hypersonic Research Project, Memorandum 57, July 20, 1960.

2. Monroe, L. L.: "Investigation of the Transmission of a Shock Wave Through an Orifice". GALCIT Hypersonic Research Project, Memorandum 46, September 25, 1958.

3. Resler, E. L.; Lin, S. C.; Kantrowitz, A.: "The Production of High Temperature Gases in Shock Tubes". J. Appl. Phys. 23, pp. 1390-1399, (1952).

4. Alpher, R. A.; White, D. R.: "Ideal Theory of Shock Tubes with Area Change Near Diaphragm". General Electric Research Laboratory Rep. 57-RL-1664, January 1957.

5. Lukasiewicz, J.: "Shock Tube Theory and Application". National Aeronautical Establishment Rep. 15, Ottawa, Canada, (1952).

6. Hall, J. G.: "Shock Tubes". University of Toronto Institute of Aerophysics, UTIA Review No. 12, Part II, May 1958.

7. Mirels, H.: "Attenuation in a Shock Tube Due to Unsteady-Boundary-Layer Action". NACA TN 3278, August 1956 (see also, TN 4021).

8. Alpher, R. A.; White, D. R.: "Flow in Shock Tubes with Area Change at the Diaphragm Section". J. Fl. Mech. 3, pp. 457-470, (1958).

9. Christiansen, W. H.: "Use of Fine Unheated Wires for Heat Transfer Measurements in the Shock Tubes". GALCIT Hypersonic Research Project, Memorandum 55, June 1, 1960.

10. Willmarth, W. W.: "Small Barium Titanate Transducer for Aerodynamic or Acoustic Pressure Measurements". Rev. of Sci. Instruments, 29, pp. 218-222, March 1958.

11. Emmons, H. W.: "Fundamentals of Gas Dynamics". Princeton High Speed Aerodynamics and Jet Propulsion Series, Vol. 3, Princeton University Press, 1958.

12. Lukasiewicz, J.: "Diffusers for Supersonic Wind Tunnels". J. Aeronautical Sci. 20, pp. 617-626, (1953).

13. Liepmann, H. W.; Puckett, A. E.: "Introduction to Aerodynamics of a Compressible Fluid". John Wiley and Sons, Inc., New York, N. Y., (1947).

14. Bull, G. V.: "Starting Processes in an Intermittent Supersonic Wind Tunnel". University of Toronto Institute of Aerophysics, UTIA Rep. 12, February 1951.

15. Emrich, R. J.; Peterson, R. L.: "Pressure Variation with Time in the Shock Tube". Lehigh University Institute of Research, T. R. 7, March 15, 1956 (see also T. R. 4, 5, and 8).

16. Ames Research Staff: "Equations, Tables and Charts for Compressible Flow". NACA Report 1135, 1953.

17. Mueller, J. N.: "Equations, Tables, and Figures for Use in the Analysis of Helium Flow at Supersonic and Hypersonic Speeds". NACA TN 4063, September 1957.

18. Rabinowicz, J.: "Aerodynamic Studies in the Shock Tube". GALCIT Hypersonic Research Project, Memorandum 38, June 10, 1957.

19. Laufer, J.; McClellan, R.: "Measurement of Heat Transfer from Fine Wires in Supersonic Flows". J. Fl. Mech. 1, pp. 276-289, (1956).

20. Spangenberg, W. G.: "Heat-Loss Characteristics of Hot-Wire Anemometers at Various Densities in Transonic and Supersonic Flow". NACA TN 3381, May 1955.

21. "Tables of Thermal Properties of Gases". National Bureau of Standards Circular 564, November 1, 1955.

22. Trimpi, R. L.; Cohen, N. B.: "A Theory for Predicting the Flow of Real Gases in Shock Tubes, with Experimental Verification". NACA TN 3375, March 1955 (see also TN 4347).

23. Lam, S. H.; Crocco, L.: "Shock Induced Unsteady Laminar Compressible Boundary Layers on a Semi-Infinite Flate Plate". Princeton University, Dept. of Aero. Eng. Rep. 428, September 1958 (see also Rep. 480).

24. Spence, D. A.; Woods, B. A.: "Boundary Layer and Combustion Effects in Shock Tube Flows". Proceedings of the Eleventh Symposium of the Colston Research Society, April 1959.

25. Demyanov, Yu A.: "The Influence of the Boundary Layer on the Character of the Flow of Gas in a Tube Behind a Moving Shock Wave". Prikl. Mat. i. Mekh. 21, 4 (1957). Also available as R. A. E. Library Translation 796, (1959).

26. Schlichting, H.: "Boundary Layer Theory", Pergamon Press, 1955.

27. Rott, H.; Hartunian, R.: "On the Heat Transfer to the Walls of a Shock Tube". Cornell School of Aeronautical Engineering, November 1955.

28. Roshko, A.: "On Flow Duration in Low-Pressure Shock Tubes". Phys. Fluids 3, pp. 835-842, November-December 1960.

29. Hartunian, R.; Russo, A.; Marrone, P.: "Boundary Layer Transition and Heat Transfer in Shock Tubes". Proceedings of the Heat Transfer and Fluid Mechanics Institute, June 1958.

30. Chisnell, R. F.: "The Motion of a Shock Wave in a Channel, with Applications to Cylindrical and Spherical Waves". J. Fl. Mech. 2, pp. 286-298, (1957).

31. Guderley, G.: "Starke Kugelige und Zylindrische Verdichtungsstösse in der Nähe des Kugelmittelpunktes bzw. der Zylinderachse", Luftfahrtforschung 19, pp. 302-312, (1942).

32. Chester, W.: "The Propagation of Shock Waves in a Channel of Non-Uniform Width". Quart. J. Mech. App. Math. 6, pp. 440-452, (1953).

33. Whitham, G.B.: "On the Propagation of Shock Waves Through Regions of Non-Uniform Area or Flow". J. Fl. Mech. 4, pp. 337-360, (1958).

34. Chester, W.: "The Propagation of Shock Waves Along Ducts of Varying Cross Section". Adv. in Appl. Mech. VI, pp. 119-152, (1960).

35. Rosciszewski, J.: "Calculations of the Motion of Non-Uniform Shock Waves". J. Fl. Mech. 8, pp. 337-367, (1960).

36. Payne, R.B.: "A Numerical Method for a Converging Cylindrical Shock". J. Fl. Mech. 2, pp. 185-200, (1957).

37. Rudinger, G.: "Passage of Shock Waves Through Ducts of Variable Cross Section". Phys. Fluid Vol 3, January 1960.

38. Laporte, O.: "On the Interaction of a Shock with a Constriction". University of California, Los Alamos Scientific Laboratory Rep. LA-1740, August 1954.

39. Friedman, M. P.: "An Improved Perturbation Theory for Shock Waves Propagating Through Non-Uniform Regions". J. Fl. Mech. 8, pp. 193-209, (1960).

40. Parks, E. K.: "Supersonic Flow in a Tube of Divergent Cross-Section". University of Toronto Institute of Aerophysics, UTIA Rep. 18, (1952).

41. Kahane, A.; Warren, W.R.; Griffith, W.C.; Marion, A.A.: "A Theoretical and Experimental Study of Finite Amplitude Wave Interactions with Channels of Varying Area". J. Aero. Sci. 21, pp. 505-524, (1954).

42. Hertzberg, A.; Kantrowitz, A.: "Studies with an Aerodynamically Instrumented Shock Tube". J. Appl. Phys, 21, pp. 874-878, (1950).

43. Bird, G.A.: "The Effect of Wall Shape on the Degree of Reinforcement of a Shock Wave Moving into a Converging Channel". J. Fl. Mech. 5, pp. 60-66, (1959).

44. Rudinger, G.: "Wave Diagrams for Nonsteady Flow in Ducts." D. Van Nostrand Co., 1955.

45. Warren, W.R.: "Interaction of Plane Waves of Finite Amplitude with Channels of Varying Cross Section". Princeton University, Dept. of Aero. Eng. Rep. 206, June 1952.

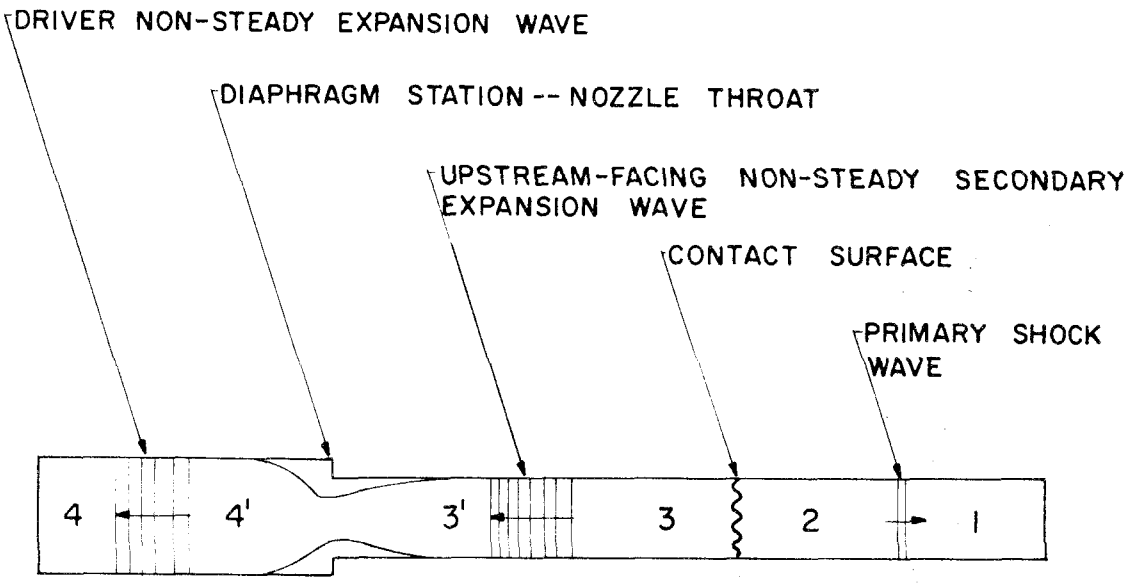


a. EXPANSION - WAVE CONFIGURATION

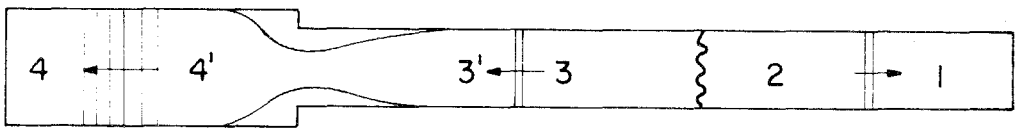


b. SHOCK - WAVE CONFIGURATION

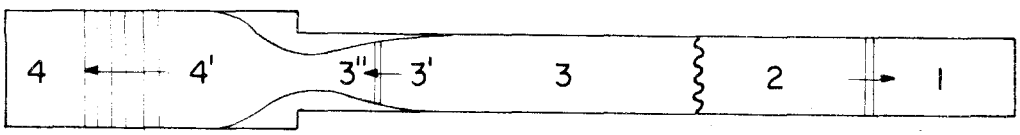


c. SHOCK-IN-NOZZLE CONFIGURATION

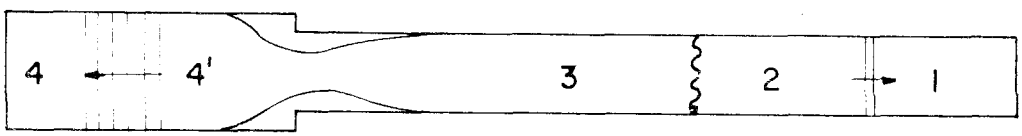


d. SUBSONIC NOZZLE CONFIGURATION

FIG. 1 SCHEMATIC SHOCK - TUBE CONFIGURATIONS

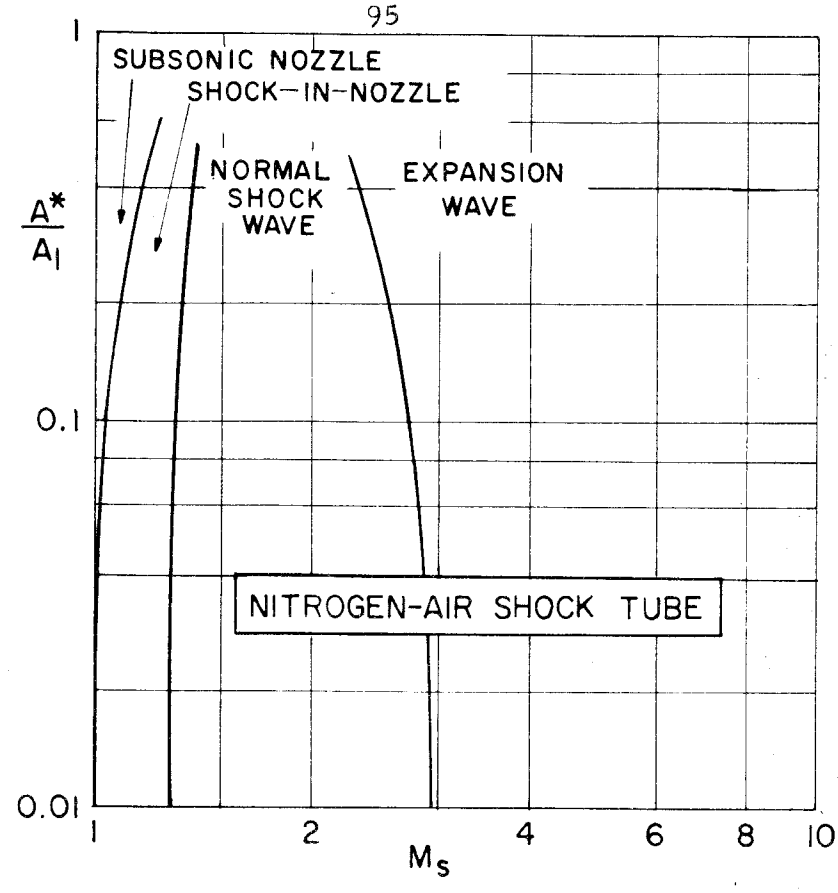


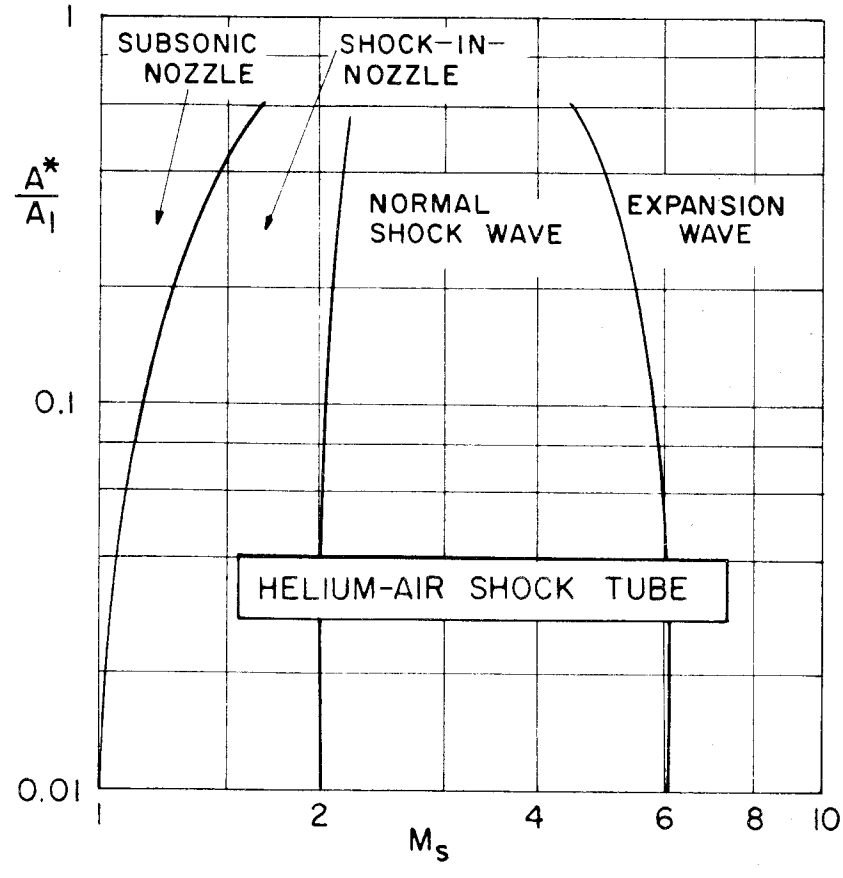


FIG. 2 CONFIGURATION BOUNDARIES FOR $A_4/A_1 = 1$

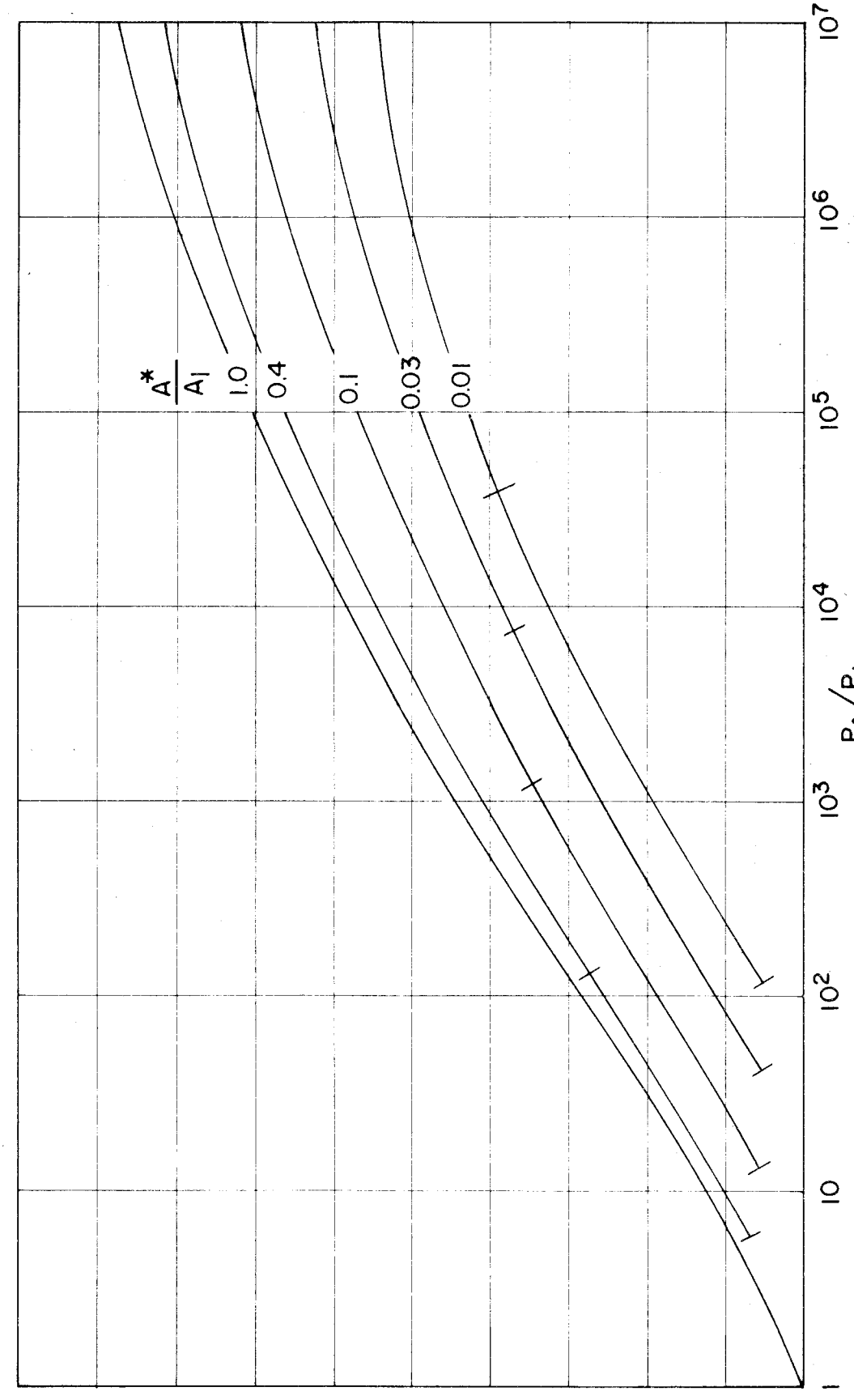


FIG. 3 BASIC PERFORMANCE -- NITROGEN-AIR SHOCK TUBE; $A_4/A_1 = 1$

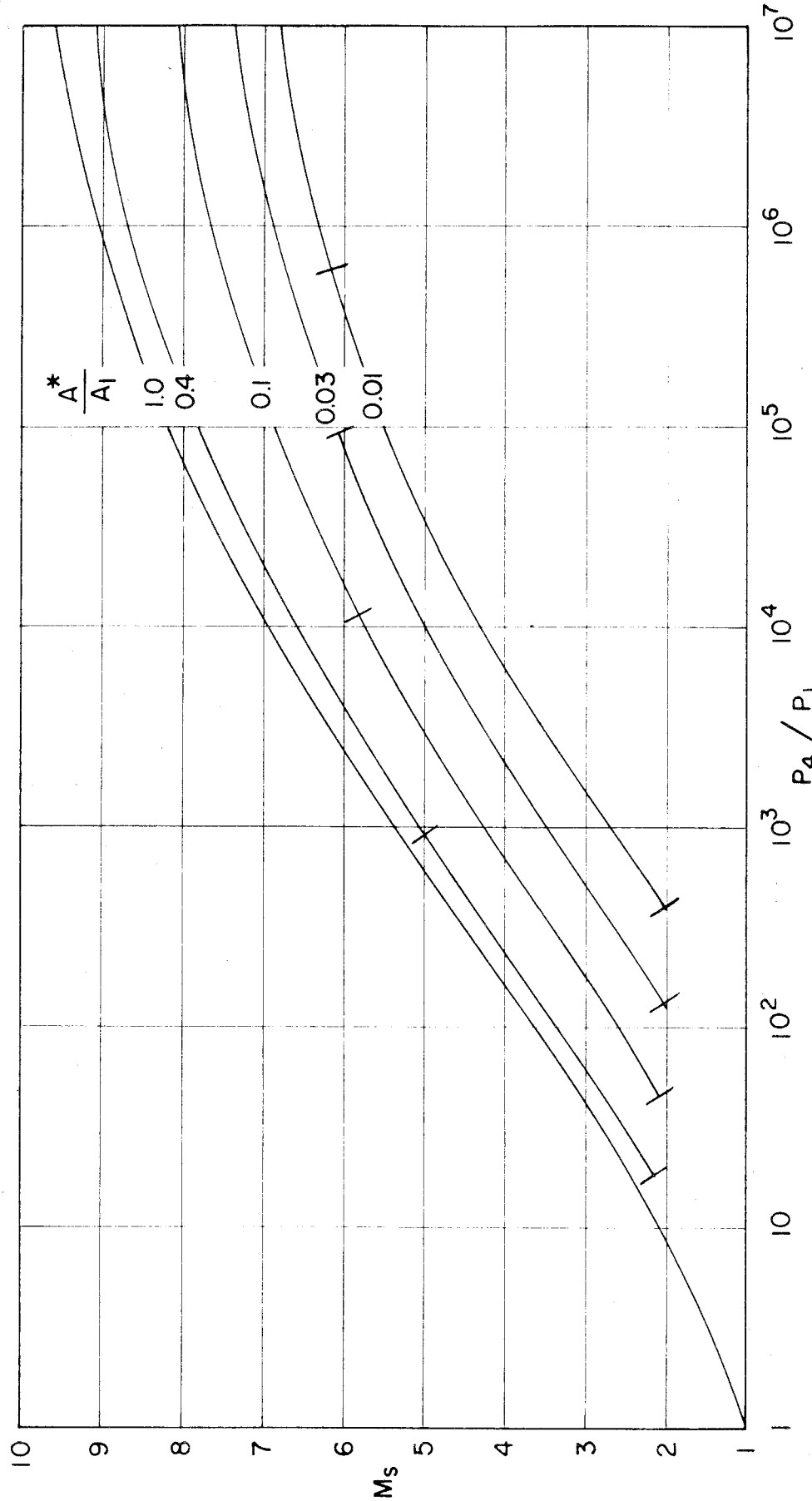


FIG. 4 BASIC PERFORMANCE -- HELIUM-AIR SHOCK TUBE; $A_4/A_1 = 1$

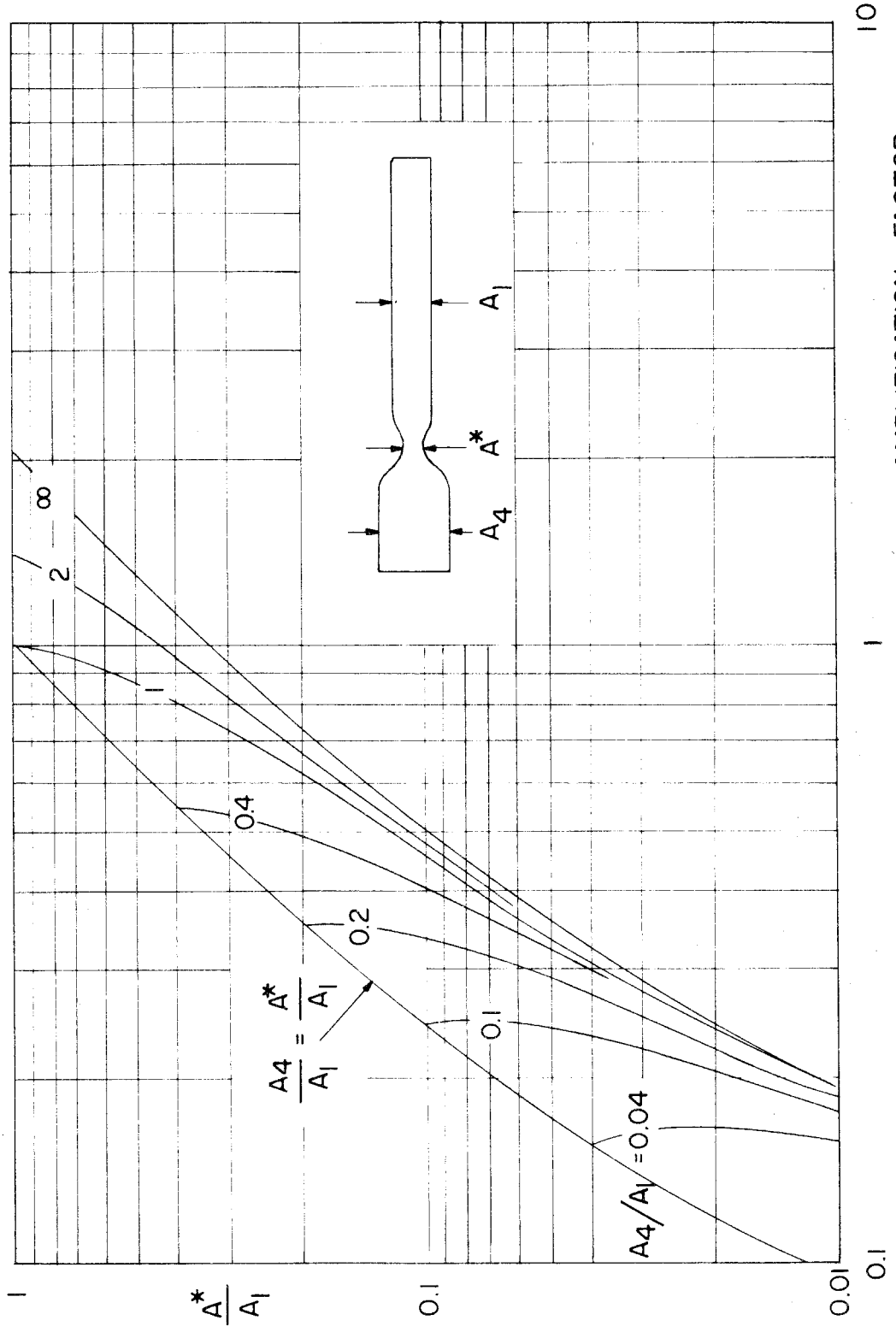


FIG. 5(a) AMPLIFICATION FACTOR FOR $\gamma = 5/3$

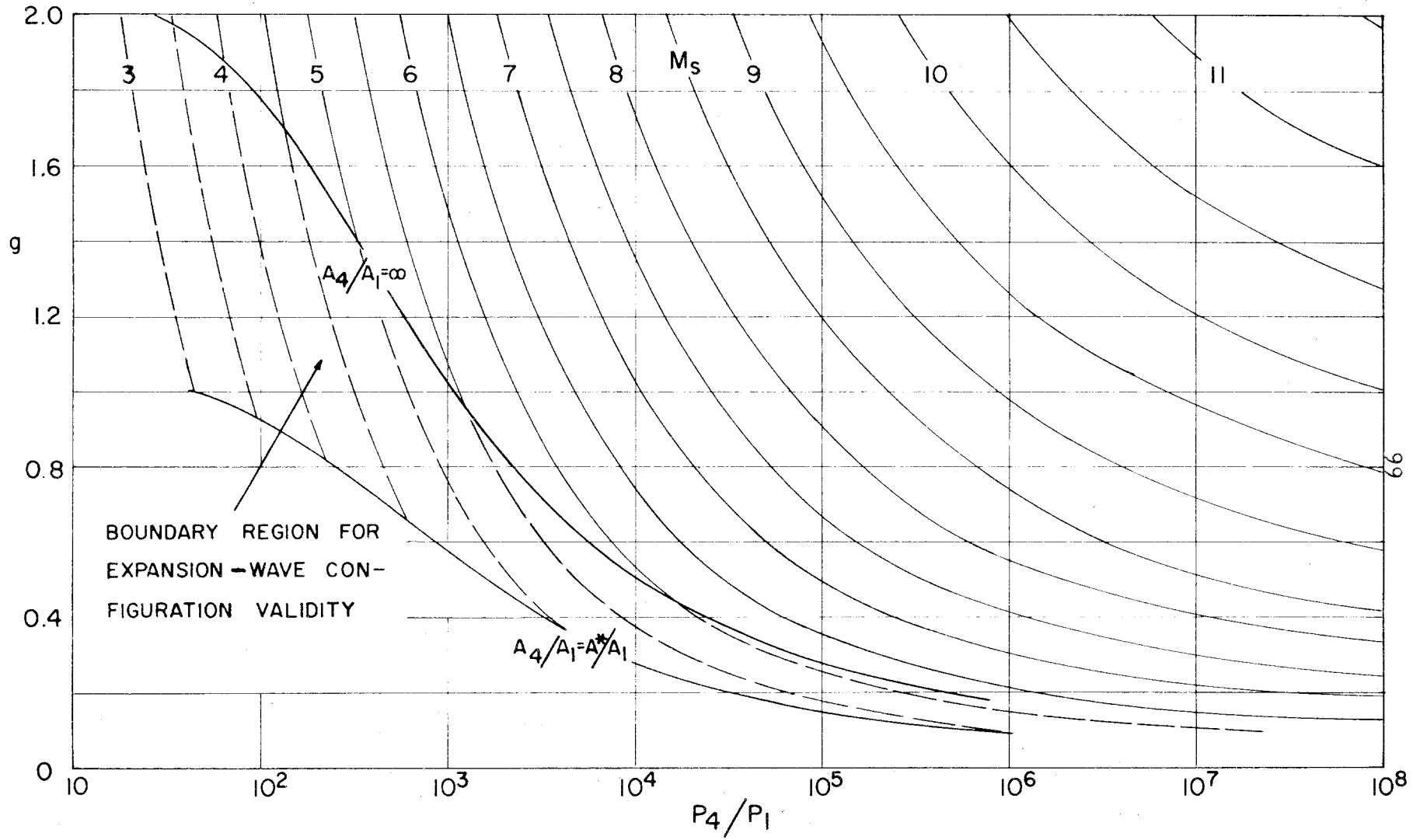


FIG. 5(b) BASIC PERFORMANCE--HELIUM-AIR SHOCK TUBE; EXPANSION-WAVE CONFIGURATION

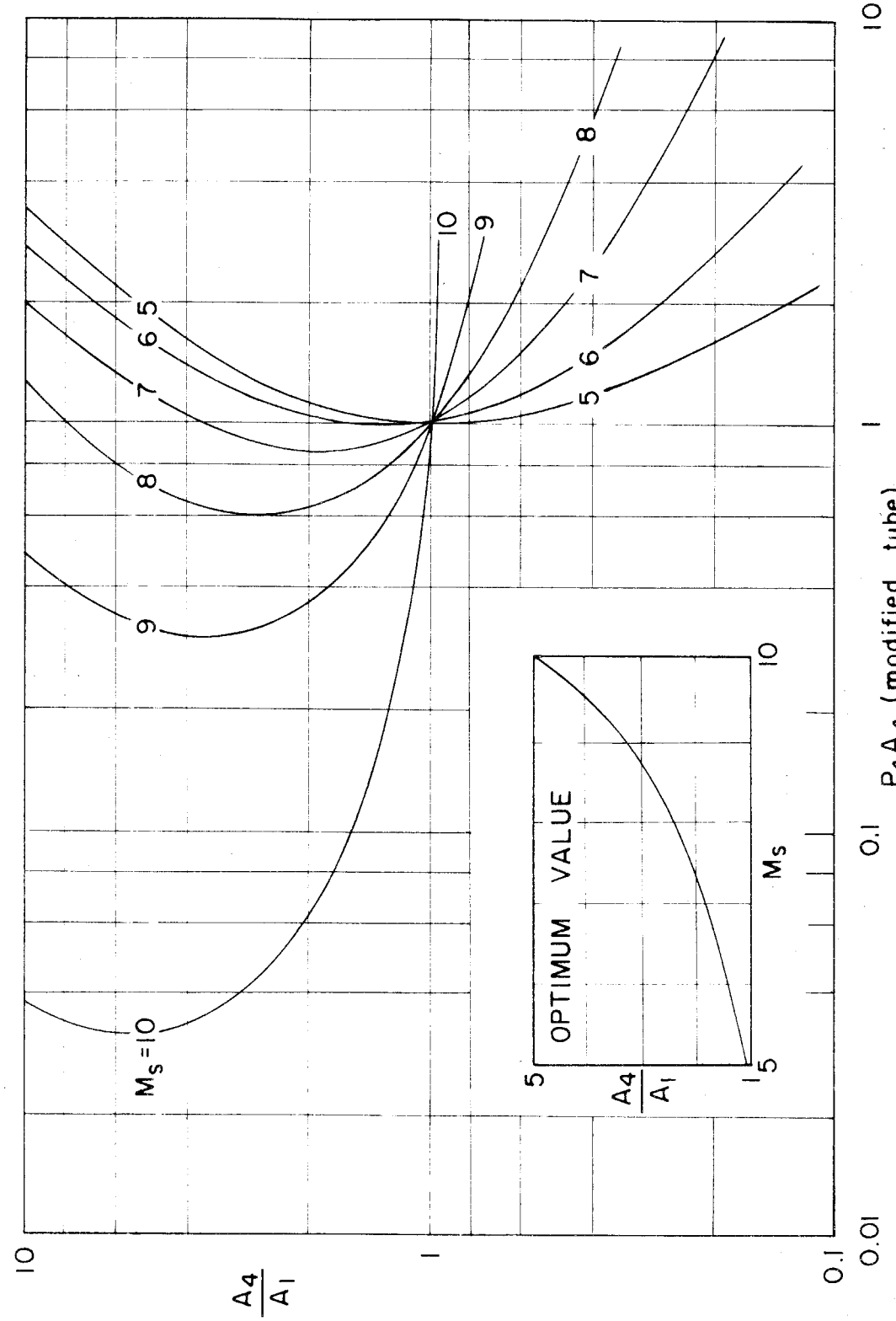


FIG. 6 OPTIMIZATION OF $A_4/A_1$ FOR ECONOMICAL OPERATION -- HELIUM-AIR SHOCK TUBE

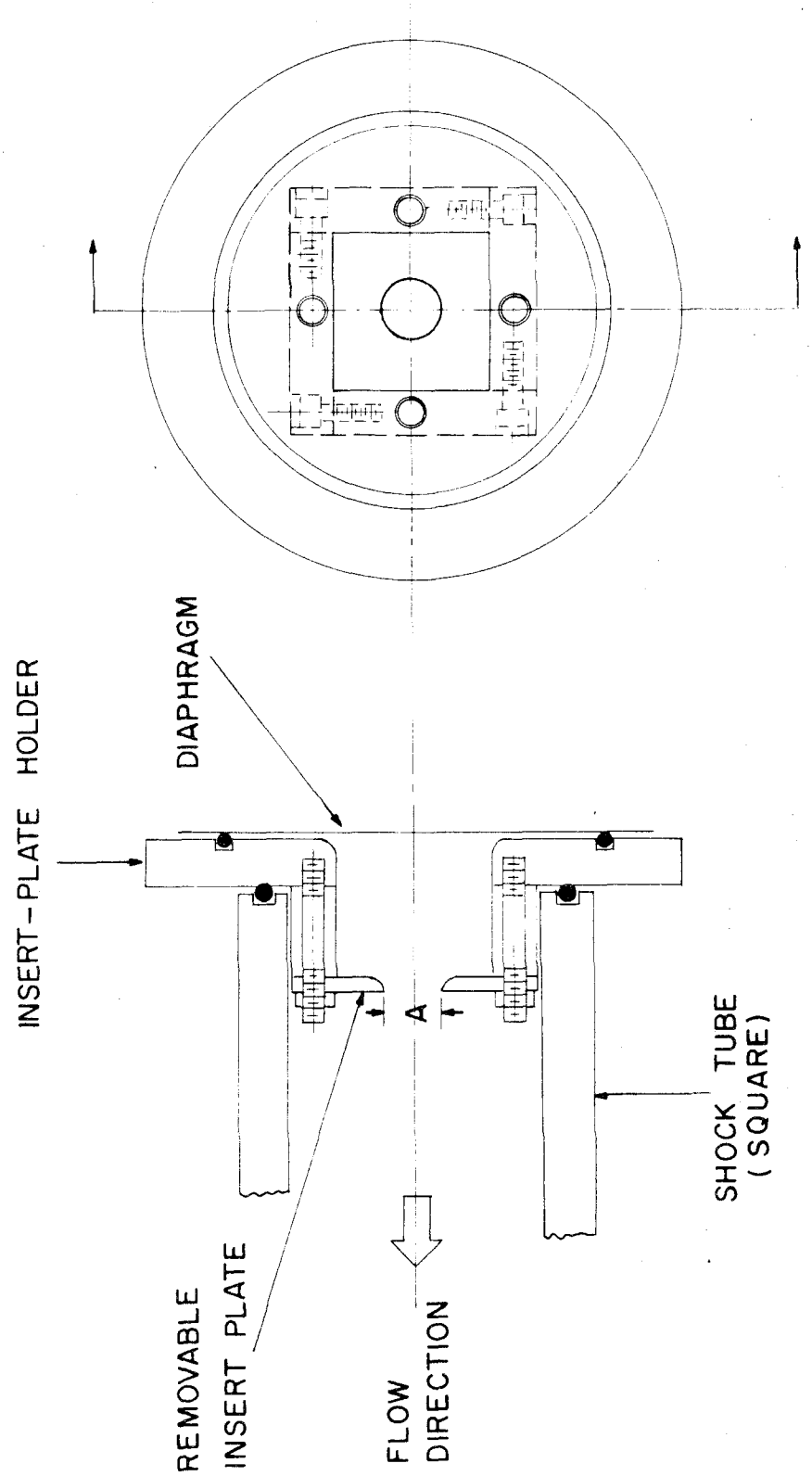


FIG. 7 DIAPHRAGM INSERT SECTION -- 1/2 SCALE

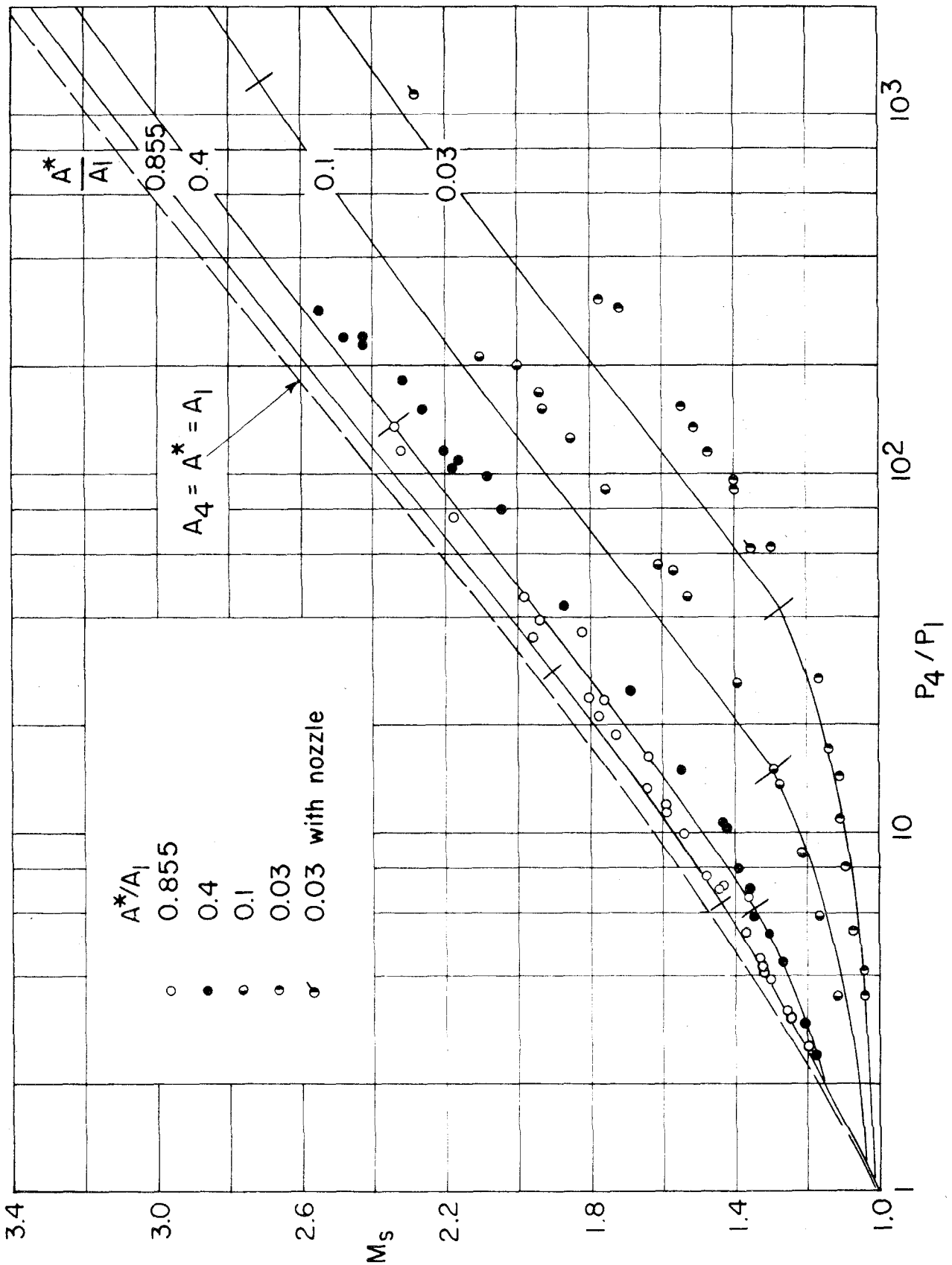


FIG. 8 UNCORRECTED DATA -- NITROGEN-AIR SHOCK TUBE; $A_4/A_1 = 0.855$

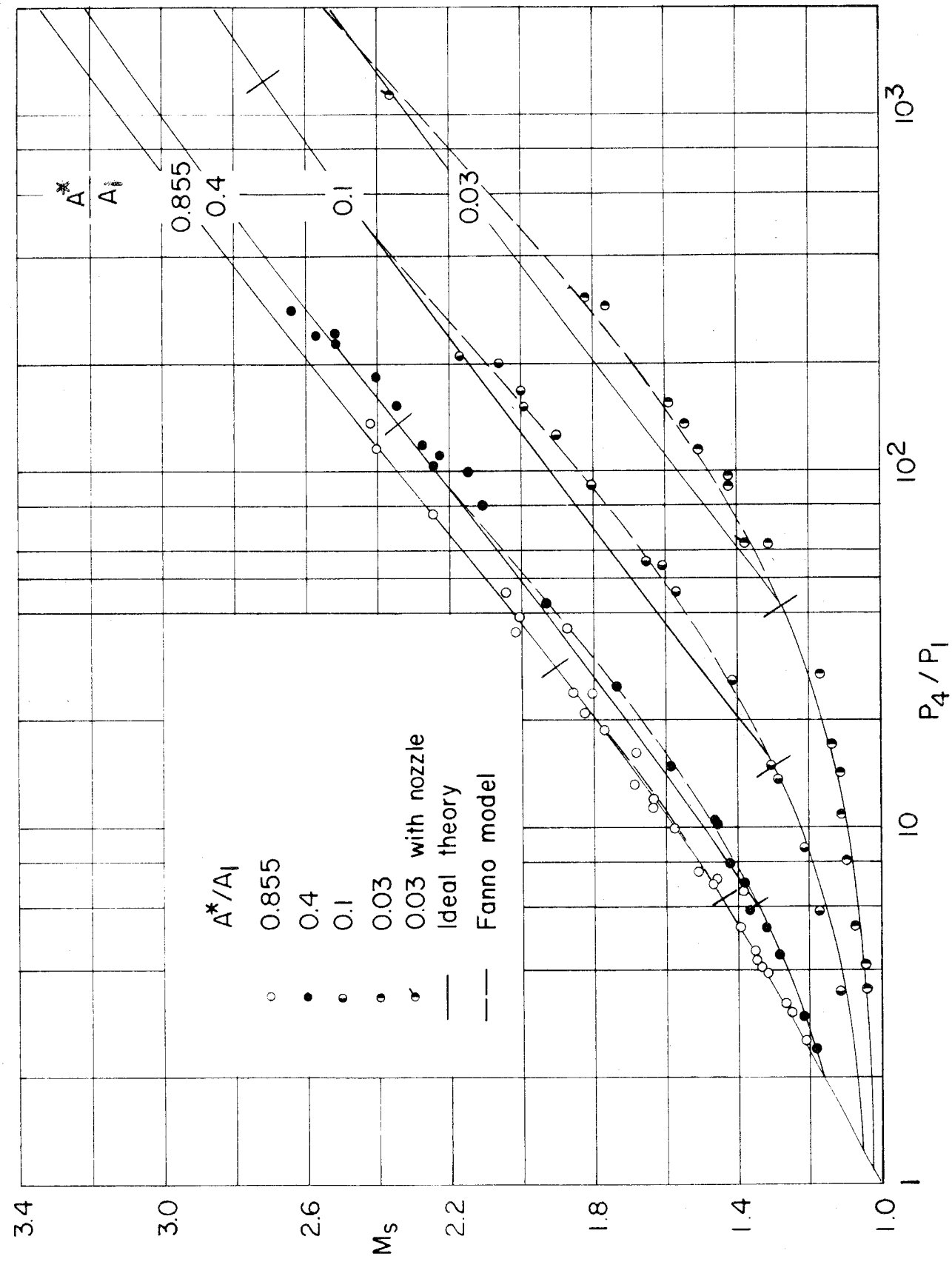


FIG. 9 CORRECTED DATA -- NITROGEN-AIR SHOCK TUBE
$A_4/A_1 = 0.855$

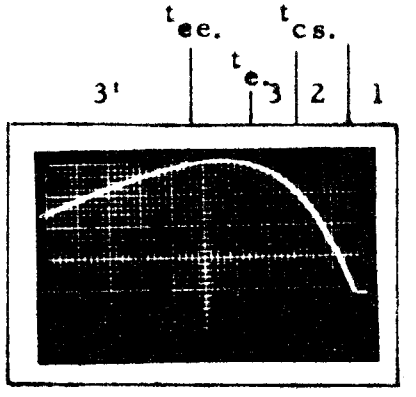


$M_s$ = 3.16
$P_1$ = 1.0 mm.
1 mv./div.
1 ms./div.
x = 15.5 ft.

$(s_2/s_{3'})_{exp.}$ = -6.9
$(s_2/s_{3'})_{th.}$ = -7.5
$(s_2/s_3)_{th.}$ = +7.5

31D2

(a) Expansion-Wave Configuration; $A^*/A_1$ = 0.1

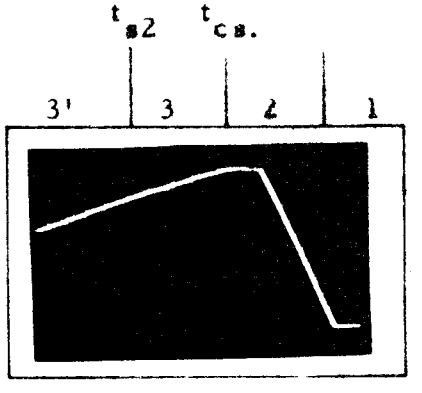


$M_s$ = 2.22
$P_1$ = 10 mm.
1 mv./div.
1 ms./div.
x = 15.5 ft.

$(s_2/s_3)_{exp.}$ = -7.7
$(s_2/s_3)_{th.}$ = -2.0
$(s_2/s_{3'})_{th.}$ = -7.8

27D1

(b) Normal Shock-Wave Configuration; $A^*/A_1$ = 0.1

**FIG. 10 ILLUSTRATIVE FINE-WIRE RESPONSE; 1½ MIL. WIRE**

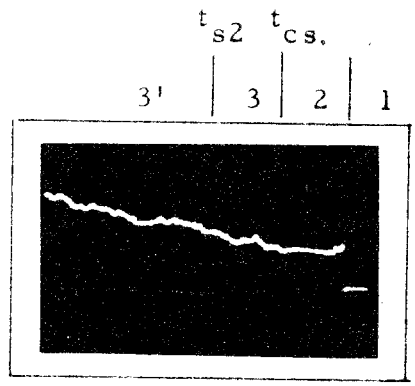


$M_s$ = 2.11
$P_1$ = 16 mm.
5 mv./div.
2 ms./div.
x = 17.5 ft.

$(P_2/P_3)_{th.}$ = 1.0
$(P_3/P_{3'})_{th.}$ = 4.2

5J6

(a) Side-Wall Trace; $A^*/A_1 = 0.1$

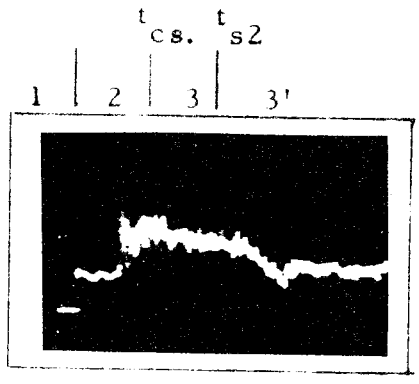


$M_s$ = 2.06
$P_1$ = 20 mm.
200 mv./div.
2 ms./div.
x = 17.5 ft.

$(P_{T_{2g}}/P_{T_{3g}})_{th.}$ = .44
$(P_{T_{3g}}/P_{T_{3'g}})_{th.}$ = .75

3F2

(b) Total-Pressure Trace; $A^*/A_1 = 0.1$

FIG. 11 ILLUSTRATIVE PRESSURE TRACES

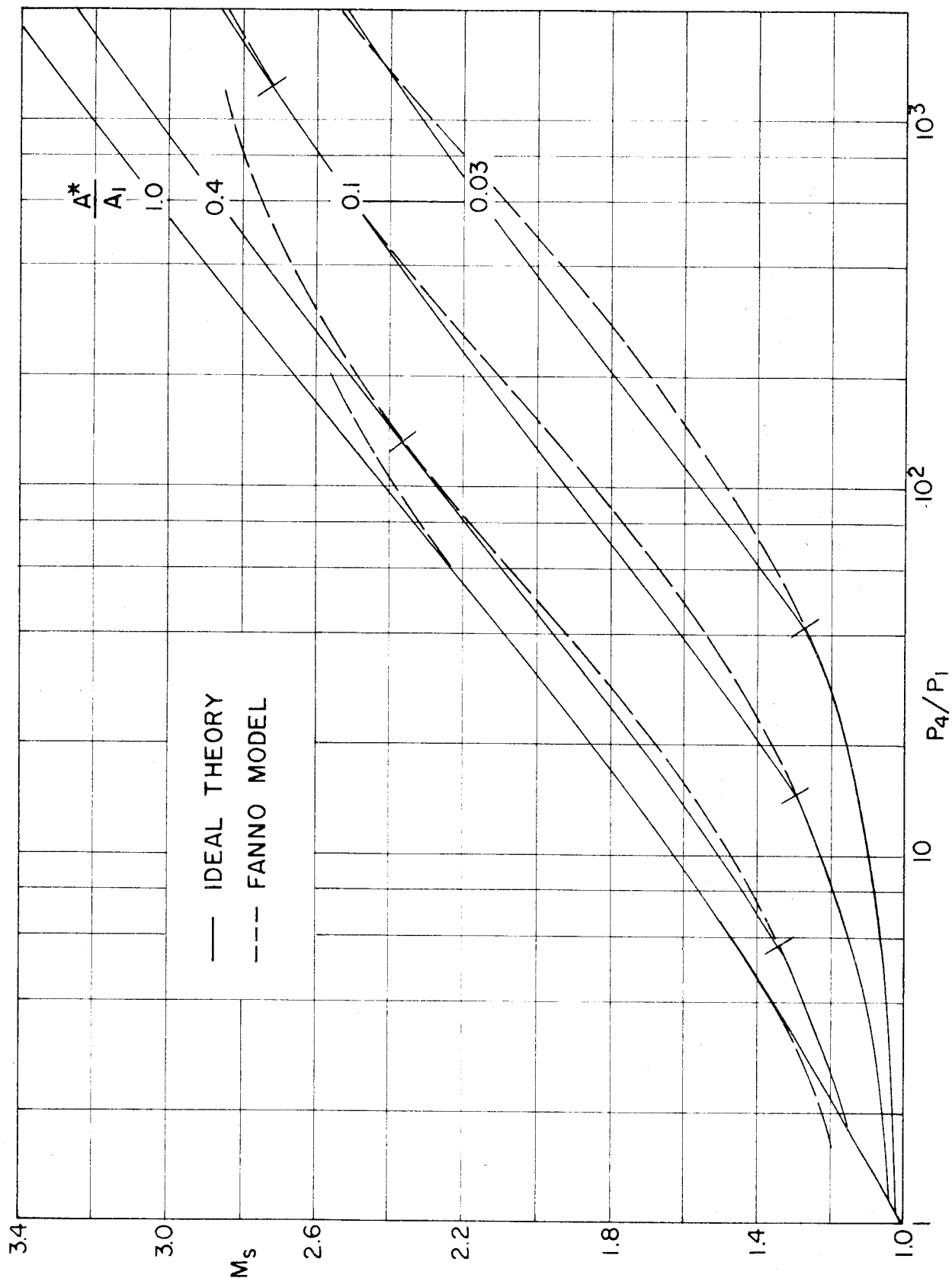


FIG. 12 THE FANNO-PROCESS MODEL--NITROGEN-AIR SHOCK TUBE; $A_4/A_1 = 1$

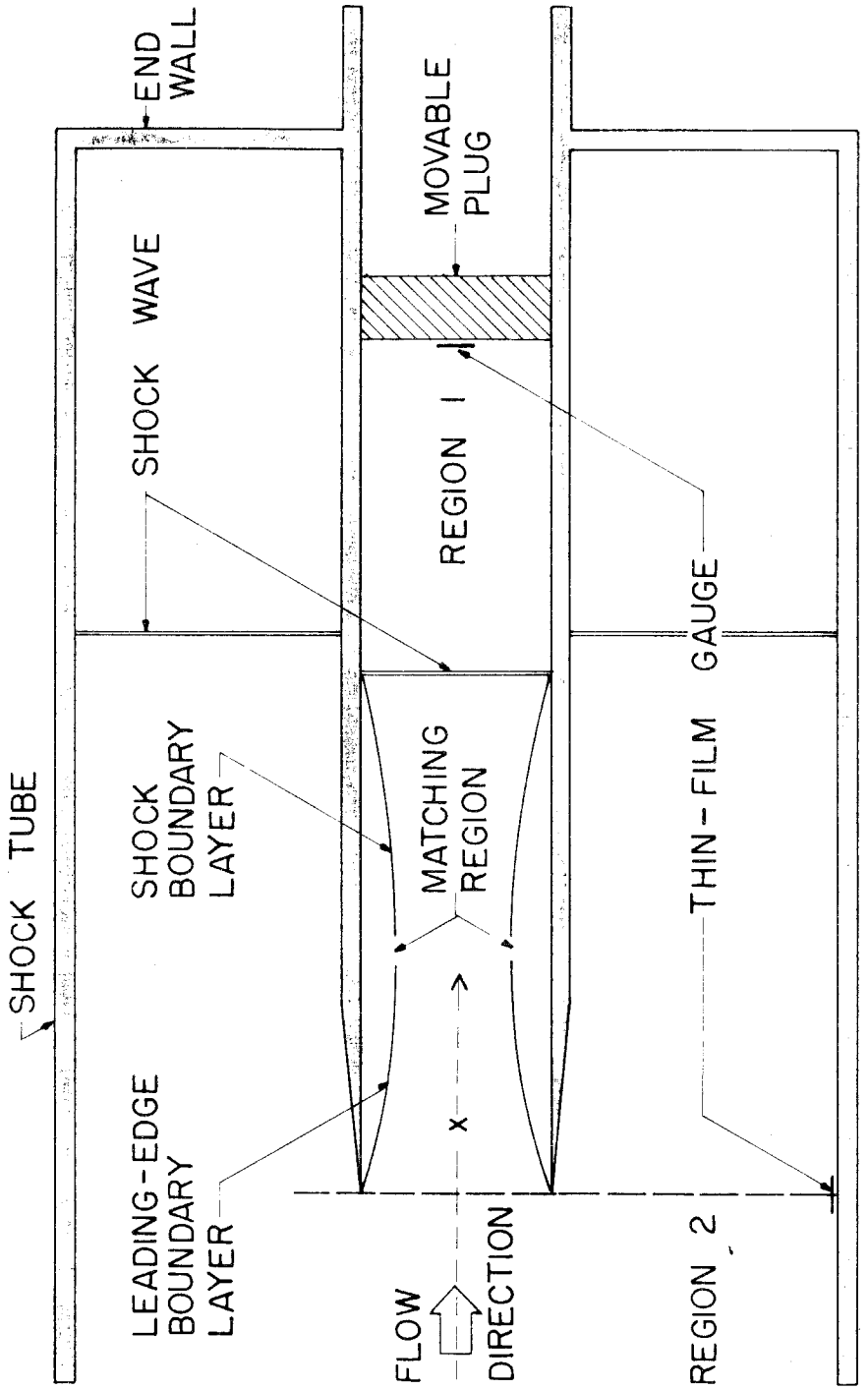


FIG. 13 SCHEMATIC OF ATTENUATION MODEL

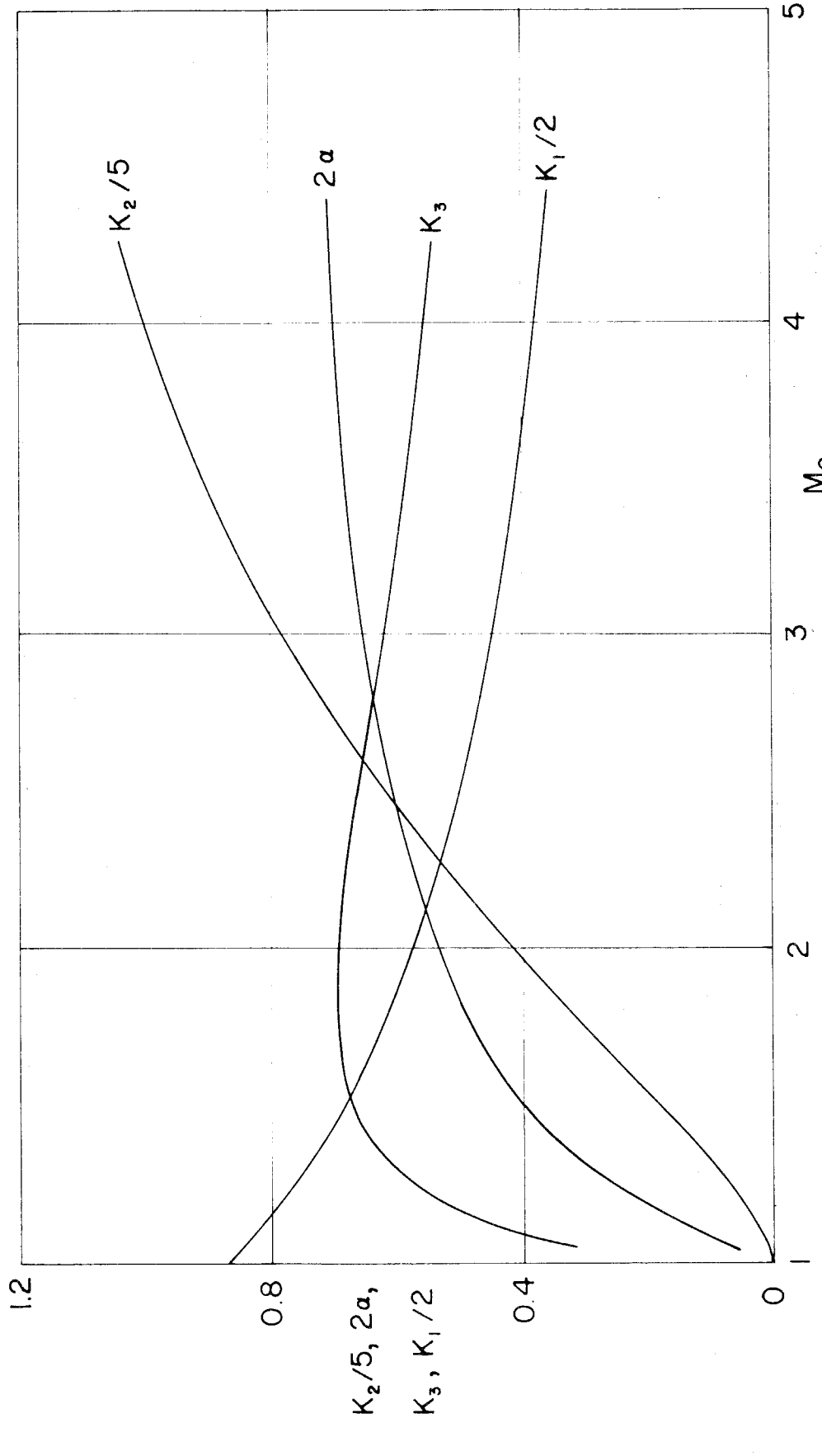


FIG. 14 BOUNDARY – LAYER PARAMETERS FOR ATTENUATION THEORY ($\gamma = 1.4$)

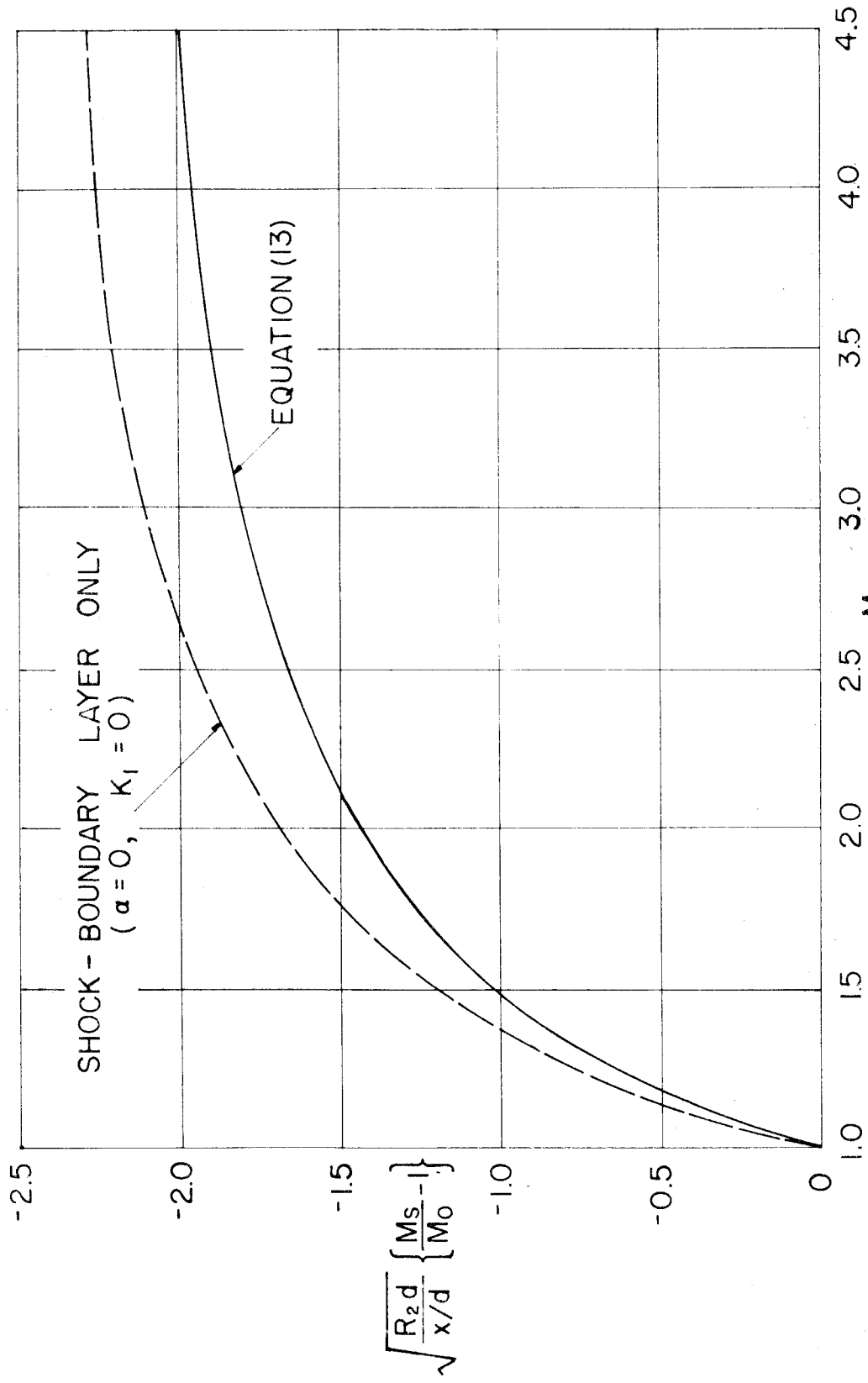


FIG. 15 ATTENUATION PARAMETER ($\gamma = 1.4$)

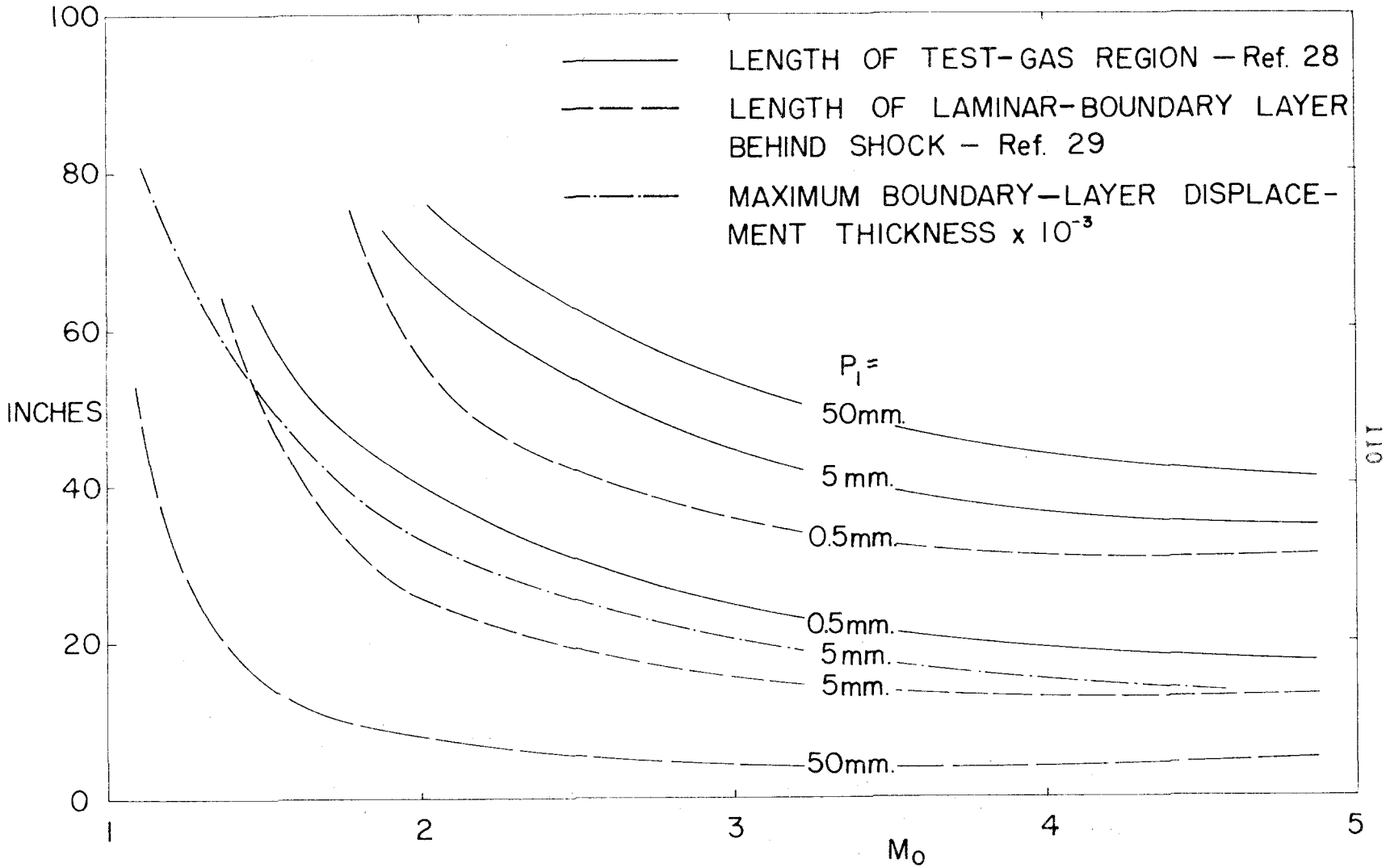


FIG. 16 FACTORS INVOLVED IN DESIGNING THE ATTENUATION EXPERIMENTS

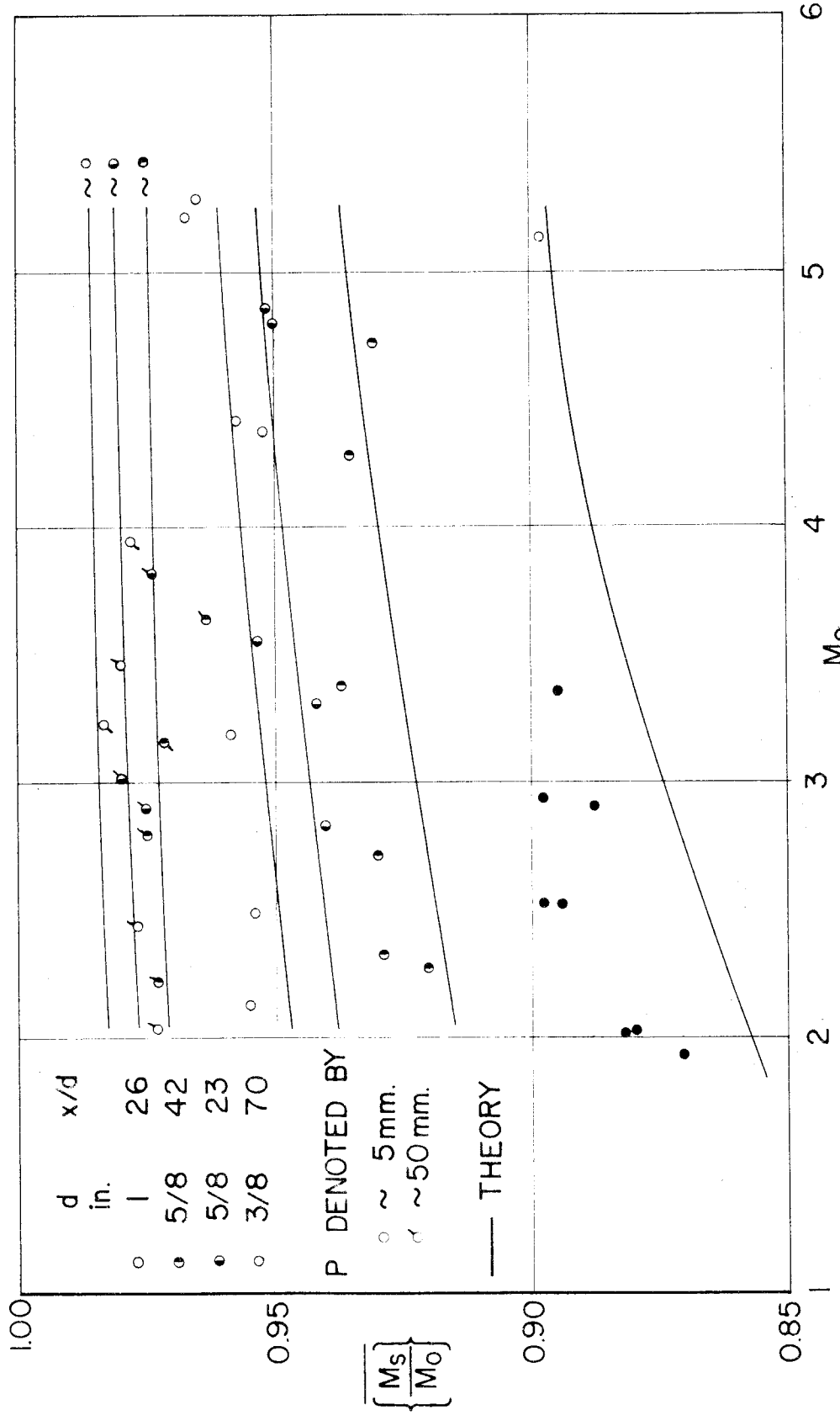


FIG. 17 ATTENUATION MEASUREMENTS

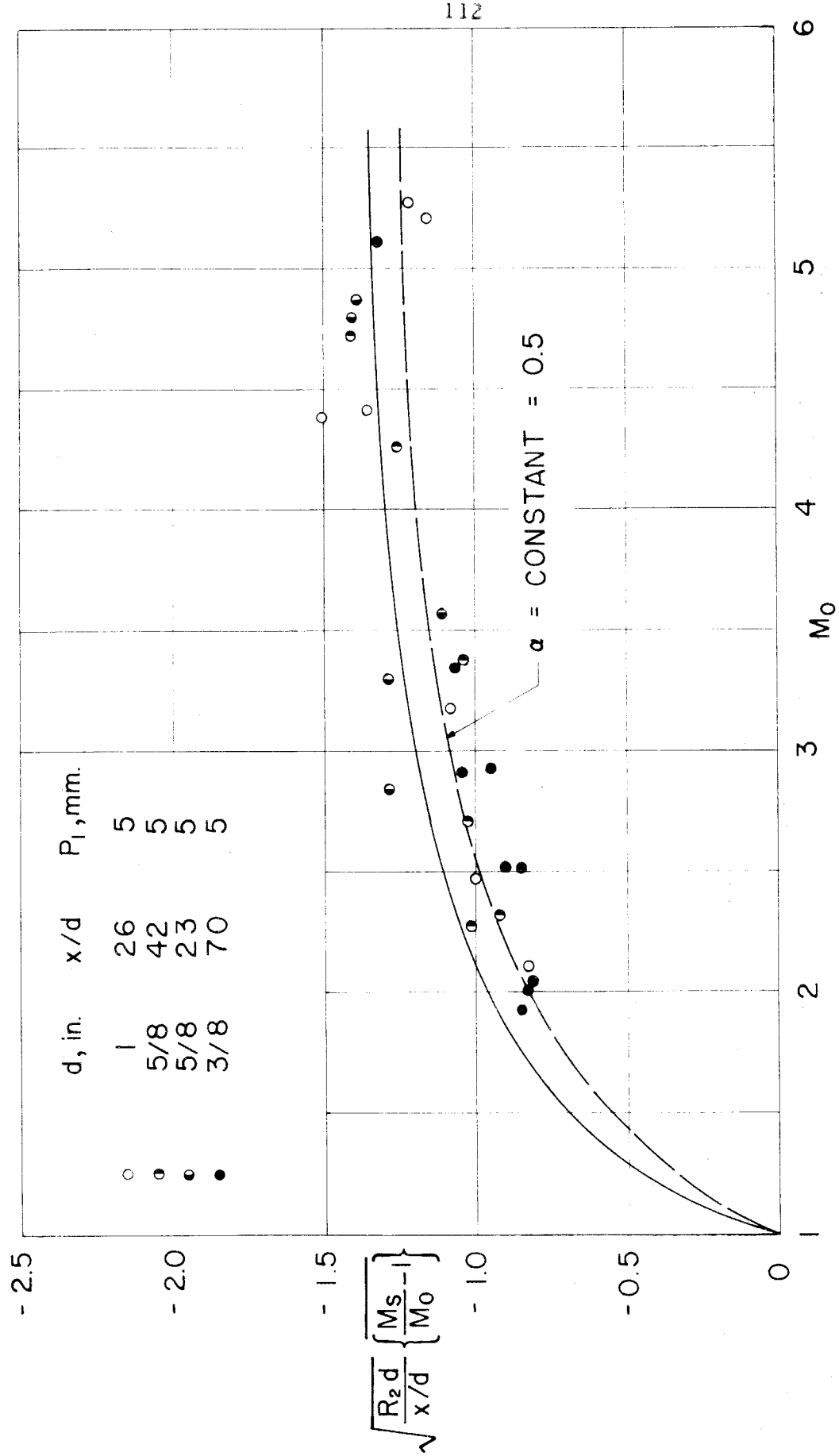


FIG. 18 COMPARISON BETWEEN ATTENUATION MEASUREMENTS AND THEORY

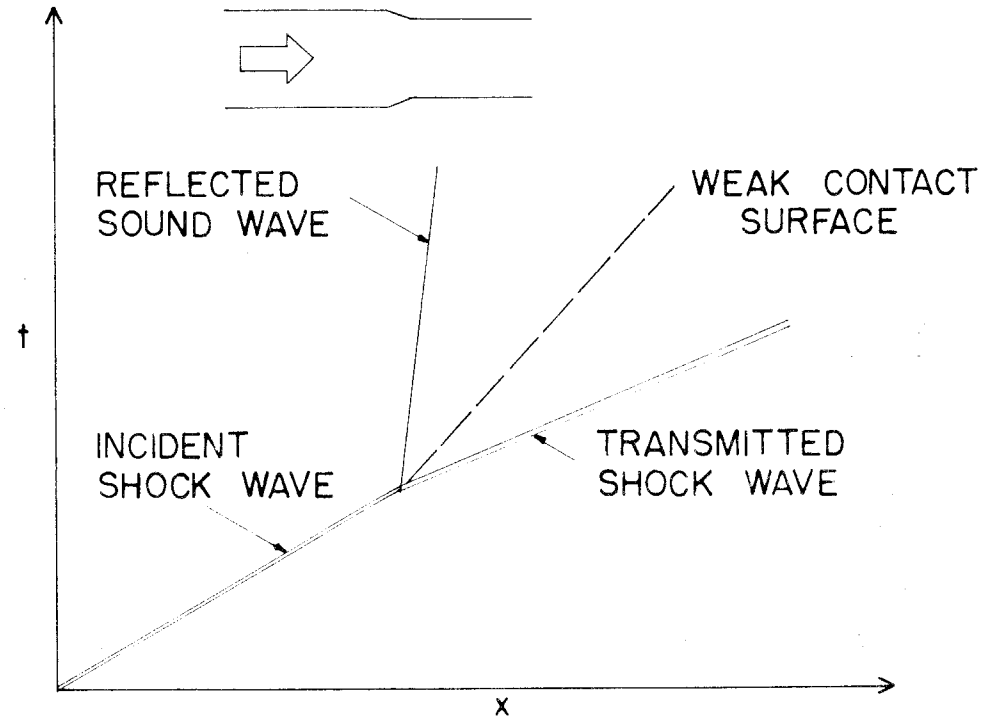


CHISNELL MODEL FOR AN INFINITESIMAL AREA CHANGE

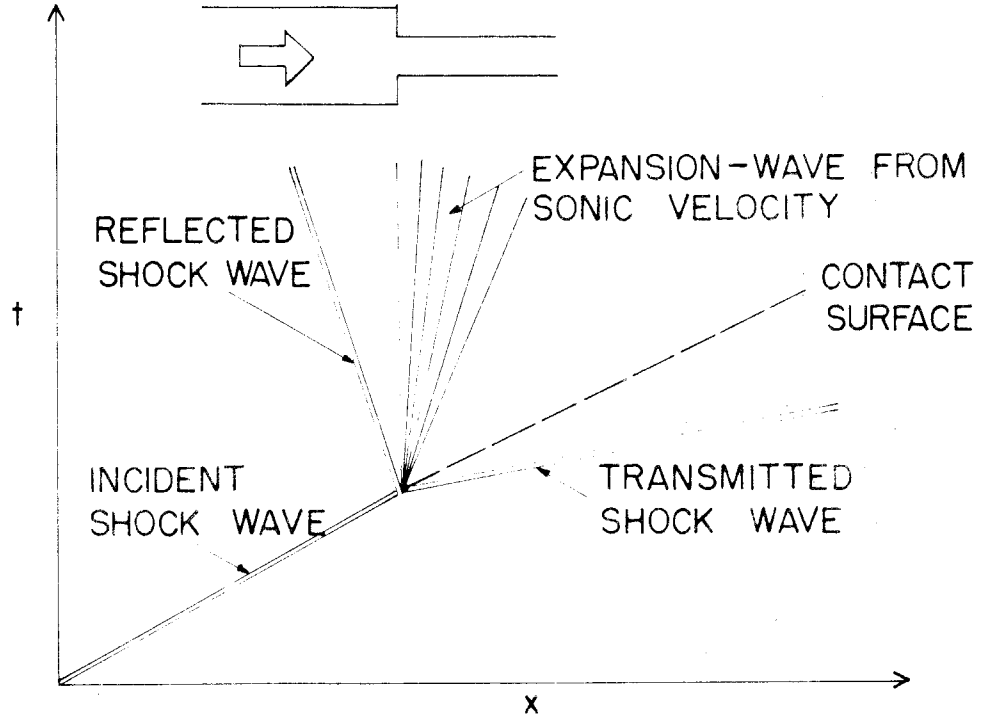


WAVE MODEL FOR FINITE INSTANTANEOUS AREA CHANGE

FIG. 19 WAVE MODELS FOR THE MOTION OF A SHOCK WAVE THROUGH AN AREA CHANGE

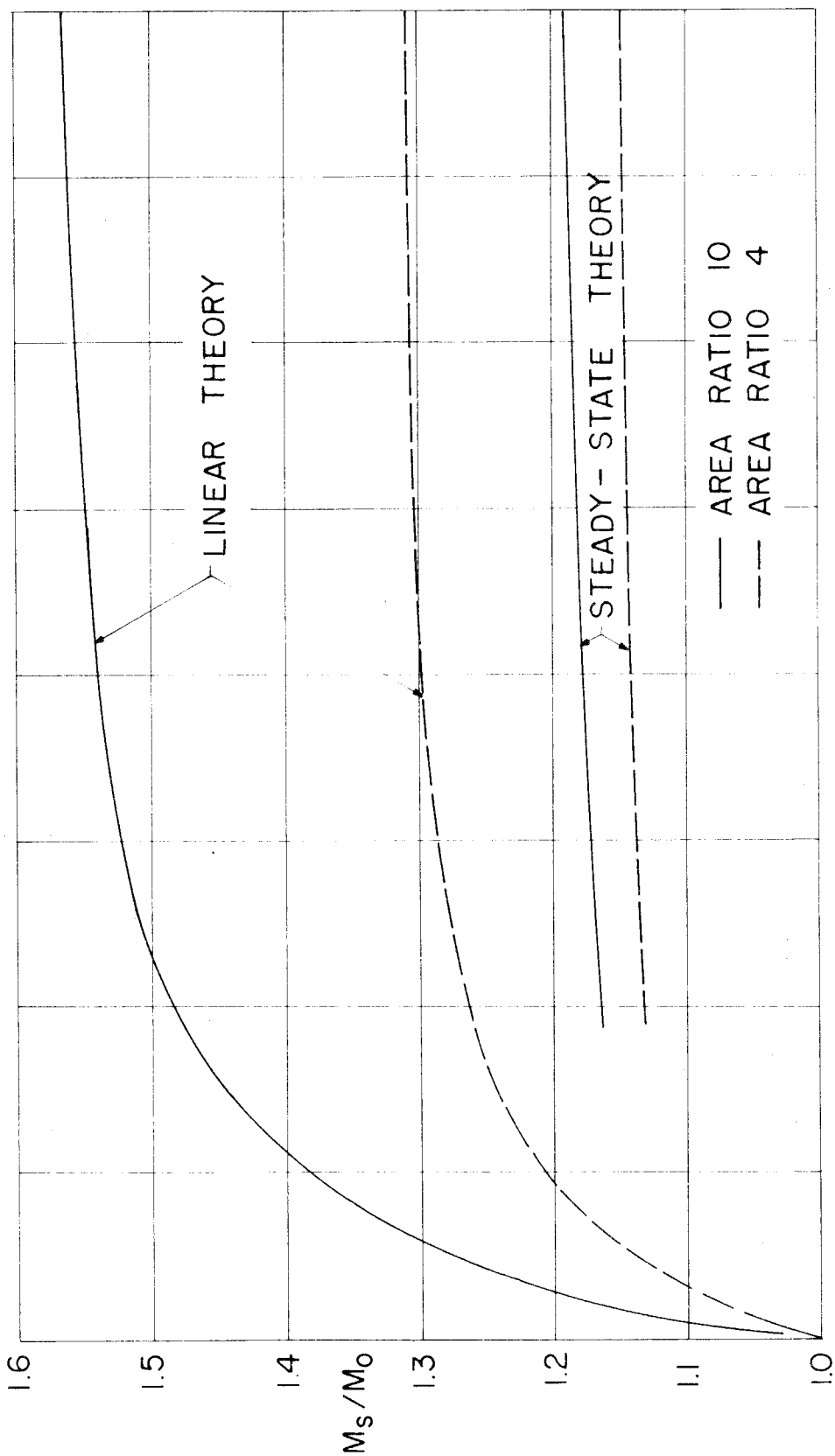


FIG. 20 COMPARISON BETWEEN SHOCK STRENGTHENING THEORIES ($\gamma = 1.4$)

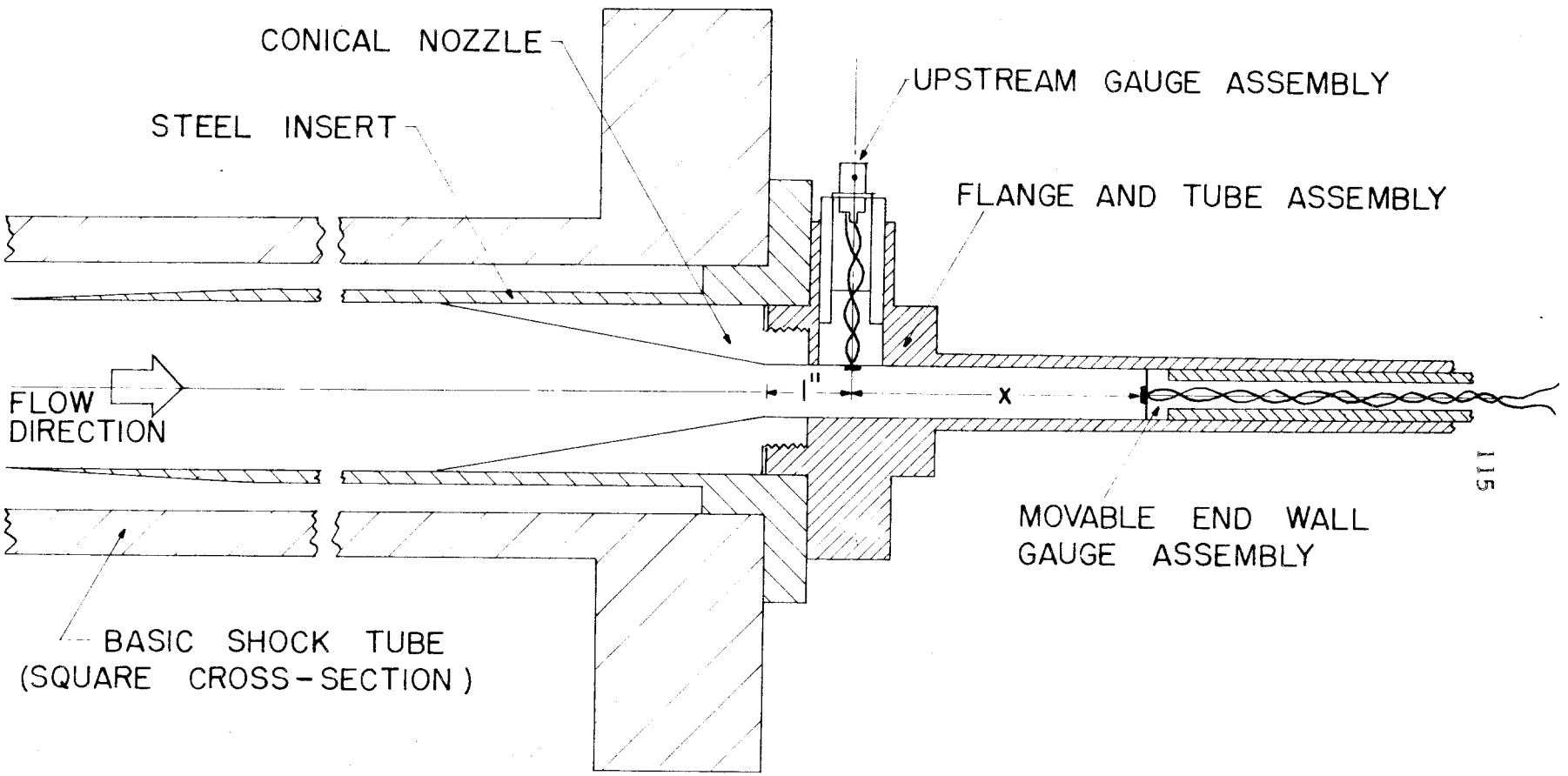


FIG. 21 NOZZLE ASSEMBLY (SIMPLIFIED) -- 1/2 SCALE

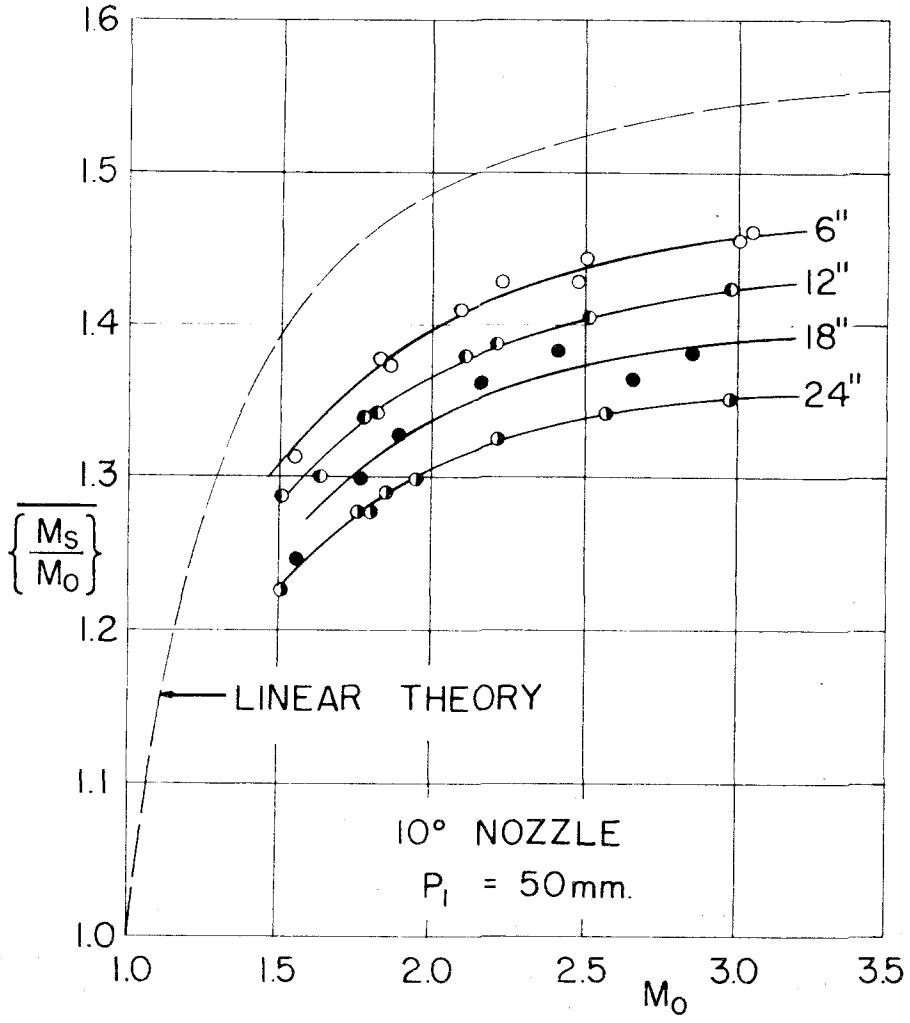


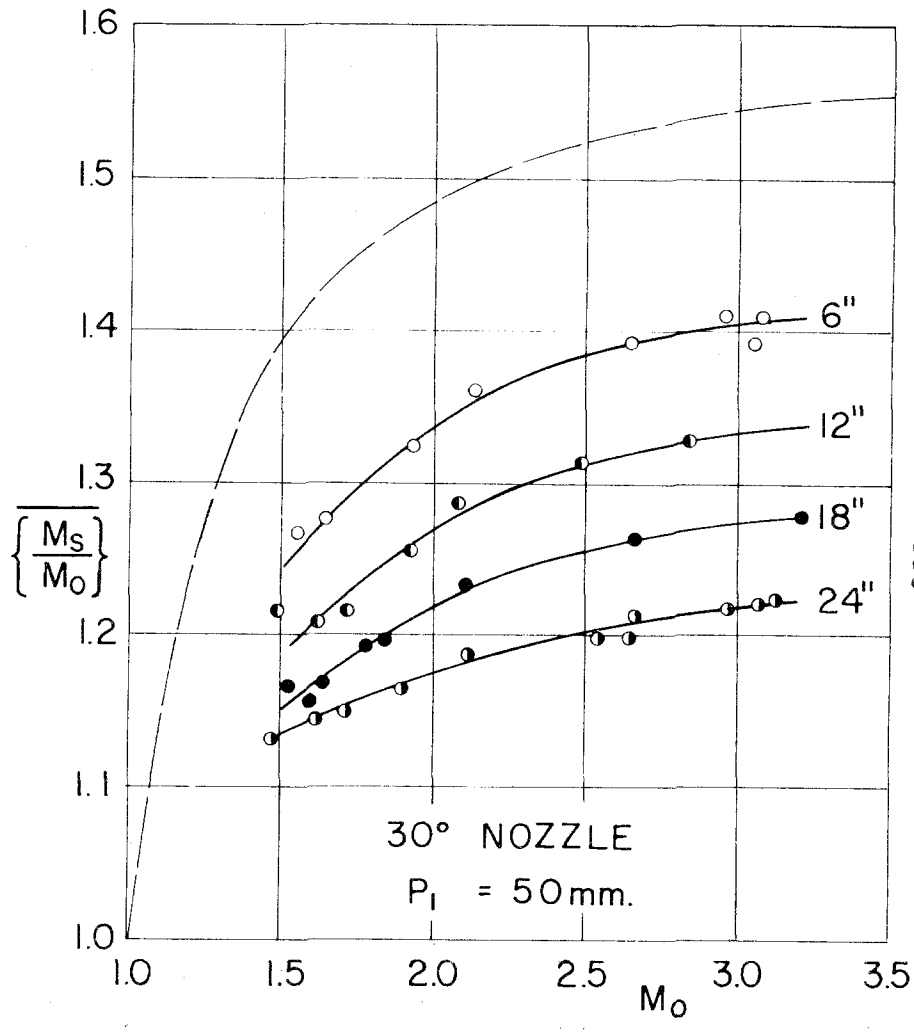


FIG. 22(a) UNCORRECTED DATA AREA RATIO = 10
(DISTANCES REFER TO DOWNSTREAM GAUGE SPACING)

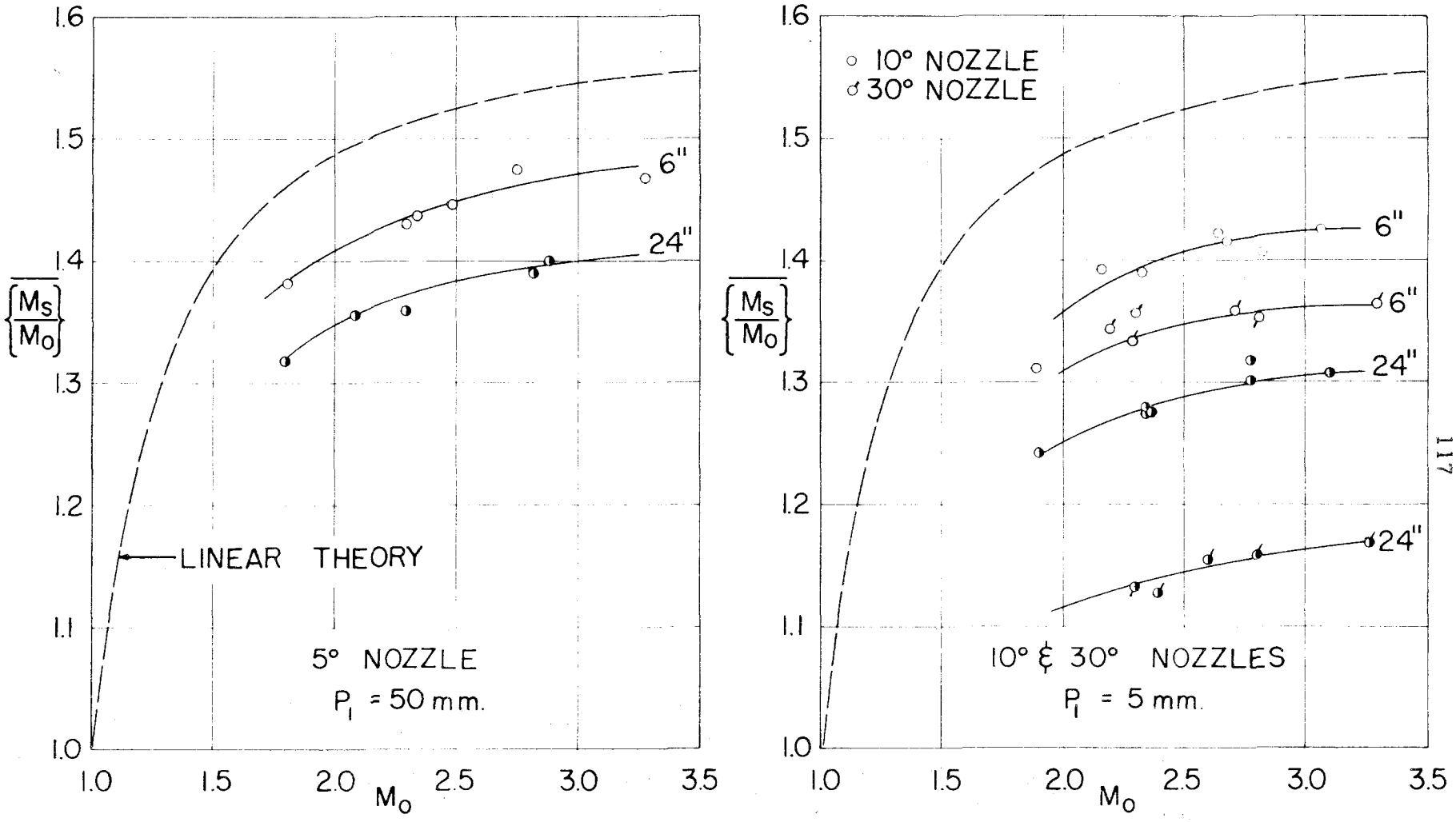


FIG. 22 (b) UNCORRECTED DATA AREA RATIO = 10
(DISTANCES REFER TO DOWNSTREAM GAUGE SPACING)

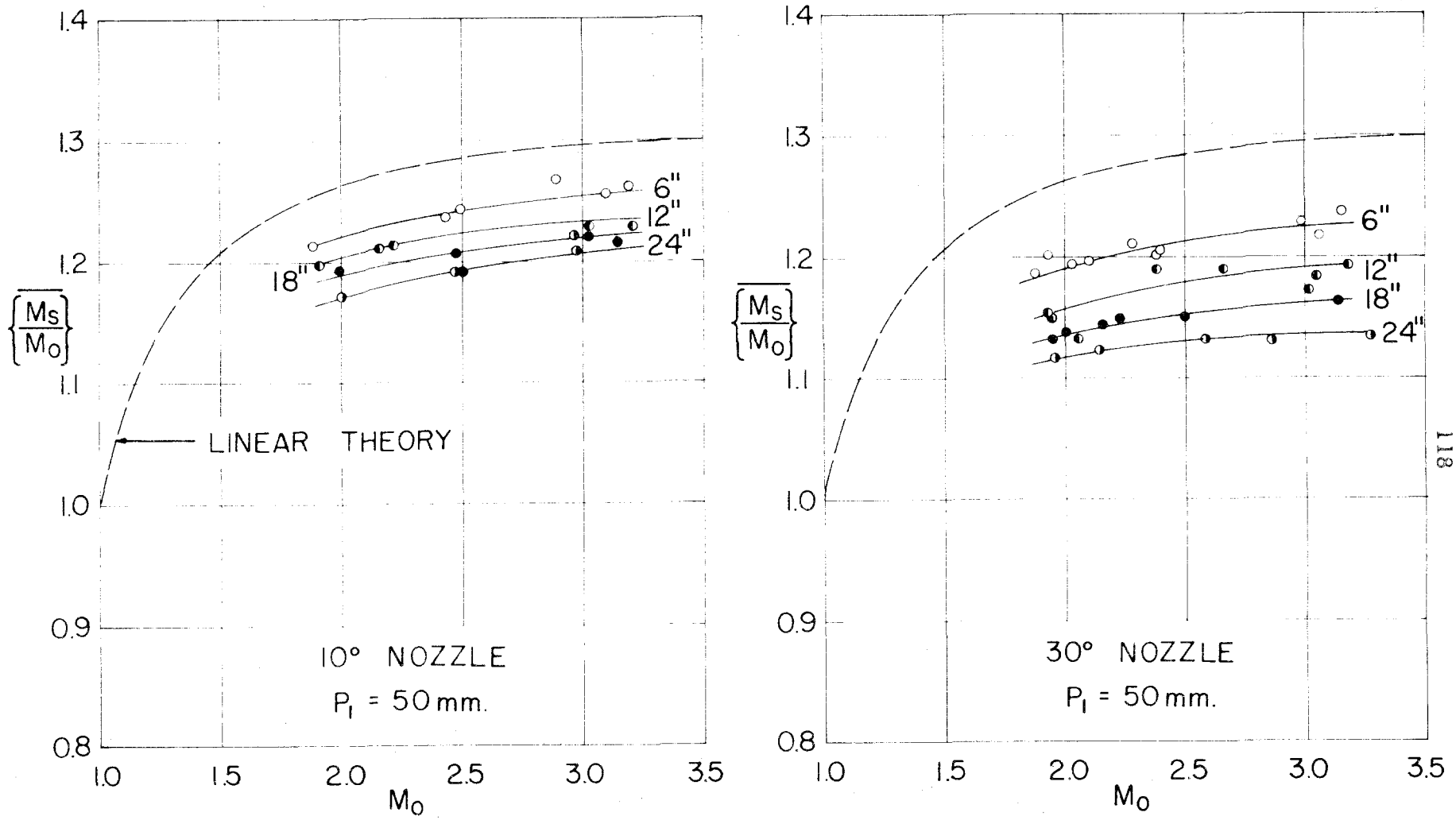


FIG. 22(c) UNCORRECTED DATA AREA RATIO = 4

(DISTANCES REFER TO DOWNSTREAM GAUGE SPACING)

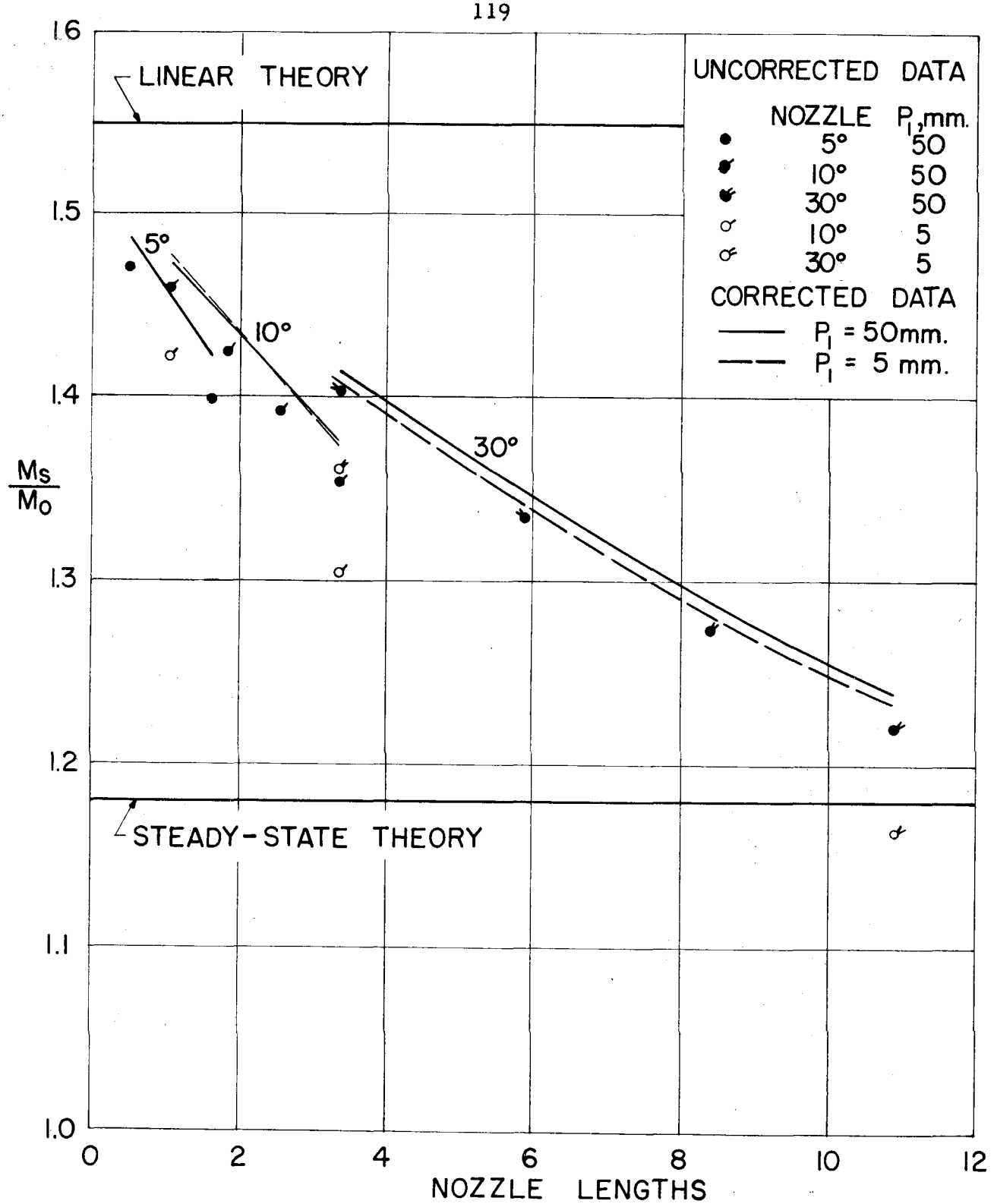


FIG. 23 TYPICAL CROSS-PLOT OF FIG. 22, SHOWING VISCOUS CORRECTION; $M_o = 3$; AREA RATIO = 10

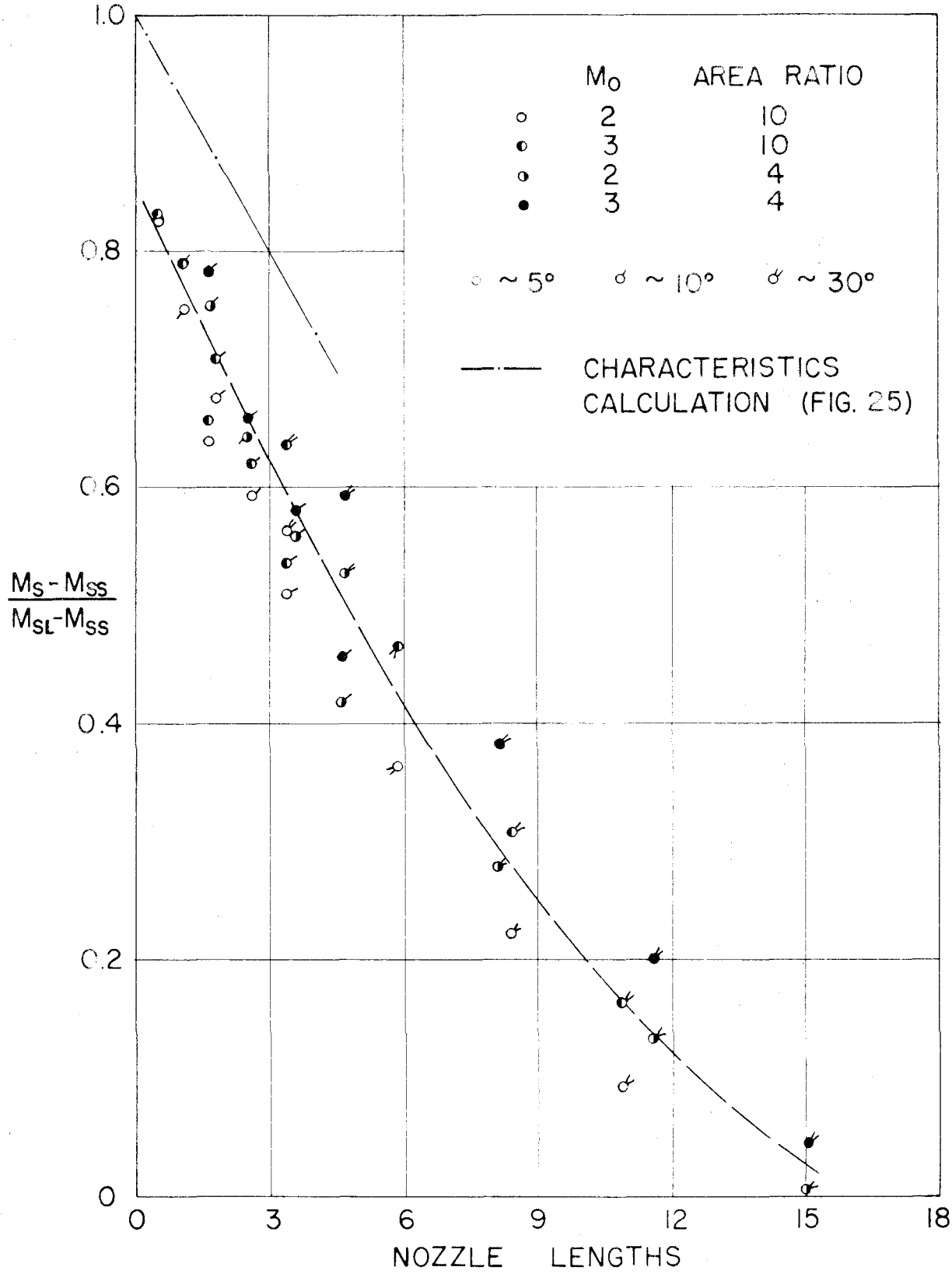


FIG. 24 NORMALIZED PLOT OF CORRECTED DATA

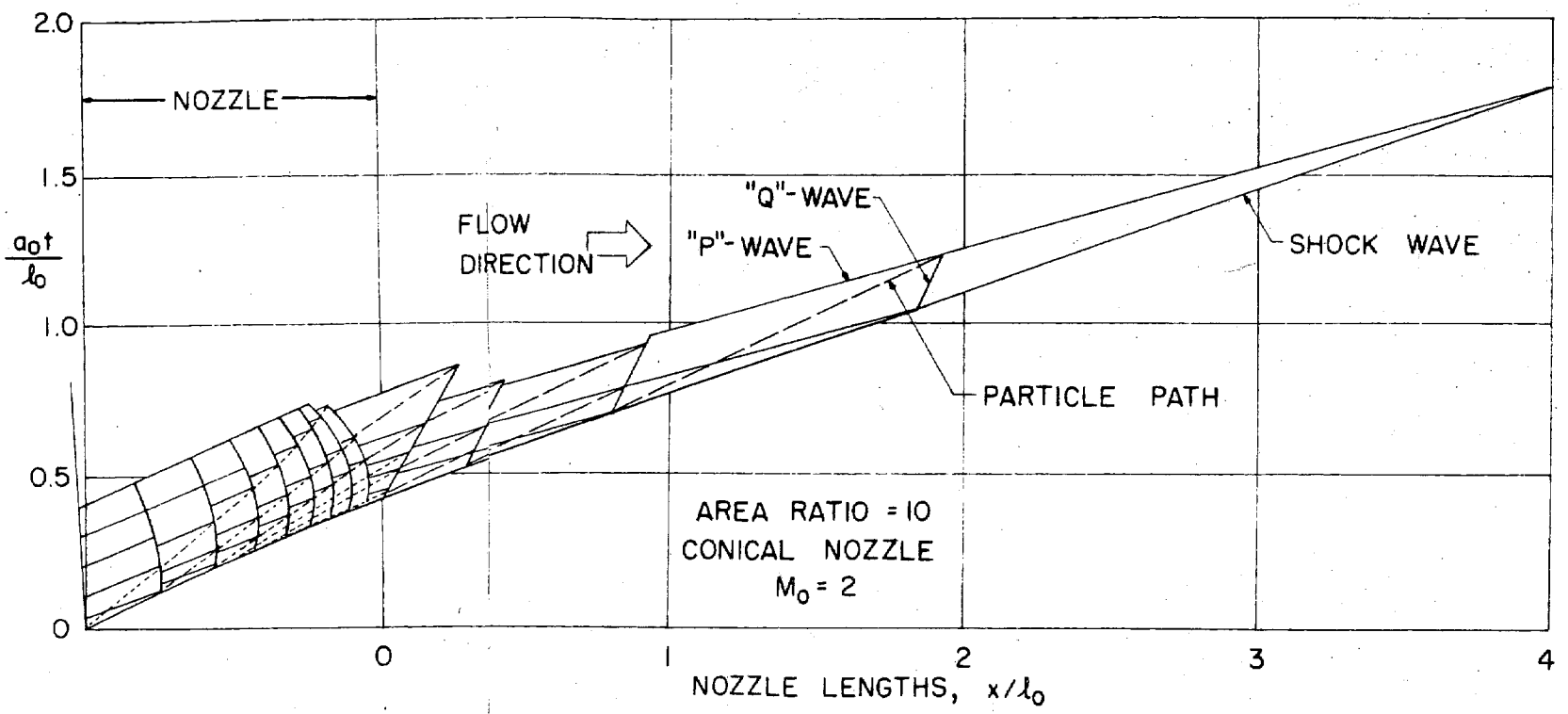


FIG. 25 CHARACTERISTICS CALCULATION -- 1/5 SCALE